

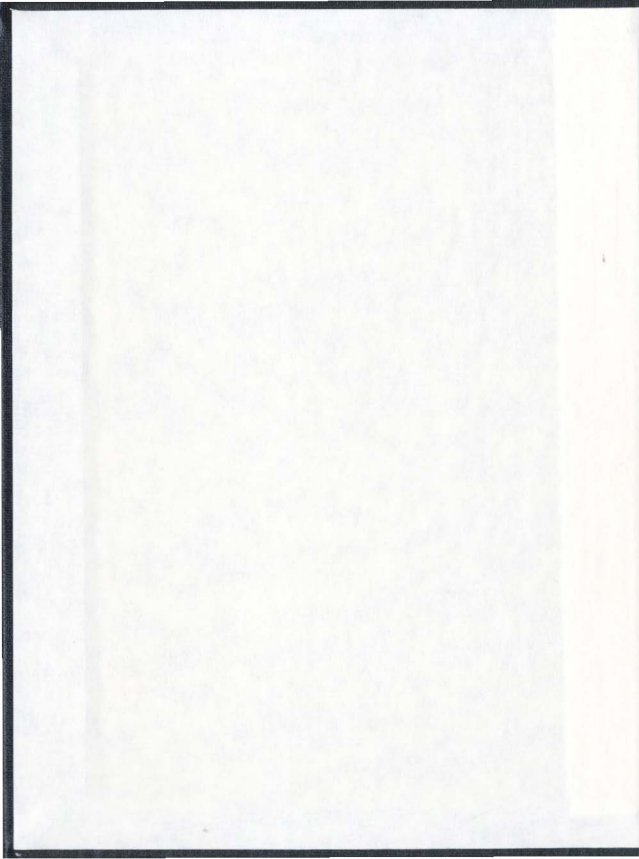
VIBRATION BASED CRACK ANALYSIS AND
DETECTION IN BEAMS USING ENERGY METHOD

CENTRE FOR NEWFOUNDLAND STUDIES

**TOTAL OF 10 PAGES ONLY
MAY BE XEROXED**

(Without Author's Permission)

XINFENG YANG



Vibration Based Crack Analysis and Detection in Beams Using Energy Method

by

Xinfeng Yang, B. Eng., M. Eng.

A thesis submitted to the School of Graduate Studies
in partial fulfillment of the requirement for
the degree of Doctor of Philosophy.

Faculty of Engineering and Applied Science
Memorial University of Newfoundland
September 2001

St. John's

Newfoundland

Canada

Acknowledgements

I would like to specially thank Dr. A. S. J. Swamidas, my thesis supervisor, for his guidance and support through my Ph. D. study at Memorial University of Newfoundland. His friendship, encouragement, experience and insightful suggestions have facilitated the successful completion of the research.

The members of my supervisory committee, Dr. R. Seshadri and Dr. K. Munaswamy, are gratefully acknowledged for their constructive comments and for their time and effort in reading the thesis.

Financial supports from NSERC grant of my supervisor, Faculty of Engineering and Applied Science, and School of Graduate Studies of Memorial University of Newfoundland are highly appreciated.

Finally, I would like to thank my family, and especially my wife Shuqin, for their never-ending love and support. Thanks also go to Mr. Li Pan, discussions with whom have been very helpful to the thesis research.

Abstract

The thesis presents a comprehensive investigation on vibrations of cracked beam structures and methodologies for crack identification. In order to determine the crack influence on structural dynamic characteristics correctly and efficiently, a vibration model for cracked beams is developed. The crack model assumes that the crack is always open during the dynamic response of the structure and considers the reduction of stiffness at the crack location; in addition it also includes the influence of stress relief around the crack region and its influence on the effective stiffness around the crack location. Computation of stiffness for the cracked beam is achieved through consideration of strain energy variation in the structure, resulting from the occurrence of a crack. The model thus generates a continuous beam vibration equation (with varying moment of inertia), which could effectively incorporate the local changes of structural properties due to the crack.

Using the model, vibration analyses of simply-supported and fixed-fixed solid rectangular beams, with one and two cracks, are carried out for computing natural frequencies and mode shapes. Changes of frequencies due to the crack are plotted considering crack size and/or crack location. It is shown that the natural frequencies would decrease as the crack size increases, and the decreases of frequencies would follow a wave-like pattern as the crack location changes. Comparisons are made with earlier results and some other experimental investigations, carried out for verifying some of these results, and shown to have a good agreement.

Frequency contour procedure is developed for crack detection. Different combinations of crack sizes and locations would give different natural frequencies, and contour lines for the same normalized frequency (as that of the measured value of the corresponding mode) could be plotted. Frequency contours for different modes in a cracked structure (having values similar to the measured values) are plotted together, and the intersection point of all the contours provides the identification of the crack location and size.

Analyses of a hollow beam model, representing a ship model, are also carried out. The beam model, with varying stiffness and mass, vibrates in water, generating added fluid mass of the ship model. Due to the eccentric nature of the added fluid mass and wave force excitation, both vertical bending vibration and coupled torsional-bending (horizontal) vibration are generated in the structure. Frequencies and mode shapes agree well with test results, obtained earlier in an experimental investigation. For a cracked backbone in the ship model, frequencies are obtained and plotted with crack size and crack location. The frequency contours are used to identify the crack size and location.

To consider shear deformation and rotary inertia effect, the vibration analyses on Timoshenko beams, with/without a crack, are also carried out. The results are compared with that of Euler beams.

Finally, forced vibration of cracked beams is considered. Frequency response, acceleration response and acceleration curvature response functions are obtained, and their changes due to a crack have been investigated. Acceleration curvature response and resonant acceleration amplitude procedures are found as suitable indicators to identify the crack.

CONTENTS

Acknowledgements	i
Abstract	ii
List of Figures	viii
List of Tables	xvii
Notations	xviii
Chapter 1 Introduction	1
1.1 Vibration Based Inspection	1
1.2 Purpose and Scope of Research	4
1.3 Organization of Thesis	6
Chapter 2 Review of Literature on Cracked Structures	8
2.1 Modeling of a Crack	8
2.1.1 Introduction	8
2.1.2 Open Crack Models	9
2.1.3 Breathing Crack Model	15
2.2 Crack Detection Methods	16
2.2.1 Frequency Changes	17
2.2.2 Mode Shape Changes	22
2.2.3 Strain and Curvature Mode Shape Changes	25
2.2.4 Flexibility Changes	27
2.2.5 Matrix Update Method	29

2.2.6	Nonlinear Method	32
2.2.7	Neural Network Method.....	35
2.3	Summary	37
Chapter 3	Basic Theory	44
3.1	Introduction	44
3.2	Vibration of Beams	45
3.2.1	Bending Vibration	45
3.2.2	Torsional Vibration	49
3.3	Galerkin's Method.....	52
3.4	General Vibration and Modal Analysis.....	54
3.5	Basic Fracture Mechanics Theory	57
3.5.1	Linear Elastic Stress Analysis for Crack Problems.....	57
3.5.2	Energy Considerations in Fracture.....	62
3.5.3	Energy Balance in a Cracked Beam under Dead-load Situation.....	64
3.6	Closure	65
Chapter 4	Crack Identification in Vibrating Beams Using Energy Method	69
4.1	Introduction	69
4.2	Solid Rectangular Beam with One or More Cracks.....	71
4.2.1	Bending Stiffness of the Beam with a Crack	71
4.2.2	Bending Stiffness of the Beam Containing Two Cracks.....	77
4.2.3	Transverse Vibration Equations for Cracked Beams	80
4.2.4	Experiments and Comparison with Theory.....	83
4.2.5	Results and Discussions	85

4.3 Crack Identification by Frequency Contours	88
4.4 Hollow Beam (Ship Backbone) Containing a Through Crack.....	91
4.4.1 Ship Model	91
4.4.2 Simplified Formulation for the Hydroelastic Model.....	92
4.4.3 Formulations for the Vertical Vibration of a Cracked Backbone Beam.....	95
4.4.4 Results and Discussions	100
4.5 Closure	102
Chapter 5 Coupled Bending-Torsional Vibration of a Cracked Hollow Beam	
Model in Water and Identification of Cracking.....	130
5.1 Introduction	130
5.2 Parameters of Model	132
5.3 Equations of Coupled Vibrations in Water	133
5.4 Natural Frequencies and Mode Shapes	136
5.5 Formulations for Cracked Backbone.....	139
5.5.1 Horizontal Bending Stiffness of Cracked Beam	140
5.5.2 Torsional Stiffness of Cracked Beam.....	143
5.6 Results and Discussions	144
5.7 Crack Detection Procedure.....	147
5.8 Closure	148
Chapter 6 Vibration and Crack Detection in Timoshenko Beam with a Crack ...	
6.1 Energy Conservation Law and Hamilton's Principle.....	161
6.2 Formulations of Vibration for a Timoshenko beam.....	162
6.3 Timshenko Beam with a Crack	166

6.4 Frequency Changes Due to Crack.....	168
6.5 Closure	169
Chapter 7 Forced Vibration of a Cracked Beam and Crack Identification	177
7.1 Formulations for Forced Beam Vibration with a Crack.....	177
7.2 Crack Identification by Acceleration Curvature Response.....	180
7.3 Crack Indication Using Resonant Acceleration Amplitude Contour	183
7.4 Closure	185
Chapter 8 Summary and Conclusions.....	197
References	205

List of Figures

Figure 2.1 Schematic of Crack Closure	40
Figure 2.2 Crack Opening and Closing (Newman [68], Backlund [69])	40
Figure 2.3 Short Beam Model	41
Figure 2.4 Beam element with a transverse crack under applied forces	41
Figure 2.5 Bilinear oscillator	42
Figure 2.6 (a) Free vibration of a bilinear oscillator;(b) Periodic square wave function ϕ_1 ; (c) Periodic square wave function ϕ_2 .	42
Figure 2.7 a. Discrete-continuous model of cantilever beam with crack; b. model of depth changes of crack as a time function.	43
Figure 2.8 Two layer back propagation network	43
Figure 3.1 A Timoshenko beam in transverse vibration	66
Figure 3.2 Displacements of a point P in torsion of a non-circular cross section	66
Figure 3.3 Mode I crack under uniform tensile stress loading	67
Figure 3.4 Mode II crack under uniform in-plane shear loading	67
Figure 3.5 Uniform out-of-plane shear stress loading (Mode III)	68
Figure 3.6 Load-displacement response as the crack grows under the dead-load loading	68
Figure 4.1 Variation of normalized bending stiffness and depth of a beam with a crack (crack location $c/l = 0.5$); — $a/h = 0.05$; $a/h = 0.25$; - - - - $a/h = 0.5$	108

Figure 4.2 Energy distribution in x-direction for a finite cracked plate (U – the strain energy over plate width, E – the elastic modulus); ——— elastic fracture mechanics theory; theory used in this paper	108
Figure 4.3 Variation of normalized bending stiffness and depth of a beam with two cracks (crack locations $c_1/l = 1/3$, $c_2/l = 2/3$); ——— $a/h = 0.05$; $a/h = 0.25$; - - - $a/h = 0.5$	109
Figure 4.4 Simply supported experimental beam	109
Figure 4.5 Experimental set up showing the electronic equipment	110
Figure 4.6 Experimental set up showing a connected beam	111
Figure 4.7 Comparison of experimental and theoretical values of frequency ratio	112
Figure 4.8 Variations of the first four frequencies as a function of crack depth for a simply supported beam (crack location $c/l = 0.5$, ω_k / ω – frequency ratio); (a) mode one; (b) mode two; (c) mode three; (d) mode four (— experimental, — theory)	112
Figure 4.9 Variations of the first four frequencies as a function of crack location for a simply supported beam (crack depth ratio $a/h = 0.25$); (a) mode one; (b) mode two; (c) mode three; (d) mode four	113
Figure 4.10 Frequencies vs. crack locations and depths for a simply supported beam; (a) mode one; (b) mode two; (c) mode three; (d) mode four	114
Figure 4.11 Variation of frequency as a function of crack depth for a simply supported beam with two cracks ($c_1/l = 1/3$, $c_2/l = 2/3$); (a) mode one; (b) mode two; (c) mode three; (d) mode four	115

Figure 4.12 Variations of the first four frequencies as a function of crack depth for a fixed-fixed beam (crack location $c/l = 0.5$); (a) mode one; (b) mode two; (c) mode three; (d) mode four 115

Figure 4.13 Variations of the first four frequencies as a function of crack depth for a fixed-fixed beam (crack location $c/l = 0$); (a) mode one; (b) mode two; (c) mode three; (d) mode four 116

Figure 4.14 Variations of the first four frequencies as a function of crack location for a fixed-fixed cracked beam (crack depth ratio $a/h = 0.25$); (a) mode one; (b) mode two; (c) mode three; (d) mode four 116

Figure 4.15 Frequencies vs. crack depths and locations for a fixed-fixed beam; (a) mode one; (b) mode two; (c) mode three; (d) mode four 117

Figure 4.16 Frequency contours for a simply supported beam with a single crack; (a) mode one; (b) mode two; (c) mode three; (d) mode four; — $\omega_c / \omega = 0.95$; $\omega_c / \omega = 0.98$; - - - - $\omega_c / \omega = 0.99$ 118

Figure 4.17 Frequency contours for a fixed-fixed beam with a single crack; (a) mode one; (b) mode two; (c) mode three; (d) mode four; — $\omega_c / \omega = 0.96$; $\omega_c / \omega = 0.98$; - - - - $\omega_c / \omega = 0.99$ 119

Figure 4.18 Crack identification by frequency contours from three different modes in a simply supported beam; — $\omega_c / \omega = 0.9708$; $\omega_c / \omega = 0.9972$; - - - - $\omega_c / \omega = 0.9744$; (Deduction: $a/h = 0.25$, $c/l = 0.5$) 120

- Figure 4.19 Crack identification by frequency contours from three different modes in a simply supported beam; — $\omega_c / \omega = 0.9947$; $\omega_c / \omega = 0.9979$; - - - $\omega_c / \omega = 0.9978$; (Deduction: $a/h = 0.1$, $c/l = 0.4$ or 0.6) 121
- Figure 4.20 Variations of the first four frequencies as a function of crack depth for a simply supported beam with an off-center mass attached (crack location ratio $c/l = 0.5$); (a) mode one; (b) mode two; (c) mode three; (d) mode four 122
- Figure 4.21 Variations of the first four frequencies as a function of crack location for a simply supported beam with an off-center mass attached (crack depth ratio $a/h = 0.25$); (a) mode one; (b) mode two; (c) mode three; (d) mode four 122
- Figure 4.22 Frequencies vs. crack depths and crack locations for a simply supported beam with an off-center mass attached; (a) mode one; (b) mode two; (c) mode three; (d) mode four 123
- Figure 4.23 Frequency contours for a simply supported cracked beam with an off-center mass attached; (a) mode one; (b) mode two; (c) mode three; (d) mode four; — $\omega_c / \omega = 0.95$; $\omega_c / \omega = 0.98$; - - - $\omega_c / \omega = 0.99$ 124
- Figure 4.24 Crack identification by frequency contours from three different modes in a simply supported beam with off-center mass attached; — $\omega_c / \omega = 0.9946$; $\omega_c / \omega = 0.9976$; - - - $\omega_c / \omega = 0.9983$; (Deduction: $a/h = 0.1$, $c/l = 0.4$) 125
- Figure 4.25 CPF ship model [87] 126
- Figure 4.26 Backbone of ship model 126
- Figure 4.27 Added mass of two-dimensional body [91] 127

Figure 4.28 Mode shapes for the uncracked backbone, W —displacement,	127
Figure 4.29 Mode shapes from tests for the uncracked backbone	128
Figure 4.30 Variations of first four normalized frequencies as a function of crack length ratio for the ship beam (backbone) model (crack location ratio $c/l=0.5$); (a) mode one; (b) mode two; (c) mode three; (d) mode four.	128
Figure 4.31 Variations of first four normalized frequencies as a function of crack location ratio for the ship beam (backbone) model (crack length ratio $a/(h+b)=0.17$); (a) mode one; (b) mode two; (c) mode three; (d) mode four.	129
Figure 5.1 Cross section of backbone at a point considering added mass	152
Figure 5.2 Displacement of a point P in coupled torsional-bending vibration of the beam.	152
Figure 5.3 Mode shapes for coupled (horizontal) bending-torsional motion (v — horizontal displacement, θ — torsional angle)	153
Figure 5.4 Mode shapes for horizontal motion only	153
Figure 5.5 Mode shapes for torsional motion only	154
Figure 5.6 A crack (2a) is located at one flank of the hollow backbone.	154
Figure 5.7 Normalized bending-torsional frequencies against crack length for a crack at $c/l=0.5$	155
Figure 5.8 Normalized bending-torsional frequencies against crack length for a crack at $c/l=0.25$	155
Figure 5.9 Normalized bending-torsional frequencies against crack length for a crack at $c/l=0.75$	156

Figure 5.10 Normalized bending-torsional frequency against crack location ratio c/l ($a/(b+h)=0.2$)	156
Figure 5.11 Normalized bending-torsional frequency against crack location ratio c/l ($a/(b+h)=0.08$)	157
Figure 5.12 Normalized bending-torsional frequency against crack location ratio c/l ($a/(b+h)=0.4$)	157
Figure 5.13 Normalized bending-torsional frequency against crack length and crack location	158
Figure 5.14 Three frequency contours for first four modes of bending-torsional motions	159
Figure 5.15 Crack identification by intersection of three contours for first, third and fourth modes (deduction: $a/(b+h)=0.2,c/l=0.5$)	160
Figure 5.16 Crack identification by intersection of three contours for first, second and third modes (deduction: $a/(b+h)=0.24,c/l=0.2$)	160
Figure 6.1 Normalized frequency vs crack depth ratio for $l/h=15, c/l=0.5$, --- Euler beam, — Timoshenko beam; (a) mode one, (b) mode two, (c) mode three, (d) mode four.	173
Figure 6.2 Normalized frequency vs crack depth ratio for $l/h=10, c/l=0.5$, --- Euler beam, — Timoshenko beam; (a) mode one, (b) mode two, (c) mode three, (d) mode four.	173
Figure 6.3 Normalized frequency vs crack depth ratio for $l/h=5, c/l=0.5$, --- Euler beam, — Timoshenko beam; (a) mode one, (b) mode two, (c) mode three, (d) mode four.	174

- Figure 6.4 Normalized frequency vs crack location ratio for $l/h=15$, $a/h=0.2$. --- Euler beam, — Timoshenko beam; (a) mode one, (b) mode two, (c) mode three, (d) mode four. 174
- Figure 6.5 Normalized frequency vs crack location ratio for $l/h=10$, $a/h=0.2$. --- Euler beam, — Timoshenko beam; (a) mode one, (b) mode two, (c) mode three, (d) mode four. 175
- Figure 6.6 Normalized frequency vs crack location ratio for $l/h=5$, $a/h=0.2$. --- Euler beam, — Timoshenko beam; (a) mode one, (b) mode two, (c) mode three, (d) mode four. 175
- Figure 6.7 Frequency ratio comparisons among Timoshenko beam, Euler beam and test results, $c/l=0.5$. --- Euler beam, — Timoshenko beam, test results of aluminum beam. 176
- Figure 7.1 Displacement frequency responses for cracked and uncracked beam excited at first natural frequency ($a/h=0.5$, $c/l=1/6$, excitation at the middle point), --- cracked beam, — uncracked beam. 187
- Figure 7.2 Displacement frequency responses for cracked and uncracked beam excited at first natural frequency ($a/h=0.5$, $c/l=1/2$, excitation at the middle point), --- cracked beam, — uncracked beam. 187
- Figure 7.3 Acceleration frequency responses for cracked and uncracked beam excited at first natural frequency ($a/h=0.5$, $c/l=1/6$, excitation at the middle point), --- cracked beam, — uncracked beam. 188

Figure 7.4 Acceleration frequency responses for cracked and uncracked beam excited at first natural frequency ($a/h=0.5$, $c/l=1/2$, excitation at the middle point), -- cracked beam, — uncracked beam.	188
Figure 7.5 Acceleration response along beam length for different excitation frequencies (excitation at the middle point of the beam, $a/h=0.5$, $c/l=5/6$)	189
Figure 7.6 Acceleration response along beam length for different excitation frequencies (excitation at the quarter point of the beam, $a/h=0.5$, $c/l=5/6$)	189
Figure 7.7 Acceleration curvature response along with beam length at different excitation frequencies (with crack location $c/l=5/6$, crack depth $a/h=0.5$, excitation at the middle point)	190
Figure 7.8 Acceleration curvature response along with beam length at the first resonant frequency (crack location $c/l=5/6$, excitation at the middle point of the beam)	190
Figure 7.9 Acceleration curvature response (at the crack location) against crack depth at the first resonant frequency (crack location $c/l=5/6$, excitation at the middle point of the beam)	191
Figure 7.10 Acceleration curvature responses for the first resonant and non resonant frequency excitations (excitation at the middle point)	191
Figure 7.11 Resonant acceleration amplitude against crack depth (crack location $c/l=1/6$; excitation at the middle point, response at the middle point)	192
Figure 7.12 Resonant acceleration amplitude against crack depth (crack location $c/l=1/3$; excitation at the middle point, response at the middle point)	192

Figure 7.13 Resonant acceleration amplitude against crack depth (crack location $c/l=0.5$; excitation at the middle point, response at the middle point)	193
Figure 7.14 Resonant acceleration amplitude against crack location (crack depth $a/h=0.25$; excitation at the middle point, response at the middle point)	193
Figure 7.15 Resonant acceleration amplitude against crack location (crack depth $a/h=0.5$; excitation at the middle point, response at the middle point)	194
Figure 7.16 Resonant acceleration amplitude vs. crack depth and location (excitation at the middle point, response at the middle point)	194
Figure 7.17 Resonant acceleration amplitude contours for first four modes	195
Figure 7.18 Resonant acceleration amplitude contours for first four modes (— 0.96, ---1.2, ----1.6)	195
Figure 7.19 Crack identification by the intersection of three contours from three different modes (deduction: $a/h=0.2$, $c/l=0.5$) (— 1.0191: first mode, --- 1.0646: third mode, ----0.9729: fourth mode)	196
Figure 7.20 Crack identification by the intersection of three contours from three different modes (deduction: $a/h=0.4$, $c/l=1/3$ or $2/3$) (— 0.9878: first mode, --- -0.9997: third mode, ----1.2256: fourth mode)	196

List of Tables

Table 4-1 Frequency comparison for four and eight terms Galerkin's method	104
Table 4-2 Frequency comparison for four and eight terms Galerkin's method	105
Table 4-3 Frequency comparison between simply supported beam with and without off-center mass attached	106
Table 4-4 Properties of CPF hydroelastic model	107
Table 4-5 Stiffness of the Backbone at the Connections of Segments	107
Table 4-6 Frequencies of Uncracked Backbone	107
Table 5-1 Properties of the Backbone [86]	150
Table 5-2 Frequencies of Uncracked Backbone	151
Table 6-1 First four frequencies for Euler and Timoshenko beams with $l/h = 15$	171
Table 6-2 First four frequencies for Euler and Timoshenko beams with $l/h = 10$	171
Table 6-3 First four frequencies for Euler and Timoshenko beams with $l/h = 5$	172
Table 6-4 Normalized frequencies for Euler and Timoshenko beams with $a/h=0.5$, $c/l=0.5$	172

Notations

A	area of cross section
A_k	acceleration resonant amplitude
ARC	acceleration response curvature
a	crack depth
b	beam width
c	crack location
$[C], c_i$	damping matrix and terms in the matrix
E	Young's modulus
E_c	Strain energy for crack growth
EI	bending stiffness of uncracked beam
EI_c	bending stiffness of cracked beam
$\{f\}$	force matrix
f_0	unit concentrated force
G	shear modulus
G_I, G_{II}, G_{III}	energy release rates for corresponding modes of cracking
$H(j\omega)$	frequency transfer function
h	beam height
I	moment inertia for uncracked beam
I_c	moment inertia for cracked beam
K_I, K_{II}, K_{III}	stress intensity factors for the three modes of cracking
$[K], k_{ij}$	stiffness matrix and terms in matrix

l	beam length
M	bending moment
m	line mass density
m_a	added fluid mass
$[M], m_{ij}$	mass matrix and terms in mass matrix
Q	shear force
U	strain energy
V	potential energy
u, v, w	three dimensional displacements
W	work by external forces
x, y, z	global coordinates
β	slope due to shear
ψ	slope due to bending
θ	rotation
ϕ	warp function for torsion
ω	frequency
ω_c	natural frequency for the cracked beam
λ	eigenvalue
$\sigma_x, \sigma_y, \sigma_{xy}$	plane stresses
$\epsilon_x, \epsilon_y, \epsilon_{xy}$	plane strains
ρ	density
ξ	modal damping factor

Chapter 1

Introduction

1.1 Vibration Based Inspection

The occurrence of defects, cracks and damages may be inevitable in engineering structures in spite of our best efforts. They are formed due to various causes. Some of them are metallurgical defects, generated as a result of improperly controlled manufacturing processes. Some may be environment induced cracks, such as stress corrosion cracking and hydrogen damage. Some may be fatigue cracks that occur under cyclic service load conditions controlled by the limited fatigue strength of materials. Some other damages may be induced due to impacts of falling weights, ramming of floating debris and ships, etc.

A crack which occurs in a structural element would reduce the local stiffness and weaken the structural strength. Even though all structures are designed to withstand the expected operational loads, they are prone to damages from overloads or repeated fatigue loads leading to cracks. The continued and undetected growth of the crack may finally lead to the collapse of the structure, and subsequently to the possible losses of human lives and tremendous revenues. Therefore, the detection of a crack at its early stage of development is important for the safety of the structure and human lives. During the past three

decades, focused efforts have been made for the development and improvement of existing and developing nondestructive inspection methods (NDI).

The use of various materials, types of structure, construction procedures, etc., have led to the development of different NDI methods. Some methods such as Visual Inspection, Ultrasonic, Radiography, Acoustic Emission, Magnetic Particle Inspection, Dye Penetrant and Eddy Current techniques, are called conventional methods which are well developed and already in use for detecting cracks/flaws in structures. The other methods such as Vibration Based Inspection, Wave Propagation and Laser techniques are new emerging methods which are undergoing development and not accepted as readily as others. Most of NDI methods could be more or less considered to be applicable to general use; but these methods also have some kinds of limitations, which make them excellent for detecting one kind of damage and useless for detecting others. The final inspection plan for any structure often includes the use of more than one inspection method.

As a newer NDI method, the Vibration Based Inspection (VBI) has been proposed as one of the most promising approaches [1], which has certain advantages compared to other conventional methods. The fundamental idea of VBI is to get information about the soundness of a structure from the measurement of its vibration characteristics; if there is a change in the vibration characteristics (which may be due to a number causes) of the structure, then such changed characteristics could be due to a decrease of stiffness caused by the presence of cracks. The cracks could be identified by the use of a number of remotely located sensors and the subsequent analysis of data obtained from them. The

dynamic characteristics such as frequencies and responses obtained from the data analysis are global parameters for structures; thus the VBI can be used as a global inspection procedure and wholesale screening is not necessary. Meanwhile, no cleaning of local areas is required compared to others. The detection of defects through VBI could be applied to cracks far away from the sensors and to areas whose surfaces are not accessible. VBI method is also cheap and quick.

Vibration based inspection, in theory, is generally developed from the investigation of simple structures such as a beam and a plate. From vibration theories of beams and plates, one knows that natural frequencies of a beam or a plate are dependent on the square root of flexural stiffness of the beam or the plate. The local flexural stiffness in a structure would change due to the crack and how much it would change, globally and locally, is dependent on the crack size and location. Given the size and location of the crack, it is possible to calculate the changes of vibration characteristics of the structure, based on the correct crack models and solution methods. Conversely, if the changes of vibration characteristics are measured from vibration response, it is also possible to detect the crack and find its location and size.

Modelling of a crack in VBI is an important step to identify the crack. The short beam model [1] was the first developed model in which the presence of a crack was considered by introducing a short beam with a reduced bending stiffness at the position of the crack. Another model, the reduced Young's modulus and moment of inertia model, was simply to assume a change in Young's modulus to represent the presence of a crack, which is

mainly used in connection with finite element analysis. The model developed later, viz., fracture mechanics model, was to model the crack zone of a beam by means of a local flexibility matrix determined using fracture mechanics concepts. At the location of the crack, the beam is considered to be connected by a spring system which has dynamic properties defined by its flexibility matrix.

Crack detection methods are developed based on crack modelling and experiments. Basically, there are two variations in vibration based crack detection methods: frequency analysis and modal analysis, which need to record sensor data in time domain and then to transform data into frequency domain using Fast Fourier transform procedures. In frequency analysis, one simple method is to compare the measured frequencies to the predicted frequencies of a cracked structure to determine the presence of the crack. Other methods are often involved in defining some parameters (indicators), which are related to frequency shifts, to determine the crack size and/or location [2]. In modal analysis, many crack indicators have been developed based on frequencies and mode shapes, which include modal assurance criteria (MAC), mode shape curvature/strain, modal sensitivity and frequency transfer function.

1.2 Purpose and Scope of Research

Among the models developed for crack characterization in VBI, the model based on fracture mechanics concepts has been widely used in analyzing the crack influence on the vibration response of structures. In this model, the local compliance at the crack location

is calculated based on fracture mechanics concepts. However, this model is mainly applied to beam structures and uses the discontinuities in beam by dividing the beam structure into two or more substructures, depending on how many cracks are on it. Substructures are connected by a bending spring which is used to model the crack. Each substructure is treated as an independent beam which has its own equation of motion. A group of vibration equations are related by continuity conditions of the bending spring. It is rather cumbersome and quite involved to apply this method to irregular beams and other structures. Meanwhile, many crack detection methods have been developed in VBI. Many procedures have been proposed to identify the presence of cracks in structures; however, the methodology to identify the location and size of a crack is still incomplete. Effective and accurate crack detection methods are required to be developed to cover the whole range of crack depths and locations.

The present research work will thus focus on developing an effective and correct crack model for beam structures using energy method. Purpose of the study is to develop crack detection methods based on results from the developed energy model to identify the crack location and crack size. The research will cover the following areas:

- i) Develop an energy based crack model for beam structures, which could be used to calculate the frequencies and mode shapes of cracked beams;
- ii) Carry out vibration analysis of Euler beams and develop a crack detection procedure;

- iii) Carry out vertical bending vibration and coupled torsional-bending vibration analyses of hollow beams and identify and detect the existence of possible cracks;
- iv) Carry out vibration analysis of Timoshenko beams and compare with Euler beams with/without cracks;
- v) Carry out forced vibration analysis of solid beams and develop crack detection methods from acceleration responses.

1.3 Organization of Thesis

The thesis is arranged according to the following format:

Chapter 2 gives a review of the relevant studies on vibration based inspection carried out by earlier researchers. Chapter 3 gives the theoretical background needed for the research; it includes basic vibration theory for beams, application of numerical Galerkin's method, representation of crack influence using fracture mechanics conceptions, and modal analysis for response estimation.

Chapter 4 describes an energy based numerical model which is used to consider the vibration of cracked beams. Galerkin's method is used to solve the vibration equations. The frequency contour method is developed to identify the crack. The analyses are carried out for simply supported and fixed-fixed beams, and a free-free hollow beam vibrating on water. The hollow beam represents a ship model with varying stiffness. The numerical results are verified by experiments carried out on cracked beam. Chapter 5

gives an analysis of torsional-bending vibration of the hollow beam model and the use of crack detection methodology developed earlier.

Chapter 6 discusses the studies on vibrations of cracked Timshenko beams. The results are compared with that of Euler beams. Forced vibration of a cracked simply-supported beam is presented in Chapter 7. The acceleration curvature response procedure and acceleration resonant amplitude contour procedure are developed for crack identification.

Finally, Chapter 8 summarizes the relevant findings of the research and gives recommendations for further studies.

Chapter 2

Review of Literature on Cracked Structures

2.1 Modeling of a Crack

2.1.1 Introduction

The basic idea in VBI is to measure the dynamic characteristics throughout the lifetime of the structure and use them as a basis for detection of the position and magnitude of cracks, if any. However, a successful detection of cracks through measuring of the dynamic characteristics is very much dependent on the exact modeling of the crack. It is known that the crack would reduce the stiffness of a structure, decrease its natural frequencies and change its vibration modes. Such changes will inevitably depend on the crack type, size and location. Correct modelling of these parameters of the crack will indicate how the dynamic characteristics change.

The established models up to now, in general, reflect only part of the changes in stiffness caused by the crack. It is almost impossible to establish a model to reflect the change of damping; this is due to the fact that damping in structures is quite complex and very sensitive to environmental conditions such as temperature, treatment of steel, etc. The modeling of a crack considering change of stiffness can be divided into open (always

open) and breathing crack (that open and close) models. In open crack models, the crack is always open during vibration. In the breathing crack model: (i) the crack opens and closes fully during part of one vibration cycle and remains closed during the remaining part of the cycle; or (ii) the crack opens partially during part of the vibration cycle (due to the compressive residual stresses left along the wakes of some fatigue crack [3,4]), closes fully and remains closed during remaining part of the vibration cycle; or (iii) the crack remains almost open during a number of vibration cycles (as a consequence of the debris deposited in the opening and closing crack, due to the continuous grinding action and the mismatched crack closure [5,6]), and then follows a procedure similar to that given in (ii). Figure 2.1 shows the schematic of crack closure. Figure 2.2 shows that crack opens and closes depending on the load applied on the crack. In most of the earlier studies carried out on cracked structures, only open crack models were used to find relationships among modal and crack parameters while very few studies considered the breathing crack model to investigate the non-linearity in cracked structures.

2.1.2 Open Crack Models

Decrease of structural stiffness due to a known open crack is constant. In other words, the stiffness of the structure is reduced by an open crack, but stiffness for this cracked structure will not change during vibratory motion. A number of analytical models have been developed to investigate the loss of stiffness due to an open crack. The methods include short beam, reduced Young's modulus and moment inertia, and fracture mechanics model.

2.1.2.1 Short Beam Model

The crack in a beam will decrease the cross-sectional area or bending stiffness EI resisting deformation. In this model the presence of a crack is taken into account by introducing a short beam element with a reduced bending stiffness at the position of the crack (Figure 2.3). The length of the short beam is assumed to be an equivalent width w of the crack. This model was probably the most commonly used model until the mid-seventies [1]. With this model, an analytical solution is easily established and finite element analysis could be easily carried out to verify the results.

Kirsmer [7] investigated the relationship between the changes in the first natural frequency of a simply supported beam and an equivalent slot width through energy considerations. The experimental data was used to calibrate the expression with respect to the equivalent width of the slot. He found that an equivalent width equal to five times the actual width of the slot gave reasonable agreement with the analytical and experimental data. Thomson and Madison [8] used a short beam model to determine the effect of a narrow groove or crack on the flexural, longitudinal and torsional vibrations of a slender bar. However, the authors pointed out that the procedure would only be applicable if the equivalent slot width was determined through experiments. Petroski [9] performed experiments on a three point bending specimen, and then used the results along with fracture mechanics theory to calculate the equivalent width of the crack.

Cracks in a beam would cause discontinuities in stress distribution (stress relief around the crack location) and local deformations (such as strain, slope, curvature, etc.) in the vicinity of the crack. Part of the beam will thus become less effective in resisting the load due to the changes in stress distribution. The main disadvantage of the short beam model is that it does not take account of this ineffectiveness of the material and the sudden change of local deformations due to the crack presence.

2.1.2.2 Reduced Young's Modulus and Moment of Inertia Model

This model is mainly used in connection with finite element analysis. Because a crack decreases local stiffness, it is convenient to assume a change in Young's modulus to represent the presence of a crack. Young's modulus is a material property. Although any change in stiffness, due to a crack, may be represented as a change in modulus, it is not a true change in modulus. This method requires only a simple modification in the finite element analysis and no new element is required. Moment of inertia reduction reflects the removal of a local portion of the structure, and in turn the variation of the local stiffness of a structure.

The complex stress/strain distribution around the tip of crack is not properly modeled in this model. In general the model is much simple and approximate. Rytter [1] pointed out that the variation in natural frequencies, with respect to the size of damage calculated by means of this model, would have poor accuracy and would be typically overestimated.

Yuen [10] used this model to investigate a damaged cantilever beam. He mainly focused on the sensitivity studies of various modal parameters, which used mode shape and mode

shape slope. Other researchers using this model include Pandey *et al* [11] and Salawu & Williams [12].

2.1.2.3 Fracture Mechanics Model

A crack existing in a structural member introduces a change of local flexibility which is a function of the crack depth. This variation changes the dynamic behavior of the system and its stability characteristics. The basic idea of this model is to model the crack zone of a beam by means of a local flexibility matrix determined using fracture mechanics concepts.

To establish the local flexibility matrix of a cracked member under general loading, consider a prismatic beam with a crack of depth a (see Figure 2.4). The beam has height h and width b . The beam is subjected to a force or moment P_i . Under a general loading, the additional displacement u_i , due to the presence of the crack, along the direction of force P_i , will be computed using Castigliano's theorem.

To this end, if Φ is the strain energy due to a crack, Castigliano's theorem requires that the additional displacement be [13]

$$u_i = \frac{\partial \Phi}{\partial P_i} \quad (2.1)$$

The strain energy Φ is given from fracture mechanics considerations as

$$\Phi = \int_0^{A_c} \frac{\partial \Phi}{\partial A} dA = \int_0^{A_c} J dA \quad (2.2)$$

where J is the strain energy density function, and A_c the crack surface. Therefore

$$u_i = \frac{\partial}{\partial P_i} \left[\int_0^A J dA \right] \quad (2.3)$$

The flexibility influence coefficient c_{ij} is given by

$$c_{ij} = \frac{\partial u_i}{\partial P_j} = \frac{\partial^2}{\partial P_i \partial P_j} \int_0^A J dA \quad (2.4)$$

Thus the flexibility matrix will be a 12×12 matrix if all the six degrees of freedom at a point (three displacements and three rotations) are taken into account for the element.

The relationship between J and the stress intensity factors, for linear elasticity, is given by

$$J = \frac{\beta}{E} K_I^2 + \frac{\beta}{E} K_{II}^2 + \frac{1+\nu}{E} K_{III}^2 \quad (2.5)$$

where ν is Poisson's ratio, E is the modulus of elasticity, K_I , K_{II} and K_{III} are the stress intensity factors for crack modes I, II and III respectively, and

$$\beta = \begin{cases} 1 & \text{for plane stress} \\ 1-\nu^2 & \text{for plane strain} \end{cases}$$

Then, the local flexibility caused by a crack can be calculated by

$$c_{ij} = \frac{1}{E} \int_0^A \frac{\partial^2}{\partial P_i \partial P_j} \left[\beta K_I^2 + \beta K_{II}^2 + (1+\nu) K_{III}^2 \right] dA \quad (2.6)$$

The influence of the ineffective material caused by the crack is inherent in the expression for the stress intensity factors and thereby in the local flexibility matrix. Thus a high level of accuracy can be expected when using this model. The level of accuracy depends on reliable expressions for the stress intensity factors and detailed description of the geometry of the cracked zone.

A beam with rectangular cross section has been the most preferred problem considered by many investigators. The stress intensity factor K_I can be written as for the bending deformation of a beam by

$$K_I = \sigma \sqrt{\pi a} f\left(\frac{a}{h}\right) \quad (2.7)$$

where σ is a characteristic stress value for the beam. The function $f\left(\frac{a}{h}\right)$ has been given in different forms by different authors. Ostachowicz and Krawczuk [14] use

$$f\left(\frac{a}{h}\right) = 1.13 - 1.374\left(\frac{a}{h}\right) + 5.749\left(\frac{a}{h}\right)^2 - 4.464\left(\frac{a}{h}\right)^3 \quad (2.8)$$

The function $f\left(\frac{a}{h}\right)$ is dependent only on the crack depth at a specific location and as such K_I in equation (2.6) has contributions only at the crack location. The effect of stress relief on either side of the crack is not taken into consideration in this model.

Irwin [15] was probably the first person to relate the local flexibility of a cracked beam to the stress intensity factor. Okamura *et al* [16] determined the local flexibility for the axial load and bending moment in a beam of rectangular cross section. They studied the variation of the first natural frequency of a free-free beam as a function of the crack depth. Ju *et al* [17] considered a beam subjected to pure bending and used the results in connection with damage detection.

Dimarogonas and Paipetis [18] established a 5x5 flexibility matrix to model the vicinity of a crack. Torsion was not included in the model. Later Papadopoulos and Dimarogonas [19] completed the matrix by adding torsion and obtained a full 6x6 flexibility matrix.

2.1.3 Breathing Crack Model

The introduction given in section 2.1.1 discusses the various possibilities that may occur during the opening and closing of a crack. The fatigue crack will open and close alternatively during the harmonic vibration of a beam or plate. This is called the breathing crack. The breathing crack model is used to analyze the opening and closing of the crack during vibration. Up to now very few studies have considered explicitly the effects of actual opening and closing of cracks on the stiffness and dynamic response of a structure. In these studies some [20,21] have used bilinear oscillators to simulate the crack, which is shown in Figure 2.5. It can be seen from the figure that when mass m_0 is not in contact with the left spring (equivalent to crack opening) the system vibrates at stiffness k_1 , and when the mass is in contact with the left spring (equivalent to crack closing) the system has stiffness k_2 ($k_2 > k_1$). In the application to a cracked beam, the beam is assumed to have two characteristic stiffnesses, one having a larger value when crack is closed and the other having a smaller value when the crack is open (see Figure 2.6). The instant of crack opening or closing is determined by the stress or strain discontinuity at the location of the crack; and the opening/closing of the crack is assumed to occur almost simultaneously. For some portion of vibration period the beam is considered to vibrate as an uncracked one; for the remaining portion of the period the

beam vibrates as a beam with fully open crack. The bilinear equations are solved by approximate methods or numerical procedures.

Krawczuk and Ostachowicz [22] assumed a time function for the crack opening and closing during one vibration period (see Figure 2.7), and then solved the consequent linear equations during small time intervals. Meanwhile, researchers [23,24,25,26] have used finite element method to analyze the opening and closing crack; and the stiffness of the cracked section was either calculated from the assumed force-displacement relationship or was the same as that of the bilinear model. Due to the complex nature of the equations and the difficulty of obtaining exact analytical solutions, several researchers [27,28,29] carried out experimental investigations and used the dynamic response to identify the nonlinearity associated with the crack opening and closing. It has been observed that the opening and closing crack makes the cracked section stiffer than it already is; this will indicate the crack depth to be much smaller than it actually is in the cracked beam. However, these papers have shown that it is difficult to relate the size and location of the crack directly from the measured crack indicators.

2.2 Crack Detection Methods

The crack would change the dynamic characteristics of a structure; therefore, use of such changes could be a possible way to detect the crack. Based on this principle, many crack detection methods have been developed: (a) frequency change; (b) mode shape change;

(c) strain and curvature changes; (d) flexibility change; (e) matrix update method; (f) nonlinear method; and (g) neural network method.

2.2.1 Frequency Changes

The natural frequencies of a structure are dependent on its stiffness and mass density. For example, the bending frequencies for a simply supported beam are given by

$$\omega_n = \left(\frac{n\pi}{l} \right)^2 \left(\frac{EI}{\mu} \right)^{\frac{1}{2}}, \quad n = 1, 2, 3, \dots \quad (2.9)$$

where l is the length of the beam, EI is bending stiffness, and μ is mass per unit length. It can be seen that the stiffness changes due to the presence of a crack will change the natural frequencies of the structure; therefore, the monitoring of frequency changes is a reasonable crack detection method. The main reason for the popularity of this approach is that the natural frequencies are rather easy to determine with a relatively high level of accuracy. In fact, one sensor placed on a structure and connected to a frequency analyzer could give the values of several natural frequencies. Further, natural frequencies are sensitive to all kinds of damages, both local and global damages.

This sensitivity of a structure to a local damage can easily be seen from equation (2.9) obtained for the natural frequency of linear uncracked beams with constant cross section and material properties. When a crack occurs, it will lead to a change in the moment of inertia I , or perhaps the distribution of mass, and thereby to changes in natural frequencies.

It is noticed from equation (2.9) that the natural frequencies depend on the square root of the stiffness. Thus the changes of frequencies might not be significant for a small crack. This is why some researchers favor other methods. However, using frequency shifts to detect damage would be much more practical in applications where such shifts can be measured very precisely in a controlled environment.

Another disadvantage is that any change in the non-structural mass or stiffness will be reflected in the natural frequencies. For example, in offshore platforms damage induced frequency shifts are difficult to distinguish from the shifts resulting from erosion of soil around the embedded portion of the pile or the increased mass due to marine growth. Therefore, it is important to record all such changes and take them into account.

The frequency change due to a crack does not modify every natural frequency of a cracked structure. A natural frequency that does not decrease cannot be used as a damage indicator, but could be used to identify possible locations of the crack. This is probably due to the fact that the damage is located at a nodal point for that mode shape and the measurements will most probably indicate unchanged values (for that frequency), precluding the possibility for identifying the frequency shift. For example, if the third frequency remains unchanged for a simply supported beam, the possible location of the crack would be at two narrow areas on the beam around the points where the displacement of the third mode shape is zero.

Usually the presence of a crack is related to a decrease in local stiffness and thereby in the natural frequencies. However, increase in natural frequencies has also been observed by Maguire [30]; he reported that when a damage was introduced in some pre-stressed concrete beams, the frequencies increased. These increases were attributed to the fact that the modulus of elasticity of concrete increased as the pre-stresses decreased.

There are a large numbers of papers related to crack detection using frequency change method. Some studies consist of calculating frequency shifts from a known type of damage. Typically, the damage is modeled mathematically, and the measured frequencies are compared to the predicted frequencies to determine the presence of the damage. Vandiver [31,32] investigated the frequency changes in first two bending modes and first torsional mode of an offshore light tower to identify damage. Numerical analysis indicated that changes in the effective mass of the tower resulting from sloshing of fluid in tanks mounted on deck would produce only 1% change in the frequencies of the three modes being considered. The author also demonstrated that failure of most members, by removing the member from the numerical model, produced changes in resonant frequencies greater than 1%, and thus damage in most of the members would be detectable.

Kenley and Dodds [33] studied changes of resonant frequencies due to crack in a decommissioned offshore platform. They found that only complete severance of a diagonal member could be detected by changes in the global modal frequencies. The

damage had to produce a 5% change in the overall stiffness before it can be detected, and 1% changes of resonant frequencies for global modes can be detected.

Tracy and Pardoen [34] gave an analysis for computing the vibration frequencies and mode shapes of a composite beam with a mid-plane delamination. The beam was divided into four sections: above, below, and on either side of the delamination, in which bending and axial vibrations were considered. The transverse deformations of the sections above and below the delamination were constrained to vibrate together so that the analysis was applied to mid-plane. The characteristic equation was solved numerically to give frequencies and mode shapes.

Man *et al* [35] gave a detailed closed form solution for the frequency of a beam containing a slot. The author reported that the minimum slot size that is detectable by their technique is 10% the beam depth.

Choy *et al* [36] used reduced modulus of one or more beam elements to simulate damage. It was assumed that the first beam element was degraded, and the modulus associated with this element was adjusted until the first natural frequency from the numerical model matched the first measured natural frequency. The process was repeated assuming the damage to be located in each of the other elements, and also repeated for the second and third natural frequencies. The location of the damaged section was obtained from the intersection of flexural rigidity versus element location curves obtained from the iterative

process using the different natural frequencies. The method could not distinguish damage at symmetrical locations in a symmetric structure.

Some studies in frequency change consist of calculating the damage parameters, e.g., crack length and/or crack location, from the frequency shifts. Adams *et al* [37] described an axial vibration response study to identify the crack from changes in the resonant frequencies associated with two modes. Stubbs *et al* [38,39] derived a relationship between changes of resonant frequencies and changes of member stiffnesses. Damage was defined as a reduction in the stiffness of one of the elements, and could be located by solving the inverse equation using measured frequencies.

Hearn and Testa [40] defined the ratio of changes in natural frequencies for various modes. The ratio could be calculated using mode shapes and pre-damaged modal properties, and the damage was identified using the measured frequency ratios. Sanders *et al* [41] used Stubbs procedure combined with an internal-state-variable theory to detect damage in composites. Skjaerbaek *et al* [42] studied a multi-story reinforced concrete frame structure and developed a procedure to detect the damage using a single response measurement. Damage was defined as average relative reduction of the stiffness matrix of the substructures that reproduce the two lowest frequencies of the whole structure.

2.2.2 Mode Shape Changes

A crack will cause a local change in the derivatives of mode shapes at the position of the damage. This has led to the application of crack detection by the mode shape change method. However, to estimate correctly the mode shape, one needs to measure responses at a large number of locations. Thus the instrumentation required and the duration of the measurement session will increase considerably if a detailed mode shape has to be estimated. This is probably the main disadvantage in using the mode shape method.

West [43] presented the first systematic use of mode shape information for the location of structural damage. In his study, he used the modal assurance criteria (MAC) to determine the level of correlation between modes from the test of an undamaged space-shuttle-orbiter body flap and the modes from the test of the flap after it had been exposed to acoustic loading. The mode shapes were partitioned using various schemes, and the change in MAC across the different partitions was used to localize the structural damage.

The MAC-value between two eigenvectors ϕ and ϕ_j was defined as

$$MAC(\phi_i, \phi_j) = \frac{|\phi_i^T \phi_j|^2}{\phi_i^T \phi_i \phi_j^T \phi_j} \quad (2.10)$$

The MAC-values express the correlation between two sets of estimates for the same mode shape. A value equal to 1 indicates a full correlation.

Rizos *et al* [44] considered the transverse vibration of an uncracked beam with an open crack. The beam was divided into two standard slender beams by the crack. The compatibility condition between the two sections was derived based on the crack strain energy function. The result was a system of equations for the frequencies and mode shapes in terms of crack length and location. To determine the crack length and position, the beam was excited at a natural frequency, and vibration amplitudes were measured only at two locations.

Fox [45] used “Node line MAC”, which was based on the measurement points close to a node point for a particular mode, to detect the crack and found it to be a more sensitive indicator of changes in mode shape caused by damage. Graphical comparison of relative changes in mode shapes proved to be the best method for detecting the damage position when only resonant frequencies and mode shapes were examined. A simple method of correlating nodal points (of modes) with the corresponding peak amplitude locations was shown to locate the damage.

Liewen and Ewins [46] suggested the so-called coordinate modal assurance criteria (COMAC), as an improvement of the MAC-factor, to detect the damage. The COMAC for point i of the beam, between two sets of mode shapes ϕ^A and ϕ^B , is defined as

$$COMAC(i) = \frac{\left[\sum_{j=1}^N |\phi_{i,j}^A \phi_{i,j}^B| \right]^2}{\sum_{j=1}^N (\phi_{i,j}^A)^2 \sum_{j=1}^N (\phi_{i,j}^B)^2} \quad (2.11)$$

where N is the number mode shapes. Thus, the COMAC compares the two sets of mode shapes in a point-wise manner.

Ko *et al* [47] used a combination of MAC, COMAC and sensitivity analysis to detect the damage in steel framed structures. The sensitivities of the calculated mode shapes to particular damage were computed to determine which DOF were the most relevant and then were used in COMAC. Mode pairs that were used in COMAC were selected by the analyses of MAC. Results from COMAC were used to identify the damage.

Kam and Lee [48] presented an analytical formulation for locating a crack and quantifying its size from the changes in the vibration frequencies and mode shapes. The first-order Taylor expansion of the modal parameters in terms of the element parameters was used for formulations. The reduced stiffness was used to locate the crack. The crack length was then determined by considering the change in strain energy due to the presence of the crack. Salawu and Williams [12, 49] compared the results of using mode shape relative change and mode shape curvature change to detect damage and pointed out that the most important factor was the selection of the modes used in the analysis.

Cornwell *et al* [50] presented a strain energy method for plate-like structures. The method only required the mode shapes of the structure before and after damage. The authors pointed that the algorithm was effective in locating areas with stiffness reductions as low as 10% using relatively few modes.

2.2.3 Strain and Curvature Mode Shape Changes

Quite a few researchers have used the changes of strain or curvature to detect cracks. The changes were found to be local and sensitive to cracks and also convenient to measure. For beams the strain and curvature at a point are related by

$$\varepsilon = \frac{y}{\rho} = \kappa y \quad (2.12)$$

where ε is the strain, ρ the radius of curvature, and κ the curvature, at the point under consideration.

Pandey *et al* [11] computed the changes in curvature mode shape in a beam by FEM and reported that the curvature change was a good damage indicator. The curvature values were computed from the displacement mode shape using the central difference approximation for mode i and degree of freedom q

$$\phi_{q,i}^{\cdot} = \frac{\phi_{q-1,i} - 2\phi_{q,i} + \phi_{q+1,i}}{h^2} \quad (2.13)$$

where h was the length of each of the two elements between the DOF $(q-1)$ and $(q+1)$.

Stubbs *et al* [51] calculated the change in modal strain energy defined by the curvature of measured mode shapes. For a linear elastic beam, the damage indicator for the p^{th} element could be written as

$$\beta_p = \left(\sum_{i=1}^n u_{ip}^d \right) / \left[\sum_{i=1}^n u_{ip}^2 \right] \quad (2.14)$$

where the u_{φ} terms were measures of the experimentally determined fractional strain energy for mode i between the endpoints of element p , denoted by a and b . The superscripts d and u indicate the damaged and undamaged specimens. For a Bernoulli-Euler beam, the fractional strain energies of undamaged and damaged beam were expressed by authors as

$$u_{\varphi}^u = \frac{\left(\int_a^b [\{\phi^u(x)\}_i]^2 dx + \int_0^a [\{\phi^u(x)\}_i]^2 dx \right)}{\left(\int_0^a [\{\phi^u(x)\}_i]^2 dx \right)}$$

$$u_{\varphi}^d = \frac{\left(\int_a^b [\{\phi^d(x)\}_i]^2 dx + \int_0^a [\{\phi^d(x)\}_i]^2 dx \right)}{\left(\int_0^a [\{\phi^d(x)\}_i]^2 dx \right)} \quad (2.15)$$

The value of β_p with the largest magnitude would indicate the member p which had the probable damaged section.

Swamidias and Chen [52] analyzed the changes of strain FRFs to detect the crack in a tripod tower platform. Artificial saw cuts were made to simulate the crack. At each cut the strains, accelerations and displacements were measured and the transfer functions were computed. The governing equation used in their study was given by

$$(-\omega^2[G] + [H])\{\varepsilon(\omega)\} = \{F(\omega)\} \quad (2.16)$$

A theoretical expression of the strain responses was given as

$$\varepsilon = [\phi^e][\Lambda]^{-1}[\varphi]\{F\} = [H^e]\{F\} \quad (2.17)$$

where $[H^e]$ was the strain transfer function, ϕ^e the strain mode shape, φ the displacement mode shape, and $[\Lambda] = (-\omega^2[M_r] + [K_r])^{-1}$. The authors demonstrated that

the strain transfer function changed by around 60% when the crack grew through the thickness, while acceleration and displacement transfer functions were not influenced much by the crack development and growth.

Chance *et al* [53] found that numerically calculated curvature from mode shapes resulted in unacceptable errors. They used measured strains instead to denote curvature directly, which dramatically improved results. Nwosu *et al* [54] evaluated strain changes generated by the presence of a crack in a tubular T-joint. They found these changes to be much greater than frequency shifts and were measurable even at a relatively large distance from the crack.

2.2.4 Flexibility Changes

The flexibility matrix is the inverse of the static stiffness matrix for a structure. The flexibility matrix relates the applied static force and resulting structural displacement as

$$\{u\} = [A]\{F\} \quad (2.18)$$

where $[A]$ is the flexibility matrix, in which each column represents the displacement pattern of structure associated with a unit force applied at the associated DOF.

The structural vibration responses can be expressed in flexibility matrix format as

$$[A][M]\{\ddot{u}\} + \{u\} = [A]\{F\} \quad (2.19)$$

Using the normalized displacement mode shapes $[\Phi]$ and natural frequencies $[\Omega]$, the flexibility matrix is given by

$$[A] = [\Phi][\Omega]^{-1}[\Phi]^T \quad (2.20)$$

Generally only the first few modes of the structure, typically the lowest-frequency modes, are measured; so the above formulation is approximate. The synthesis of the complete static flexibility matrix would require the measurement of all mode shapes and frequencies.

In principle, the damage is detected using the flexibility matrix by comparing the flexibility matrix obtained from the damaged structure to the flexibility matrix obtained from the undamaged structure. It is obvious that the stiffness matrix could also be used to detect damage in a similar manner. From the above equation, it can be seen that the flexibility has an inverse relationship to the square of the frequencies; therefore, the measured flexibility matrix is more sensitive to changes in the lower frequency modes of the structure.

Pandey and Biswas [55] detected and located the damage by using changes in flexibility of the structure. Their numerical and experimental results showed that proper estimates of the damage condition and the location of damage could be obtained from just the first two measured modes of the structure.

Toksoy and Aktan [56] computed the measured flexibility of a bridge and examined the cross-sectional deflection profiles. They found that anomalies in the deflection profile can identify the damage even without a baseline data set.

Mayes [57] measured flexibility from the results of a modal test on a bridge to locate the damage. Zhang and Aktan [58] used the uniform load flexibility to calculate the curvature of the uniform load surface which was appropriate to identify the damage from the author's view. The uniform load flexibility matrix was constructed by summing the columns of the measured flexibility matrix.

2.2.5 Matrix Update Method

The presence of crack in a structure would change structural modal matrices consisting of mass, stiffness and damping contributions. In this method, the updated matrix is obtained by modifying the original modal matrix to reproduce as closely as possible the measured static or dynamic response from the data. The crack is detected by comparing the updated matrix to the original correlated matrix. To solve for the updated matrix, a constrained optimization problem is usually developed based on the structural equations of motion, the nominal model and the measured data.

The structural equations of motion of an undamaged structure for a n -DOF system are given as [2]

$$[M^u]\ddot{x} + [C^u]\dot{x} + [K^u]x = \{f(t)\} \quad (2.21)$$

The eigenvalue equation for the above equation is given by

$$((\lambda_i^u)^2 [M^u] + (\lambda_i^u) [C^u] + [K^u])\{\phi^u\}_i = \{0\} \quad (2.22)$$

where λ_i^u and $\{\phi^u\}_i$ are the i^{th} eigenvalue and eigenvector of the undamaged structure.

Let λ_i^d and $\{\phi^d\}_i$ stand for the eigenvalues and eigenvectors corresponding to the damaged structure. Substituting these quantities into the above eigenvalue equation will give

$$((\lambda_i^d)^2 [M^d] + (\lambda_i^d) [C^d] + [K^d])\{\phi^d\}_i = \{E\}_i \quad (2.23)$$

where $\{E\}_i$ is defined as the modal force error, or residual force, for the i^{th} mode of the damaged structure. This vector represents the harmonic force excitation that would have to be applied to the undamaged structure represented by $[M^u]$, $[C^u]$ and $[K^u]$ at the frequency of λ_i^d so that the structure would respond with mode shape $\{\phi^d\}_i$. For the damaged structure, the eigenvalue equation can be expressed as

$$((\lambda_i^d)^2 [M^d] + (\lambda_i^d) [C^d] + [K^d])\{\phi^d\}_i = \{0\} \quad (2.24)$$

where the damaged modal matrices are defined as the modal matrices of the undamaged structure minus a perturbation

$$\begin{aligned} [M^d] &= [M^u] - [\Delta M] \\ [C^d] &= [C^u] - [\Delta C] \\ [K^d] &= [K^u] - [\Delta K] \end{aligned} \quad (2.25)$$

Substituting the above equation into the eigenvalue equation for the damaged structure yields

$$((\lambda_r^d)^2 [M^* - \Delta M] + (\lambda_r^d) [C^* - \Delta C] + [K^* - \Delta K]) \{\phi^d\}, = \{0\} \quad (2.26)$$

Moving the perturbation terms to the right side of the equation then yields

$$((\lambda_r^d)^2 [M^*] + (\lambda_r^d) [C^*] + [K^*]) \{\phi^d\}, = ((\lambda_r^d)^2 [\Delta M] + (\lambda_r^d) [\Delta C] + [\Delta K]) \{\phi^d\}, \quad (2.27)$$

The left side of this equation consists of known quantities and has previously been defined as the modal force error. Thus we have

$$((\lambda_r^d)^2 [\Delta M] + (\lambda_r^d) [\Delta C] + [\Delta K]) \{\phi^d\}, = \{E\}, \quad (2.28)$$

The above equation is the basis for solving the modal matrix for damaged structure.

Liu [59] used the optimal update technique to identify the damage in a truss structure. The author reported that if sufficient modal data are available, the elemental properties could be directly computed using the measured modal frequencies and measured mode shapes. The method is used to locate the damaged member of a truss structure, using the first four measured modes.

Kim and Bartkowicz [60] demonstrated the damage detection capabilities of the matrix update method for a three dimensional truss structure. The numerical and experimental results showed that the number of sensors is the most critical parameter for damage detection, followed by the number of the measured modes.

Doebling *et al* [61] presented a method of selecting vibration modes for finite element model update. The modes were selected using the maximum strain energy stored in the damaged structural configuration. The authors pointed that these modes provided more information about changes in the structural load paths resulting from damage. However,

this procedure required accurate identification and mass normalization of the damaged structure's mode shapes.

2.2.6 Nonlinear Method

Shen and Chu [20] used a bilinear crack model (Figure 2.5) to deal with the fatigue crack postulated to open when the normal strain near the crack tip was positive, and to be closed otherwise. The stress, strain and displacement distributions were assumed in the cracked beam, considering the crack contact effect. Using a variational theorem, they obtained the equations of motion and associated boundary conditions for the vibration of a uniform beam containing one fatigue crack. A bilinear equation of motion for each vibration mode of a simply supported beam was formulated using a Galerkin's procedure. The dynamic response of the bilinear equation under a concentrated forcing excitation was calculated through a numerical analysis. A clear nonlinear behavior was found on time history and frequency spectrum for each vibration mode. The authors pointed out that the change in the dynamic behavior could be used to deduce the size and location of the crack. However, the authors do not describe the details of how to consider the effects of crack closing in the numerical analysis.

Chu and Shen [21] used two square wave functions to model stiffness change and proposed a new closed-form solution for bilinear oscillators under low-frequency excitation. The equation of motion was given by

$$\ddot{u} + [\omega_1^2 \phi_1(t) + \omega_2^2 \phi_2(t)]u = 0 \quad (2.29)$$

where ω_1 and ω_2 were frequencies corresponding to two stiffnesses (one for crack opening and one for crack closing), and $\phi_1(t)$ and $\phi_2(t)$ were two square wave functions which were defined by (see Figure 2.6)

$$\phi_1(t) = \begin{cases} 1 & \text{for } u > 0 \\ 0 & \text{for } u < 0 \end{cases} \quad (2.30)$$

and

$$\phi_2(t) = 1 - \phi_1(t) \quad (2.31)$$

The proposed solution provided the spectral pattern and the magnitude of each harmonic component for a damaged rectangular beam according to the size and location of the crack. The authors suggested that this procedure was a possible crack detection approach considering the spectral response under low frequency harmonic excitation.

Collins, Plaut and Wauer [62] used the bilinear model to consider the crack closing and opening in a shaft due to its rotation. The crack was assumed to be open when the elongation of the all the points on the crack face was positive. Otherwise, the crack was considered closed. Six coupled equations were obtained for the rotating circular shaft with simply supported ends. Galerkin's method was used with a two-term approximation for each of the six displacements which resulted in twelve second-order ordinary differential equations. Then the twelve equations were solved numerically by the Adams–Moulton technique. Time histories and frequency spectra were compared for shafts without and with a crack for which the crack depth was one-fifth of the shaft diameter. The responses to a single axial impulse and periodic axial impulses were also determined.

The procedure appeared to provide an effective means for detecting cracks in rotating shafts.

Friswell and Penny [63] presented an equivalent one degree of freedom nonlinear model of a cracked beam vibrating in its first mode. The variance of the stiffness due to the crack closing and opening was determined by analysis of vibrational time domain signals. The crack closing or opening depended on the sign of the curvature of the beam at the crack location. Analysis of the frequency response function for the beam vibration, under impact and sinusoidal excitations, showed that it was not possible to detect the two values of effective stiffness.

Abraham and Brandon [64] used the time varying connection matrices representing the interaction forces at crack surfaces to consider the crack opening and closing. The crack became the boundaries of sub-intervals over which linear equations governed the general motion of the system. A Timoshenko beam under transverse and longitudinal vibrations was investigated. The authors assumed that the system was under steady state motion and the connection matrices were periodic functions with respect to time. Thus the connection matrices alternated between two values, corresponding to the cases when the crack was open and when it was closed (intact beam). Then the connection matrices were expressed by Fourier series. The solution was obtained by truncating the Fourier series, which gave approximate results.

Krawczuk and Ostachowicz [22] presented a discrete-continuous model of transverse vibrations of a beam with a closing crack. The local stiffness at the position of the crack was calculated on the basis of fracture mechanics concepts. In order to take into account the crack opening and closing, the authors used the assumption that the depth of the crack was subjected to variations in time according to the following relationship (Figure 2.7)

$$\begin{aligned} a(t) &= a_0 [1 - \sin(\Omega t)], & \text{for } t \in (0, T_v / 2) \\ a(t) &= a_0, & \text{for } t \in (T_v / 2, T) \end{aligned} \quad (2.32)$$

where Ω is the vibration frequency of the beam and $T_v = 2\pi/\Omega$ is the period of beam's vibration. Due to the crack opening and closing which resulted in variations of the stiffness or flexibility in the plane of the crack, the authors used small time intervals of vibration equations in which the stiffness could be assumed to be constant. Using the results in one interval as the initial conditions for next interval, the procedure of solving the open crack vibration in a beam could then be used to solve the problem.

2.2.7 Neural Network Method

Neural network methods have been developed only during the recent years. They aim at locating and sizing the damage in complex structures. The most popular method used is the multi-layer perception concept (MLP) trained by back propagation, which is usually called the backprop neural network. Figure 2.8 shows a typical two-layer back-propagation network.

Neural networks are computational models inspired by the neuron architecture and operation of the human brain. They were developed to mimic the pattern recognition capabilities of the human brain. The strength of neural network solutions lies in their pattern recognition capabilities. A neural network is an assembly of a large number of highly connected processing units, the so-called nodes or neurons. The neural networks are capable of self-organization and knowledge acquisition. Neural networks “learn” from examples and exhibit some structural capability for generalization. Training consists of providing a set of known input-output patterns to the network. The outputs of one layer (nodes) are multiplied by the weights, and summed, and shifted by a bias. Then they are used as inputs to the next layer. The network iteratively adjusts the weights and bias by minimizing the error between the predicted and measured outputs so as to obtain the desired outputs with a requested level of accuracy.

Kudva *et al* [65] used a backprop neural network to detect the damage in a stiffened plate with a 4x4 array of bays. The damage was modeled by cutting holes of various diameters in the plate at the center of the bays. A static uniaxial load was applied to the structure, and the strain gauge readings were taken from elements in the bays. The neural network was used to identify the map from the strain gauge data to the location and size of the hole. The structure of the network was chosen to be two hidden layers, each with the same number of hidden nodes as the number of inputs. The network was trained with 3, 12, or 32 patterns. The authors found that the above neural network was able to predict the location of the damaged bay without an error, but there were errors of 50%, more or less, on the prediction of the hole size.

Leath and Zimmerman [66] used an MLP neural network, based on a training algorithm, to identify the damage in a four-element cantilevered beam. The training algorithm was designed to fit the data with a minimal number hidden nodes. The damage in the beam was modeled by reducing Young's modulus up to 95%. The neural network was used to identify the map from the first two bending frequencies to the level of damage in each member. The algorithm was able to identify the damage with a maximum error of 35%.

Szwczyk and Hajela [67] used a counter-propagation neural network to detect damage in a truss structure. The counter-propagation network builds what is essentially an adaptive look-up table from the data. The advantages of the counter-propagation network are that the body of data does not have to be cycled through more than once. The disadvantage of this network is that it may take a very large number of training points to adequately sample the desired function. In this study, the damage was modeled by reducing Young's modulus in the truss members up to 100%. The error of verification was about 30%.

2.3 Summary

Several models have been developed for "always open" cracks, viz., (i) A short beam model that uses a short beam element with reduced bending stiffness at the position of the crack to represent the presence of a crack, and whose application, in many cases, leads to an analytical solution or to a simple finite element analytical procedure; but this model does not take into account the ineffective material and local deformations in the vicinity

of the crack; (ii) The reduced Young's modulus and moment of inertia model that assumes a change in Young's modulus or a removal of a local portion of the structure so as to represent the presence of a crack; but the complex stress/strain distribution around the tip of crack is not considered in this model; and (iii) The fracture mechanics model that computes the local flexibility/stiffness terms using the concepts of fracture mechanics. The decrease in the magnitude of the terms of the stiffness matrix reflects the presence of the crack; the model has been mainly applied to beams or truss structures, and the structure is divided into substructures by the crack. The crack is modelled into a bending or torsional spring which connects substructures; however, the actual beam stiffness is continuous and the model does not consider stress relief at crack surfaces.

For crack opening and closing, only a few studies have been carried out, in which nonlinear crack models have been developed. The bilinear oscillator is the mainly used one. In this model, the beam is assumed to have two characteristic stiffnesses, one having a larger value when crack is closed and the other having a smaller value when the crack is open. The crack is assumed fully open and fully closed, alternatively. The instant of crack opening or closing is determined by parameters such as the stress/strain discontinuity at the location of the crack.

Based on the above models, several crack detection methods have been developed. They include methods based on frequency changes, mode shape changes, strain/curvature mode shape changes, flexibility changes, matrix updates and neural network. The frequency change method uses the changes of natural frequency of structures to identify

the crack. The natural frequency is a global parameter in structural vibration, and is easy to obtain from measurements. However, the changes of frequencies will be small if the crack is not big enough. This would make the detection a bit difficult. The mode shape changes method uses the changes of mode shapes to detect the crack. This method is sensitive to the crack due to the local derivative changes of mode shapes at the position of a crack. However, the instrumentation required and the duration of the measurement session will increase considerably if a detailed mode shape has to be estimated. Strain mode shape and curvature mode shape changes methods are similar to the mode shape change method; but they use more sensitive parameters such as curvature, strain and stress. Other crack detection methods are generally based on the measurement of frequencies and mode shapes.

To model the crack better, this study will develop a continuous beam analysis approach, which considers the continuous stiffness and stress/energy relief close to the crack surfaces. Due to the complex distribution of stresses and plastic deformation around the crack tip, it is difficult to analyze the vibration of a cracked structure by the use of stress functions. Energy method is exclusively applied in general vibration analysis to derive the equations of motion. Energy approach in fracture mechanics provides an easy way to calculate energy release of a cracked structure, and would become an effective tool for the development of the model. Crack detection will be investigated in this study for developing better procedures for crack size and location identification.

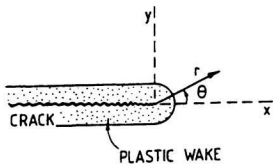


Figure 2.1 Schematic of Crack Closure

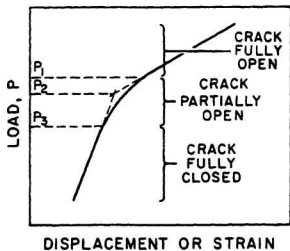


Figure 2.2 Crack Opening and Closing (Newman [68], Backlund [69])

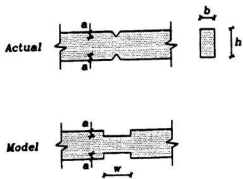


Figure 2.3 Short Beam Model

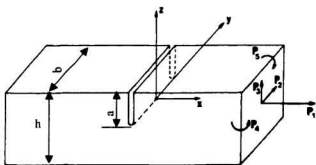


Figure 2.4 Beam element with a transverse crack under applied forces

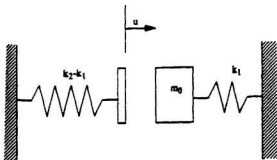


Figure 2.5 Bilinear oscillator

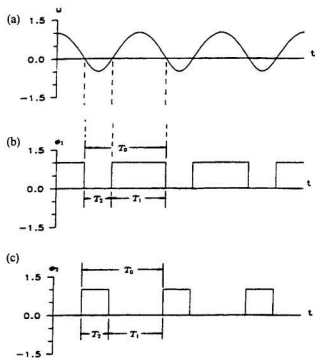


Figure 2.6 (a) Free vibration of a bilinear oscillator;(b) Periodic square wave function ϕ_1 ; (c) Periodic square wave function ϕ_2 .

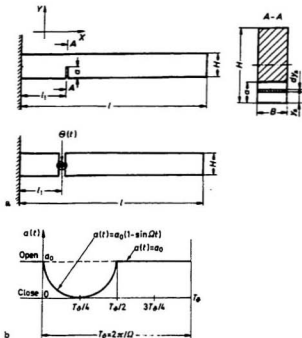


Figure 2.7 a. Discrete-continuous model of cantilever beam with crack; b. model of depth changes of crack as a time function.

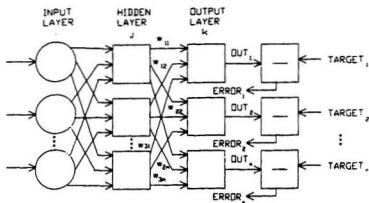


Figure 2.8 Two layer back propagation network

Chapter 3

Basic Theory

3.1 Introduction

In dealing with any problem related to vibration and diagnostics, basic equations of motion are formulated by considering the dynamic equilibrium or total energy of the system, and equations are solved in time, frequency or Laplace domain; in this study, Laplace and frequency domains are considered. For cracked beams considered in this study, the results obtained earlier for uncracked beams are used in the dynamic analysis, considering both the bending and torsional vibrations of the beam. Differential equations of motion for cracked beams are quite complicated and often do not have exact analytical solutions. The Galerkin's method is therefore utilized to solve such equations. Since the structure is cracked, fracture mechanics principles are utilized to formulate the problem. Knowledge of stress and energy determination in cracked structures would be a necessary prerequisite to model cracks in vibration analysis. For forced vibration of cracked beams, modal analysis is carried out. The basic theoretical results, used for the above-mentioned studies, are given in this chapter to give a better insight into the reading of the subsequent chapters.

3.2 Vibration of Beams

3.2.1 Bending Vibration

Transverse vibrations of beams, in which shear deformation and rotary inertia are taken into account, are included in the study. Shear deformation effects are substantial for shorter beams. In such a case, the slope of the beam is not merely equal to the bending rotation of the cross section, but also includes distortion due to shear. Therefore, the problem needs to be described by two variables. Consider the element of a beam of length dx shown in Figure 3.1. If w is the displacement of the centerline of the beam, $\frac{\partial w}{\partial x}$ the total slope, ψ the slope due to bending, the slope due to shear will be [70]

$$\beta = \frac{\partial w}{\partial x} - \psi \quad (3.1)$$

The relation between the shear force and shear deformation is given by

$$Q = k'GA\beta = k'GA\left(-\psi + \frac{\partial w}{\partial x}\right) \quad (3.2)$$

where G is the shear modulus, A is area of the cross section and k' is a numerical factor depending on the shape of the cross section, being $5/6$ for a rectangular cross section, and $9/10$ for a circular section. The relationship between the bending moment and the bending deformation is given by

$$M = EI \frac{\partial \psi}{\partial x} \quad (3.3)$$

where EI is bending stiffness of the beam. Newton's law for transverse and rotational motion yields

$$m\ddot{w} = \frac{\partial Q}{\partial x} + f(x,t) \quad (3.4)$$

$$J\ddot{\psi} = \frac{\partial M}{\partial x} + Q \quad (3.5)$$

where Q is the transverse shear force acting on the element, $f(x,t)$ is the distributed dynamic load on the beam, m is the mass per unit length, and J is the mass moment of inertia.

$$J = \frac{m}{A} I = r^2 m \quad (3.6)$$

in which r is the radius of gyration about the neutral axis. Substitution of equations (3.2) and (3.3) into equations (3.4) and (3.5) yields

$$\begin{aligned} \frac{\partial}{\partial x} \left[k'GA \left(\frac{\partial w}{\partial x} - \psi \right) \right] - m \frac{\partial^2 w}{\partial t^2} + f(x,t) &= 0 \\ \frac{\partial}{\partial x} \left(EI \frac{\partial \psi}{\partial x} \right) + k'GA \left(\frac{\partial w}{\partial x} - \psi \right) - r^2 m \frac{\partial^2 \psi}{\partial t^2} &= 0 \end{aligned} \quad (3.7)$$

Eliminating ψ , for a constant cross section, equation (3.7) will result in

$$EI \frac{\partial^4 w}{\partial x^4} - (r^2 m + \frac{mEI}{k'GA}) \frac{\partial^4 w}{\partial x^2 \partial t^2} + m \frac{\partial^2 w}{\partial t^2} + \frac{r^2 m^2}{k'GA} \frac{\partial^4 w}{\partial t^4} + f + \frac{r^2 m}{k'GA} \frac{\partial^2 f}{\partial t^2} - \frac{EI}{k'GA} \frac{\partial^2 f}{\partial x^2} = 0 \quad (3.8)$$

If shear deformation and rotary inertia are neglected, free bending vibration [without any applied forces, viz., $f(x,t)=0$] for a beam can be obtained from the equation (3.8) as

$$-EI \frac{\partial^4 w}{\partial x^4} = m \frac{\partial^2 w}{\partial t^2} \quad (3.9)$$

The solution for the above equation (3.9) is assumed as

$$w = W(x)e^{i\omega t} \quad (3.10)$$

Substitution of equation (3.10) into (3.9) yields

$$EI \frac{d^4 W}{dx^4} - m\omega^2 W = 0 \quad (3.11)$$

The solution for equation (3.11) is given by

$$W = C_1 \cosh(kx) + C_2 \sinh(kx) + C_3 \cos(kx) + C_4 \sin(kx) \quad (3.12)$$

where $k = \left(\frac{\omega}{\sqrt{EI/m}} \right)^{\frac{1}{2}}$ and C_1, C_2, C_3 and C_4 are undetermined constants. These

constants are determined by the use of boundary conditions. For bending vibration of single span beams, four boundary conditions are used for solving the equation (3.12), which yield four algebraic equations in terms of C_1, C_2, C_3 and C_4 . The condition for the existence of a solution for these algebraic equations is that the determinant of these equations be zero. This gives the frequency equation for the determination of frequency ω . Three cases can be considered for the solution, viz., (i) both ends simply supported; (ii) both ends fixed; and (iii) both ends freely moving in space.

(i) For a simply supported beam with length l , the four boundary conditions are:

$$\begin{aligned} W(0) = W(l) = 0 \\ \left(\frac{d^2 W}{dx^2} \right)_{x=0} = \left(\frac{d^2 W}{dx^2} \right)_{x=l} = 0 \end{aligned} \quad (3.13)$$

After the application of the boundary conditions, the frequency equation is obtained as

$$\sin(kl) = 0 \quad (3.14)$$

The mode shape is given by

$$W = \sin(kx) \quad (3.15)$$

(ii) For a fixed-fixed beam, boundary conditions are:

$$\begin{aligned} W(0) = W(l) = 0 \\ \left(\frac{dW}{dx}\right)_{x=0} = \left(\frac{dW}{dx}\right)_{x=l} = 0 \end{aligned} \quad (3.16)$$

Frequency equation is obtained as

$$1 - \cosh(kl)\cos(kl) = 0 \quad (3.17)$$

The mode shape is given by

$$W = \sin(kx) - \sinh(kx) + \frac{\cos(kl) - \cosh(kl)}{\sin(kl) + \sinh(kl)} [\cos(kx) - \cosh(kx)] \quad (3.18)$$

(iii) For a free-free beam, boundary conditions are

$$\begin{aligned} \left(\frac{d^2W}{dx^2}\right)_{x=0} = \left(\frac{d^2W}{dx^2}\right)_{x=l} = 0 \\ \left(\frac{d^3W}{dx^3}\right)_{x=0} = \left(\frac{d^3W}{dx^3}\right)_{x=l} = 0 \end{aligned} \quad (3.19)$$

Frequency equation is obtained as

$$(kl)^2 [1 - \cosh(kl)\cos(kl)] = 0 \quad (3.20)$$

and the mode shape is given by

$$W = \sin(kx) + \sinh(kx) + \frac{\cos(kl) - \cosh(kl)}{\sin(kl) + \sinh(kl)} [\cos(kx) + \cosh(kx)] \quad (3.21)$$

Discussions on the solutions of equation (3.8) are deferred till Chapter Six, wherein a detailed solution procedure is given for cracked beams considering transverse shear deformation and rotary inertia.

3.2.2 Torsional Vibration

For the general beam such as a rectangular beam, the cross section would not remain plane after deformation under torsion. The cross section would undergo warping which generates an axial displacement. Figure 3.2 shows the displacements of a point P , located on the body, in y and z directions due to rotation as well as the displacement in x direction due to warping and rotation. The warping function is denoted by $\phi(y, z)$ and rotation is denoted by θ , then displacements are given as [71]

$$\begin{aligned} u &= \phi \frac{\partial \theta}{\partial x} \\ v &= -z\theta \\ w &= y\theta \end{aligned} \quad (3.22)$$

Neglecting the axial strain ϵ_x , the shear strains are obtained as

$$\begin{aligned} \gamma_{xy} &= \left(\frac{\partial \phi}{\partial y} - z \right) \frac{\partial \theta}{\partial x} \\ \gamma_{xz} &= \left(\frac{\partial \phi}{\partial z} + y \right) \frac{\partial \theta}{\partial x} \end{aligned} \quad (3.23)$$

The shear stresses are given by

$$\begin{aligned}\tau_{xy} &= G\left(\frac{\partial\phi}{\partial y} - z\right)\frac{\partial\theta}{\partial x} \\ \tau_{xz} &= G\left(\frac{\partial\phi}{\partial z} + y\right)\frac{\partial\theta}{\partial x}\end{aligned}\quad (3.24)$$

where G is the material shear modulus. The potential energy is obtained as

$$U = \frac{1}{2} \int_0^l \int_A G \left[\left(\frac{\partial\phi}{\partial y} - z \right)^2 + \left(\frac{\partial\phi}{\partial z} + y \right)^2 \right] \left(\frac{\partial\theta}{\partial x} \right)^2 dA dx = \frac{1}{2} \int_0^l G I_n \left(\frac{\partial\theta}{\partial x} \right)^2 dx \quad (3.25)$$

where l is the length of the beam, and A is the area of the cross section. From the above equation, the torsional rigidity could be expressed as

$$G I_n = G \int_A \left[\left(\frac{\partial\phi}{\partial y} - z \right)^2 + \left(\frac{\partial\phi}{\partial z} + y \right)^2 \right] dA \quad (3.26)$$

The differential equation for torsional vibration could be obtained as

$$G I_n \frac{\partial^2\theta}{\partial x^2} - \rho I_p \frac{\partial^2\theta}{\partial t^2} = 0 \quad (3.27)$$

where I_p is the polar moment of inertia and ρ is material density.

For a circular beam warping could be neglected, i.e., $\phi(y, z) = 0$ and $I_n = I_p$; then one obtains the torsional vibration equation for a solid cylindrical body as

$$G \frac{\partial^2\theta}{\partial x^2} = \rho \frac{\partial^2\theta}{\partial t^2} \quad (3.28)$$

The solution for the above equation is assumed as

$$\theta = \Theta(x)e^{i\omega t} \quad (3.29)$$

Substitution of equation (3.29) into (3.28) yields

$$G \frac{d^2 \Theta}{dx^2} + \rho \omega^2 \Theta = 0 \quad (3.30)$$

The above equation has the following solution

$$\Theta = C_1 \cos\left(\sqrt{\frac{\rho}{G}} \alpha x\right) + C_2 \sin\left(\sqrt{\frac{\rho}{G}} \alpha x\right) \quad (3.31)$$

where C_1 and C_2 are undetermined constants. Application of boundary conditions to equation (3.31) will yield two algebraic equations for C_1 and C_2 . The condition for existence of a solution for the algebraic equations is that its coefficient determinant is zero. This will give a frequency equation which determines natural frequencies. Two cases are considered, viz., (i) both ends fixed; and (ii) both ends free.

(i) For a fixed-fixed beam with length l , boundary conditions are

$$\Theta(0) = \Theta(l) = 0 \quad (3.32)$$

Frequency equation is obtained as

$$\sin\left(\sqrt{\frac{\rho}{G}} \alpha l\right) = 0 \quad (3.33)$$

The mode shape is given by

$$\Theta = \sin\left(\sqrt{\frac{\rho}{G}} \alpha x\right) \quad (3.34)$$

(ii) For a free-free or simply supported beam, boundary conditions are

$$\left(\frac{\partial \Theta}{\partial x}\right)_{x=0} = \left(\frac{\partial \Theta}{\partial x}\right)_{x=l} = 0 \quad (3.35)$$

Frequency equation is obtained as

$$\sqrt{\frac{\rho}{G}} \omega \sin\left(\sqrt{\frac{\rho}{G}} \omega l\right) = 0 \quad (3.36)$$

The mode shape is given by

$$\Theta = \cos\left(\sqrt{\frac{\rho}{G}} \omega x\right) \quad (3.37)$$

Discussions on the solution of equation (3.27) are deferred till Chapter Five, wherein the coupled torsional-bending vibration of a cracked beam is discussed in great details.

3.3 Galerkin's Method

Galerkin's method is the most widely used one of the various weighted residual methods, which works directly with a differential equation. It achieves the best approximation by minimizing the error in satisfying a differential equation over the system. For the beam vibration, the differential equation could be written as

$$LW(x) = \lambda \mu(x)W(x) \quad (3.38)$$

where L is a differential operator of order 2 or 4. For the transverse vibration of a beam,

$LW(x) = EI \frac{d^4 W}{dx^4}$, $\mu(x) = \rho A$, λ is eigenvalue, ρ is material density, A is area of the cross-section, and EI is bending stiffness. The solution $W(x)$ is subject to given boundary

conditions. The assumption is that the problem does not have a close-form solution, so that one can consider an approximate solution in the form

$$W(x) \equiv W^{(n)}(x) = \sum_{j=1}^n C_j W_j(x) \quad (3.39)$$

where W_j are called independent trial functions chosen from a set of functions satisfying the boundary conditions. Because $W^{(n)}(x)$ does not satisfy the equation (3.38), there is an error at every point. This error is called the residual which could be expressed as

$$R = LW^{(n)} - \lambda^{(n)} \mu W^{(n)} \quad (3.40)$$

To reduce the error to the largest extent possible, the coefficients C_j in equation (3.39) are sought such that these values would make the following integral to be zero, i.e.,

$$\int_0^l W_i R dx = \int_0^l W_i (LW^{(n)} - \lambda^{(n)} \mu W^{(n)}) dx = 0 \quad (3.41)$$

Substituting equation (3.39) into the above equation, one obtains

$$\int_0^l W_i \left(\sum_{j=1}^n C_j L W_j - \lambda^{(n)} \sum_{j=1}^n C_j \mu W_j \right) dx = \sum_{j=1}^n (k_{ij} - \lambda^{(n)} m_{ij}) C_j = 0 \quad (3.42)$$

or in matrix format

$$[K]\{C\} = \lambda^{(n)}[M]\{C\} \quad (3.43)$$

where

$$k_{ij} = \int_0^l W_i L W_j dx \quad (3.44)$$

$$m_{ij} = \int_0^l W_i \mu W_j dx \quad (3.45)$$

are constant coefficients. Equation (3.42) will consist of n linear equations in C_1, C_2, \dots, C_n . For the existence of the solution, the determinant of the coefficient matrix should be zero. This will yield the natural frequencies and, subsequently, the vibration modes.

From equation (3.41), we can see that when the number of trial functions $W_j(x)$ approaches infinity, the only manner in which the integral could be zero is that the residual itself is zero, i.e.,

$$\lim_{n \rightarrow \infty} R = \lim_{n \rightarrow \infty} (LW^{(n)} - \lambda^{(n)} \mu W^{(n)}) = LW - \lambda \mu W = 0 \quad (3.46)$$

which shows that the solution of the equation (3.41) converges to the solution of the differential equation. After determination of the coefficients C_j , equation (3.39) will become the best solution for the differential equation. Quite often, several properly selected trial functions will give much accurate solution for the problem.

3.4 General Vibration and Modal Analysis

Dynamical characteristics for a structure could be described by a set of vibration modes and natural frequencies; therefore, vibration analyses for the structure, specially that of a complex structure, are usually carried out on discrete models.

Invariably, any structure could be modelled as a multi-degree-of freedom system. The properties of the multi-degrees-of-freedom system are expressed by its mass matrix [M], stiffness matrix [K], damping matrix [C] and the forces {f} that act in the direction of the

various displacement degrees of freedom $\{u\}$. The motion equation for such a system is given by

$$[M]\{\ddot{u}\} + [C]\{\dot{u}\} + [K]\{u\} = \{f\} \quad (3.47)$$

Let $[\Phi]$ be the normal modes of the system. For a linear system,

$$\begin{aligned} [\Phi]^T [M] [\Phi] &= I = \text{diag}[1, 1, \dots, 1] \\ [\Phi]^T [K] [\Phi] &= \text{diag}[\omega_1^2, \omega_2^2, \dots, \omega_n^2] \end{aligned} \quad (3.48)$$

The damping matrix is assumed to be uncoupled according to the following formulation

$$[\Phi]^T [C] [\Phi] = \text{diag}[c_1, c_2, \dots, c_n] \quad (3.49)$$

Equation (3.49) is generally satisfied when the damping is a linear combination of the mass matrix and stiffness of the form:

$$[C] = a[M] + b[K] \quad (3.50)$$

where a and b are real scalar constants, and this type of damping is called proportional damping. For proportional damping or for the case wherein off-diagonal terms in the matrix $[\Phi]^T [C] [\Phi]$ can be neglected, we could set up

$$[\Phi]^T [C] [\Phi] = \text{diag}[2\xi_i \omega_i] \quad (3.51)$$

where

$$\xi_i = a/(2\omega_i) + b\omega_i / 2 \quad (3.52)$$

Then equation (3.47) can be uncoupled with the linear transformation

$$\{u\} = [\Phi]\{q\} \quad (3.53)$$

which gives uncoupled equations of the following form:

$$\ddot{q}_i + 2\xi_i \omega_i \dot{q}_i + \omega_i^2 q_i = [\Phi]^T \{f\} \quad (3.54)$$

For free vibration, one obtains

$$\ddot{q}_i + 2\xi_i \omega_i \dot{q}_i + \omega_i^2 q_i = 0 \quad (3.55)$$

The solution for free vibration could be expressed as

$$q_i = A_i e^{-\xi_i \omega_i t} \sin(\omega_{di} t + \varphi_i) \quad (3.56)$$

$$\omega_{di} = \omega_i (1 - \xi_i^2)^{1/2} \quad (3.57)$$

where A_i and φ_i are constants that are determined by initial conditions. Final response is obtained using the equation $\{u\} = [\Phi] \{q\}$. For forced vibration, given by equation (3.54), wherein the structure undergoes a harmonic motion with frequency ω ,

$$q_i = Q_i e^{j\omega t} \quad (3.58)$$

The excitation function could be written as

$$\{f\} = \{F\} e^{j\omega t} \quad (3.59)$$

Substitution of equations (3.58) and (3.59) into equation (3.54) leads to

$$Q_i = \frac{[\Phi]^T \{F\}}{\omega_i^2 + 2j\xi_i \omega_i \omega - \omega^2} \quad (3.60)$$

Using equation (3.53), the response for forced vibration is given by

$$\begin{aligned} \{u\} &= [\Phi][\omega_i^2 + 2j\xi_i \omega_i \omega - \omega^2]^{-1} [\Phi]^T \{F\} e^{j\omega t} \\ &= [H(j\omega)] \{F\} e^{j\omega t} \end{aligned} \quad (3.61)$$

where

$$[H(j\omega)] = [\Phi][\omega_i^2 + 2j\xi_i \omega_i \omega - \omega^2]^{-1} [\Phi]^T \quad (3.62)$$

is the frequency transfer response function matrix. $H_n(j\omega)$ is the response in degree of freedom r due to a unit harmonic excitation with frequency ω applied in degree of freedom s . From equation (3.62), it can be seen that

$$H_n(j\omega) = \sum_{r=1}^n \frac{\phi_r \phi_r^T}{\omega_r^2 + 2j\zeta_r \omega_r \omega - \omega^2} \quad (3.63)$$

3.5 Basic Fracture Mechanics Theory

Stresses in a cracked structure could be obtained using linear elastic fracture mechanics theory, and could be expressed in terms of complex functions. Using these stresses, the strain energy distribution can numerically be calculated, which will be used in verification of the model developed in next chapter. Energy consideration based on Griffith theory is used to investigate the decrease/increase of strain energy during the crack growth, under different loading conditions [72].

3.5.1 Linear Elastic Stress Analysis for Crack Problems

An analytic function could be constructed as [73]

$$Z(z) = \text{Re } Z + i \text{Im } Z \quad (3.64)$$

where $z = x + iy$ is a complex variable, Re denotes the real part of Z , Im denotes the imaginary part of Z . Use of Cauchy-Riemann conditions gives

$$\begin{aligned}\operatorname{Re} Z' &= \operatorname{Re} \frac{dZ}{dz} = \frac{\partial \operatorname{Re} Z}{\partial x} = \frac{\partial \operatorname{Im} Z}{\partial y} \\ \operatorname{Im} Z' &= \operatorname{Im} \frac{dZ}{dz} = \frac{\partial \operatorname{Im} Z}{\partial x} = -\frac{\partial \operatorname{Re} Z}{\partial y}\end{aligned}\quad (3.65)$$

It can be shown that

$$\nabla^2 \operatorname{Re} Z = \nabla^2 \operatorname{Im} Z = 0 \quad (3.66)$$

Introducing the notation

$$\begin{aligned}\bar{Z} &= \int Z dz = \operatorname{Re} \bar{Z} + i \operatorname{Im} \bar{Z} \\ \bar{\bar{Z}} &= \iint Z dz = \int \bar{Z} dz = \operatorname{Re} \bar{\bar{Z}} + i \operatorname{Im} \bar{\bar{Z}}\end{aligned}\quad (3.67)$$

Westergaard defined an Airy function [74]

$$U = \operatorname{Re} \bar{\bar{Z}} + y \operatorname{Im} \bar{\bar{Z}} \quad (3.68)$$

which would satisfy the bi-harmonic equation for plane stress problems, viz.,

$$\nabla^2 \nabla^2 U = 0 \quad (3.69)$$

The stresses are therefore determined by

$$\sigma_x = \frac{\partial^2 U}{\partial y^2} = \operatorname{Re} Z - y \operatorname{Im} Z' \quad (3.70)$$

$$\sigma_y = \frac{\partial^2 U}{\partial x^2} = \operatorname{Re} Z + y \operatorname{Im} Z' \quad (3.71)$$

$$\tau_{xy} = -\frac{\partial^2 U}{\partial x \partial y} = -y \operatorname{Re} Z' \quad (3.72)$$

For a through crack (length $2a$) in an infinite plate, subjected to uniform equal stress σ in both directions (opening crack mode or Mode I), shown in Figure 3.3, the boundary conditions could be stated as

$$\sigma_x + i\tau_{xy} = 0 \quad \text{for } y=0, -a < x < a \quad (3.73)$$

$$\sigma_x = \sigma_y = \sigma \quad \text{for } x, y \rightarrow \text{infinity} \quad (3.74)$$

It is found that the following function satisfies the boundary conditions described above.

$$Z = \frac{\sigma}{\sqrt{z^2 - a^2}} \quad (3.75)$$

Inserting equation (3.75) into the equations (3.70), (3.71) and (3.72), one obtains stresses for a plane crack problem under uniform stress loading in x and y directions.

$$\sigma_x = \operatorname{Re}\left(\frac{\sigma}{\sqrt{z^2 - a^2}}\right) - y \frac{\partial}{\partial x} \operatorname{Im}\left(\frac{\sigma}{\sqrt{z^2 - a^2}}\right) \quad (3.76)$$

$$\sigma_y = \operatorname{Re}\left(\frac{\sigma}{\sqrt{z^2 - a^2}}\right) + y \frac{\partial}{\partial x} \operatorname{Im}\left(\frac{\sigma}{\sqrt{z^2 - a^2}}\right) \quad (3.77)$$

$$\tau_{xy} = -y \frac{\partial}{\partial x} \operatorname{Re}\left(\frac{\sigma}{\sqrt{z^2 - a^2}}\right) \quad (3.78)$$

The stresses can be calculated numerically for linear elastic fracture using the above equations. It could be seen that the stresses given by the above equations are close to infinity at the crack tips while the real stresses around crack tips would be limited to the yield stress of the material, because the local region become plastic under the applied yield stresses. For stresses of interest, near the crack tip, equations (3.76), (3.77) and (3.78) could be expressed, using polar coordinates, as

$$\sigma_x = \frac{K_I}{\sqrt{2\pi r}} \cos \frac{\theta}{2} \left(1 - \sin \frac{\theta}{2} \sin \frac{3\theta}{2}\right) \quad (3.79)$$

$$\sigma_y = \frac{K_I}{\sqrt{2\pi r}} \cos \frac{\theta}{2} \left(1 + \sin \frac{\theta}{2} \sin \frac{3\theta}{2}\right) \quad (3.80)$$

$$\tau_{xy} = \frac{K_I}{\sqrt{2\pi r}} \cos \frac{\theta}{2} \sin \frac{\theta}{2} \cos \frac{3\theta}{2} \quad (3.81)$$

where

$$K_I = \sigma \sqrt{\pi a} \quad (3.82)$$

is the stress intensity factor for opening mode crack, and θ is the angular coordinate to the point under consideration (see Figure 3.3).

If the plate containing the crack is subjected to the uniform stress in only one (y) direction (perpendicular to the crack), the Airy stress function is selected as

$$U = \operatorname{Re} \bar{Z} + y \operatorname{Im} \bar{Z} + \frac{\sigma}{2}(x^2 - y^2) \quad (3.83)$$

where

$$Z = \frac{\sigma z}{\sqrt{z^2 - a^2}} - \frac{\sigma}{2} \quad (3.84)$$

Stresses will then be

$$\sigma_x = \operatorname{Re} \left(\frac{\sigma z}{\sqrt{z^2 - a^2}} \right) - y \frac{\partial}{\partial x} \operatorname{Im} \left(\frac{\sigma z}{\sqrt{z^2 - a^2}} \right) - \sigma \quad (3.85)$$

$$\sigma_y = \operatorname{Re} \left(\frac{\sigma z}{\sqrt{z^2 - a^2}} \right) + y \frac{\partial}{\partial x} \operatorname{Im} \left(\frac{\sigma z}{\sqrt{z^2 - a^2}} \right) \quad (3.86)$$

$$\tau_{xy} = -y \frac{\partial}{\partial x} \operatorname{Re} \left(\frac{\sigma z}{\sqrt{z^2 - a^2}} \right) \quad (3.87)$$

For mode II (sliding mode) crack, which is subjected to pure shear loading in the plane of x and y , shown in Figure 3.4, the stress function is chosen as

$$U_{II} = -y \operatorname{Re} \bar{Z} \quad (3.88)$$

where

$$Z = \frac{z}{\sqrt{z^2 - a^2}} \quad (3.89)$$

Stresses are determined as

$$\sigma_x = 2 \operatorname{Im} \bar{Z} + y \operatorname{Re} Z' \quad (3.90)$$

$$\sigma_y = -y \operatorname{Re} Z' \quad (3.91)$$

$$\tau_{xy} = \operatorname{Re} Z - y \operatorname{Im} Z' \quad (3.92)$$

Stresses near the crack tips could also be expressed, using the polar coordinates, as

$$\sigma_x = -\frac{K_{II}}{\sqrt{2\pi r}} \sin \frac{\theta}{2} \left(2 + \cos \frac{\theta}{2} \cos \frac{3\theta}{2} \right) \quad (3.93)$$

$$\sigma_y = \frac{K_{II}}{\sqrt{2\pi r}} \cos \frac{\theta}{2} \sin \frac{\theta}{2} \cos \frac{3\theta}{2} \quad (3.94)$$

$$\tau_{xy} = \frac{K_{II}}{\sqrt{2\pi r}} \cos \frac{\theta}{2} \left(1 - \sin \frac{\theta}{2} \sin \frac{3\theta}{2} \right) \quad (3.95)$$

where

$$K_{II} = \tau \sqrt{\pi a} \quad (3.96)$$

is the stress intensity factor for sliding mode crack.

For mode III (tearing mode) crack which is subjected to a shear loading in the antiplane, shown in Figure 3.5, the stress function could be selected as

$$U_{III} = \frac{1}{\mu} \operatorname{Im} \bar{Z} \quad (3.97)$$

where $Z = \frac{z}{\sqrt{z^2 - a^2}}$ and $\mu = \frac{E}{2(1+\nu)}$ is elastic shear modulus.

The stresses are obtained as

$$\begin{aligned}\tau_{\theta} &= \text{Im } Z \\ \tau_{\rho} &= \text{Re } Z\end{aligned}\tag{3.98}$$

Using polar coordinates, stresses near the crack tips could be expressed as

$$\begin{aligned}\tau_{\theta} &= -\frac{K_{III}}{\sqrt{2\pi r}} \sin \frac{\theta}{2} \\ \tau_{\rho} &= \frac{K_{III}}{\sqrt{2\pi r}} \cos \frac{\theta}{2}\end{aligned}\tag{3.99}$$

where

$$K_{III} = \tau \sqrt{\pi a}\tag{3.100}$$

is stress intensity factor for tearing mode crack.

3.5.2 Energy Considerations in Fracture

The crack will consume energy to form its two crack surfaces when it propagates. The energy comes from stored strain energy and/or work done by external loads. The total potential energy of the system could be written as [72]

$$\Pi = U - W\tag{3.101}$$

where U is strain energy and W is work done by external loads. During crack growth, decrease of potential energy per unit crack area will be equal to the energy dissipated in unit propagation of crack area. Let Γ denote the energy spent in increasing the crack area, then we have

$$\frac{\partial \Pi}{\partial A} + \frac{\partial \Gamma}{\partial A} = 0 \quad (3.102)$$

Generally strain energy will include elastic energy and plastic energy. The plastic energy is generated as a result of plastic deformation during crack growth. For brittle materials, the plastic energy would be negligible; therefore Griffith theory gives the definition of strain energy release rate as

$$G = \frac{\partial \Gamma}{\partial A} = \frac{\partial W}{\partial A} - \frac{\partial U^e}{\partial A} \quad (3.103)$$

where U^e is elastic strain energy. G is also called crack driving force. It has been shown that the strain energy release rates are related to stress intensity factors according to following relationships:

$$G_I = \frac{K_I^2}{\tilde{E}} \quad (3.104)$$

where $\tilde{E} = E$ for plane stress, and $\tilde{E} = \frac{E}{1-\nu^2}$ for plane strain.

$$G_{II} = \frac{K_{II}^2}{\tilde{E}} \quad (3.105)$$

$$G_{III} = \frac{1+\nu}{E} K_{III}^2 \quad (3.106)$$

If the crack is subjected to a complex loading, related to all three crack modes, the strain energy release rate will be

$$G = G_I + G_{II} + G_{III} \quad (3.107)$$

When the crack propagates from 0 to a , the energy consumed by the crack growth could be calculated as

$$E_c = \int_0^a GdA = \int_0^a GBda \quad (3.108)$$

where B is the width of crack surface.

3.5.3 Energy Balance in a Cracked Beam under Dead-load Situation

Suppose a beam contains a crack, and the beam is subjected to a dead load which is maintained constant during the crack growth. If a crack has propagated Δa , say, under a constant bending moment (due to dead-load loading assumption), the applied moment will perform some work W which will not only assist the crack growth but also increase the structural strain energy [72]. Since the externally applied moment remains unaltered due to the crack growth Δa , using Clapeyron's theorem [72], the work W is twice the increase of elastic strain energy, and the final strain energy of the system is increased. Figure 3.6 shows the load-displacement response under dead-load assumption for crack growth from a_1 to a_2 . The energy before crack growth is represented by the area (OAC) and after the growth by the area (OBD) . During crack growth (under the constant load P) the load P performs work given by the area $(ABCD)$. The increase of strain energy would be $(OBD) - (OAC) = (ABCD)/2$. Mathematical expressions are as follows:

$$\begin{aligned} W &= E_c + \Delta U = 2\Delta U \\ E_c &= \Delta U \end{aligned} \quad (3.109)$$

where E_c is energy for crack growth, and ΔU the increase of elastic strain energy in a cracked beam. The final strain energy of the cracked beam is

$$U_c = U + \Delta U = U + E_c \quad (3.110)$$

where U is strain energy of the beam prior to crack growth. This procedure is utilized in formulating the deformation of the cracked beam.

3.6 Closure

In this chapter, the necessary equations and formulations utilized in the subsequent derivations of governing equations for cracked structures are given for easy reference and reading of the chapters that follow. Chapter 4 utilizes the equations given in section 3.2.1, 3.2.2, 3.3, 3.5.1, 3.5.2 and 3.5.3 to derive the basic formulations and solutions obtained for a cracked beam and other comparisons given therein. Similarly other chapters will be using the relevant section of this chapter to formulate and solve the governing equation obtained therein.

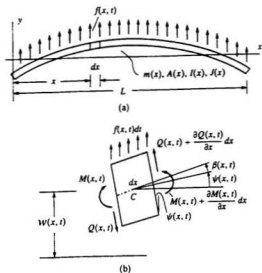


Figure 3.1 A Timoshenko beam in transverse vibration

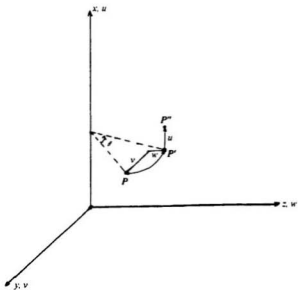


Figure 3.2 Displacements of a point P in torsion of a non-circular cross section

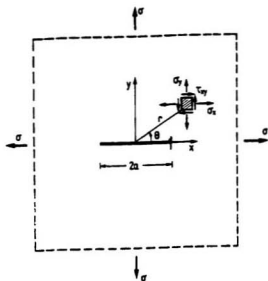


Figure 3.3 Mode I crack under uniform tensile stress loading

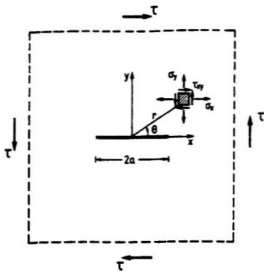


Figure 3.4 Mode II crack under uniform in-plane shear loading

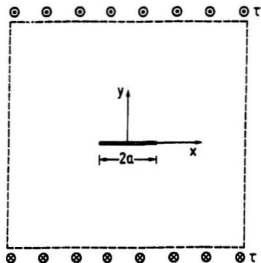


Figure 3.5 Uniform out-of-plane shear stress loading (Mode III)

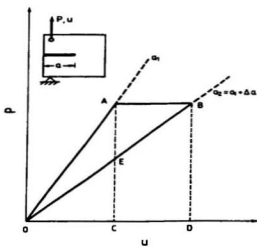


Figure 3.6 Load-displacement response as the crack grows under the dead-load loading

Chapter 4

Crack Identification in Vibrating Beams Using Energy Method

4.1 Introduction

As outlined in chapter three, for vibration analyses of cracked beams and possible crack detection, fracture mechanics procedure is generally preferred [1]. The procedure assumes that a crack occurring in a beam would reduce the local stiffness around the location of the crack. In using the fracture mechanics model, one type of formulation calculates the local flexibility using Castigliano's second theorem as applicable to fracture mechanics [18,19].

For better modelling of a crack in the beam, some researchers have used the variational principle to develop continuous vibration equations for cracked beams with assumptions of stresses/strains/displacements. Christides and Barr [75] first proposed an exponential-type function (crack disturbance function) to model the stress/strain variation around the crack zone, in which one parameter was to be determined by experiments. Based on the assumed stress, strain and displacement expressions, the vibration equations of beams with symmetrical cracks were derived using Hu-Washizu variational principle [76,77]. Shen *et al.* [78,79] followed a similar procedure to investigate the vibration of cracked beams with single or symmetrical cracks, solution to which was obtained using

Galerkin's method with many terms. Recently Chondros and Dimarogonas [80], using Christides and Barr's theory as a background material, have generated some solutions for the crack functions in vibrations of a cracked cantilever beam using fracture mechanics principle and Castigliano's theorem. Displacements and stresses were assumed as

$$\begin{aligned}
 u &= -z\{[1 + f(x, z)]w(x, t)\}' \\
 w &= [1 + f(x, z)]w(x, t) \\
 \gamma_{xz} &= [-z + m(x, z)]S(x, t) \\
 \sigma_{xx} &= [-z + m(x, z)]T(x, t)
 \end{aligned} \tag{4.1}$$

where $f(x, z)$ and $m(x, z)$ were crack disturbance functions, and $S(x, t)$ and $T(x, t)$ were unknown functions. The disturbance function $f(x, z)$ was determined as

$$f = -3\pi(1 - \nu^2)h^2\alpha^2(L_0 - L) / [zL_0^2(L_0^2 + \nu h^2 / 4)] \tag{4.2}$$

where α is crack depth ratio (a/h), and L is crack location (beam length = L_0). According to their computations, one crack disturbance function $m(x, z)$ gets canceled and disappears in the final vibration equation, while the other function $f(x, z)$ seems to be constant along the beam; this function also tends to infinity along the neutral axis. Such crack disturbance functions could result in unrealistic displacements/stresses, which would not represent the displacements/stresses due to a crack. Later Chondros *et al* [81] obtained the crack function for a simply supported beam (varying as a function of its distance from crack), which is given by

$$f = -6\pi(1 - \nu^2)h^2\Phi_1(\alpha)(x - L)^2 / [zL_0(L_0^2 + \nu h^2 / 4)] \tag{4.3}$$

where $\Phi_1(\alpha)$ is modification function for stress intensity factor, which is a function of crack depth ratio (a/h). It can be seen that the crack disturbance function is still infinite at the neutral axis, which would lead to infinite displacements/stresses.

In this thesis investigation, a continuous vibration theory for cracked beams will be developed by modeling the energy variation along the beam length due to the crack.

4.2 Solid Rectangular Beam with One or More Cracks

4.2.1 Bending Stiffness of the Beam with a Crack

For the uncracked beam, subjected to a bending moment M , the strain energy in the beam is given by

$$U = \frac{1}{2} \int_0^L \frac{M^2}{EI} dx \quad (4.4)$$

When a crack is formed on one side of the beam, and then it grows from zero to a under a constant external bending moment, the energy consumed for crack growth, based on fracture mechanics (see equation 3.108), is

$$E_c = \int_0^a G dA = \int_0^a G b da \quad (4.5)$$

where b is the width of the beam, and G the strain energy release rate. For the transverse vibration of the beam, the crack is mainly subjected to direct bending stresses and the effect of shear stresses can be neglected; therefore, only the effect of first mode crack needs to be considered in the analysis. If the shear and transverse tearing forces are dominant, effects due to modes II and III should be considered. This gives the strain energy release rate as

$$G = \frac{K_I^2}{E} \quad (4.6)$$

where K_I is the stress intensity factor for first mode crack, and E is the Young's modulus. For a solid rectangular cross-section beam of depth h and width b , K_I is given as [72]

$$K_I = \frac{6M\sqrt{\pi a}}{bh^2} F(a) \quad (4.7)$$

where h is the depth of the beam; and for $a/h < 0.6$ (for higher values of a/h , a tabular format is given in reference [82], which could be used in a numerical manner), the crack geometry factor is

$$F(a) = 1.12 - 1.4\left(\frac{a}{h}\right) + 7.33\left(\frac{a}{h}\right)^2 - 13.8\left(\frac{a}{h}\right)^3 + 14\left(\frac{a}{h}\right)^4 \quad (4.8)$$

Finally using equation (4.5) the energy consumed in generating the crack becomes

$$E_c = D(a)M^2 \quad (4.9)$$

where

$$D(a) = \frac{18\pi F_s(a)a^2}{Ebh^4}$$

$$F_s(a) = 1.254 - 2.091\left(\frac{a}{h}\right) + 9.19\left(\frac{a}{h}\right)^2 - 20.574\left(\frac{a}{h}\right)^3 + 41.243\left(\frac{a}{h}\right)^4$$

$$- 69\left(\frac{a}{h}\right)^5 + 98.92\left(\frac{a}{h}\right)^6 - 85.87\left(\frac{a}{h}\right)^7 + 39.2\left(\frac{a}{h}\right)^8 \quad (4.10)$$

If $EI_c(x)$ is the bending stiffness of the cracked beam with the crack being always open, the final strain energy in the cracked beam could be alternatively expressed as

$$U_c = \frac{1}{2} \int_0^l \frac{M^2}{EI_c(x)} dx \quad (4.11)$$

where $I_c(x)$ is moment inertia of the beam with an open crack. It must be remembered that under the dead-load assumption, the external dynamic moment applied to the beam is constant over the length of the beam. For other cases where bending moments vary and shear forces are present, suitable variation of bending moment along the length could be considered and the derivations modified; in addition effect due to mode II cracking should also be incorporated.

From fracture mechanics considerations, the stresses/strains are highly concentrated around the crack tip and the crack region, and reach the nominal stress at a location far away from the crack. So it can be assumed that the increase of strain energy due to crack growth, under constant applied moment, is concentrated mainly around the crack region. In order to represent mathematically the strain energy variation along the cracked beam length, the distribution of E_c (equal to the increase of strain energy) along the beam is postulated (by the present researcher) to be similar to

$$\frac{Q(a,c)}{1 + \left(\frac{x-c}{k(a)a}\right)^2} \quad (4.12)$$

where $Q(a,c)$ and $k(a)$ are terms to be determined such that

$$E_c = \int_0^l \frac{Q(a,c)}{1 + \left(\frac{x-c}{k(a)a}\right)^2} dx \quad (4.13)$$

and c is the distance to the crack location from one end of the beam. Expression (4.12) has the maximum value at the crack location ($x = c$) and approaches zero far away from the crack, which indicates that changes of strain energy occur mainly around crack, and

very little away from the crack location. This makes the strain energy variation to be concentrated largely around the crack region. From equations (4.9) and (4.13), one obtains

$$Q(a,c) = \frac{D(a)M^2}{k(a)a \left[\arctan\left(\frac{l-c}{k(a)a}\right) + \arctan\left(\frac{c}{k(a)a}\right) \right]} \quad (4.14)$$

Substitution of equations (4.4), (4.11) and (4.13) into equation (3.110) yields

$$\frac{1}{2} \int_0^l \frac{M^2}{EI_c(x)} dx = \frac{1}{2} \int_0^l \frac{M^2}{EI} dx + \int_0^l \frac{Q(a,c)}{1 + \left(\frac{x-c}{k(a)a}\right)^2} dx \quad (4.15)$$

From the above equation, the modified bending stiffness of the cracked beam is obtained as

$$EI_c(x) = \frac{EI}{1 + \frac{EI R(a,c)}{1 + \left(\frac{x-c}{k(a)a}\right)^2}} \quad (4.16)$$

$$\text{where } R(a,c) = \frac{2D(a)}{k(a)a \left[\arctan\left(\frac{l-c}{k(a)a}\right) + \arctan\left(\frac{c}{k(a)a}\right) \right]} \quad (4.17)$$

At the location of crack, i.e., at $x = c$, one has

$$h_{eq}|_{x=c} = h - a \quad (4.18)$$

$$\frac{EI}{EI_c}|_{x=c} = \frac{bh^3/12}{b(h_{eq}|_{x=c})^3/12} = \frac{bh^3/12}{b(h-a)^3/12} \quad (4.19)$$

where $h_{eq}|_{x=c}$ is the equivalent height of the beam at the position of the crack. The EL_c given by equation (4.16) and equivalent height (h_{eq}), computed thereby, will vary along the length of the beam. Using equations (4.16) and (4.19), one obtains

$$k(a) = \frac{3\pi F_s(a)(h-a)^3 a}{[h^3 - (h-a)^3]h} \quad (4.20)$$

[The quantity $\left\{ \arctan\left(\frac{l-c}{k(a)a}\right) + \arctan\left(\frac{c}{k(a)a}\right) \right\}$ is approximately equal to π when the crack is not near the ends of the beam]. It can be seen that if no crack is present in the beam, i.e., $a = 0$, then the parameters $D(a) = 0$, $Q(a,c) = 0$, $R(a,c) = 0$ and $k(a) = 0$; from equation (4.16) the equivalent stiffness EL_c becomes the stiffness of the uncracked beam. The variations of normalized equivalent stiffness and normalized equivalent height (h_{eq}) of the cracked beam (along its length) are shown in Figure 4.1 [calculated from equation (4.16)].

To verify the reasonableness of energy distribution given by equations (3.110) and (4.13), the strain energy along the x-axis in a cracked plate (width of 40 units and unit thickness) under uniform tension stress (plane stress) is calculated based on equations (3.110) and (4.13). At the same time, strain energy is computed numerically using Westergaard's method (complex functions, equations (3.84) to (3.87)) [74] used in linear elastic fracture mechanics. The two curves of energy distribution are plotted in Figure 4.2, which are close to one another except near the crack zone. It can be seen from Figure 4.2 that, outside the crack influence zone, the energy distribution is nearly constant, and the change of strain energy (due to both formulations) will be nearly zero (outside the crack

influence zone) [assumed in equation (4.13)]. Thus, the increase of strain energy under dead-load is quite concentrated around the crack zone.

Based on elastic fracture mechanics approach, the stresses near the crack tip tend to be very large or infinite, so does the strain energy. But, in reality, stresses and strain energy cannot approach infinity, and consequently plastic deformation occurs around the crack tip; therefore, a part of the increased strain energy under the dead-load loading is stored as plastic energy at the crack tip. The magnitude of the plastic strain energy is difficult to calculate and is dependent on the stress cycling and the consequent residual strain left around the crack tip. Since cracking in beams can be characterized as plane stress cracking, under cyclic loading the plastic energy stored around the crack tip is very small; hence the contribution from crack tip plasticity to the energy stored in the beam is rather small. Consequently use of LEFM principles to characterize the crack phenomena is valid. Also using equation (4.13), the strain energy is assumed to be concentrated around the crack tip, and the total energy increase is set almost to the correct value. The final strain energy distribution would then be a reasonable one. From Figure 4.2, the difference in energy between the exact solution and the developed approximate solution is small, and the closeness of energy concentration around the crack tip and total increase of energy are also guaranteed by equation (4.13); therefore, the crack energy function represented by equation (4.13) is considered to be valid for the problems investigated in this thesis.

4.2.2 Bending Stiffness of the Beam Containing Two Cracks

Under a constant external bending moment M , the energy supplied for the growth of two cracks is

$$E_c = E_{c1} + E_{c2} = \int_0^{a_1} G_1 b da_1 + \int_0^{a_2} G_2 b da_2 \quad (4.21)$$

where a_1 & a_2 are depths of two cracks, and G_1 & G_2 are strain energy release rates for the two cracks. Similarly, for the transverse vibration of the beam, the first mode crack effect is dominant; and only the influence of the first mode crack is considered in this study.

$$G_1 = \frac{K_{I1}^2}{E}, \quad G_2 = \frac{K_{I2}^2}{E} \quad (4.22)$$

The two stress intensity factors are given as

$$K_{I1} = \frac{6M\sqrt{\pi a_1}}{bh^2} F(a_1), \quad K_{I2} = \frac{6M\sqrt{\pi a_2}}{bh^2} F(a_2) \quad (4.23)$$

where for $a_1/h < 0.6$ and $a_2/h < 0.6$ crack geometry factors are

$$\begin{aligned} F(a_1) &= 1.12 - 1.4\left(\frac{a_1}{h}\right) + 7.33\left(\frac{a_1}{h}\right)^2 - 13.8\left(\frac{a_1}{h}\right)^3 + 14\left(\frac{a_1}{h}\right)^4 \\ F(a_2) &= 1.12 - 1.4\left(\frac{a_2}{h}\right) + 7.33\left(\frac{a_2}{h}\right)^2 - 13.8\left(\frac{a_2}{h}\right)^3 + 14\left(\frac{a_2}{h}\right)^4 \end{aligned} \quad (4.24)$$

Finally equation (4.21) becomes

$$E_c = E_{c1} + E_{c2} = [D_1(a_1) + D_2(a_2)]M^2 \quad (4.25)$$

where

$$D_1(a_1) = \frac{18\pi F_s(a_1)a_1^2}{Ebh^4}, \quad D_2(a_2) = \frac{18\pi F_s(a_2)a_2^2}{Ebh^4} \quad (4.26)$$

The function $F_s(a)$ is given in equation (4.10). Following the earlier derivations given in equation (4.9), for each crack growth, the energy consumed can be expressed by

$$E_{c1} = D_1(a_1)M^2, \quad E_{c2} = D_2(a_2)M^2 \quad (4.27)$$

when the cracks are close together, the energy consumed in crack formulation cannot be superposed near the crack region, since the interaction is nonlinear. Hence a more rigorous analysis is needed to include the crack interaction effects. If the two cracks are not very close to each other so that the stress field for each crack could be treated separately using fracture mechanics theory, then the increase of strain energy due to crack growths under constant external bending moment could be assumed to be distributed in the beam according to the following functions (similar to the case for one crack),

$$\frac{Q_1(a_1, c_1)}{1 + \left(\frac{x - c_1}{k_1(a_1)a_1}\right)^2} \text{ and } \frac{Q_2(a_2, c_2)}{1 + \left(\frac{x - c_2}{k_2(a_2)a_2}\right)^2} \quad (4.28)$$

where $Q_1(a_1, c_1)$, $Q_2(a_2, c_2)$ and $k_1(a_1)$, $k_2(a_2)$ are terms to be determined such that

$$E_{c1} = \int_0^l \frac{Q_1(a_1, c_1)}{1 + \left(\frac{x - c_1}{k_1(a_1)a_1}\right)^2} dx, \quad E_{c2} = \int_0^l \frac{Q_2(a_2, c_2)}{1 + \left(\frac{x - c_2}{k_2(a_2)a_2}\right)^2} dx \quad (4.29)$$

with c_1 and c_2 being distances to the crack locations from one end of the beam. Using equations (4.27) and (4.29), one obtains

$$Q_1(a_1, c_1) = \frac{D_1(a_1)M^2}{k_1(a_1)a_1 \left[\arctan\left(\frac{l-c_1}{k_1(a_1)a_1}\right) + \arctan\left(\frac{c_1}{k_1(a_1)a_1}\right) \right]} \quad (4.30)$$

and

$$Q_2(a_2, c_2) = \frac{D_2(a_2)M^2}{k_2(a_2)a_2 \left[\arctan\left(\frac{l-c_2}{k_2(a_2)a_2}\right) + \arctan\left(\frac{c_2}{k_2(a_2)a_2}\right) \right]} \quad (4.31)$$

Substitution of equations (4.4), (4.11), (4.21), (4.25) and (4.29) into equation (3.110)

yields

$$\frac{1}{2} \int_0^l \frac{M^2}{EI_c} dx = \frac{1}{2} \int_0^l \frac{M^2}{EI} dx + \int_0^l \frac{Q_1(a_1, c_1)}{1 + \left(\frac{x-c_1}{k_1(a_1)a_1}\right)^2} dx + \int_0^l \frac{Q_2(a_2, c_2)}{1 + \left(\frac{x-c_2}{k_2(a_2)a_2}\right)^2} dx \quad (4.32)$$

From equation (4.32), the bending stiffness of the beam with two cracks is obtained as

$$EI_c = \frac{EI}{1 + \frac{EIR_1(a_1, c_1)}{1 + \left(\frac{x-c_1}{k_1(a_1)a_1}\right)^2} + \frac{EIR_2(a_2, c_2)}{1 + \left(\frac{x-c_2}{k_2(a_2)a_2}\right)^2}} \quad (4.33)$$

where

$$R_1(a_1, c_1) = \frac{2D_1(a_1)}{k_1(a_1)a_1 \left[\arctan\left(\frac{l-c_1}{k_1(a_1)a_1}\right) + \arctan\left(\frac{c_1}{k_1(a_1)a_1}\right) \right]} \quad (4.34)$$

$$R_2(a_2, c_2) = \frac{2D_2(a_2)}{k_2(a_2)a_2 \left[\arctan\left(\frac{l-c_2}{k_2(a_2)a_2}\right) + \arctan\left(\frac{c_2}{k_2(a_2)a_2}\right) \right]} \quad (4.35)$$

At the two crack locations, i.e., at $x = c_1$ and $x = c_2$, one has

$$\frac{EI}{EI_{c1}} = \frac{bh^3/12}{b(h-a_1)^3/12}, \quad \frac{EI}{EI_{c2}} = \frac{bh^3/12}{b(h-a_2)^3/12} \quad (4.36)$$

where EI_{c1} and EI_{c2} are equivalent bending stiffnesses at each of the crack positions, respectively. Using equations (4.33) and (4.36), one obtains

$$k_1(a_1) = \frac{3\pi F_n(a_1)(h-a_1)^3 a_1}{[h^3 - (h-a_1)^3]h}, \quad k_2(a_2) = \frac{3\pi F_n(a_2)(h-a_2)^3 a_2}{[h^3 - (h-a_2)^3]h} \quad (4.37)$$

[it is to be noted that $|c_1 - c_2| \gg a_1$ or a_2 when the two cracks are assumed to be far apart].

The variations of normalized equivalent stiffness and depth (along the beam length) for two cracks are shown in Figure 4.3. It can be seen that the effect due to crack interaction is marginal unless the crack becomes large, viz., $a/h > 0.5$. For more cracks on the beam, the same procedure could be utilized to compute the bending stiffness of the cracked beam, if the cracks do not interact considerably with one other.

4.2.3 Transverse Vibration Equations for Cracked Beams

For an Euler beam, the vibration equation can be expressed using Newton's approach as

$$\frac{\partial^2}{\partial x^2} \left[EI_c \frac{\partial^2 w}{\partial x^2} \right] + m \frac{\partial^2 w}{\partial t^2} = 0 \quad (4.38)$$

where m is the mass density along the beam length; in spite of the crack, the mass m per unit length will remain constant throughout the length of the beam.

Assuming the separation of variables concept, let $w = W(x)H(t)$, and substituting into the above equation (4.38), one obtains the characteristic equation as

$$\frac{d^2}{dx^2} \left[EI_c \frac{d^2 W}{dx^2} \right] + m\omega_c^2 W = 0 \quad (4.39)$$

where ω_c is the natural frequency of the cracked beam.

To solve for natural frequencies and mode shapes, a four-term Galerkin's method is used.

For a simply supported beam, the trial functions are selected as [see equation (3.15)]

$$W = C_1 W_1 + C_2 W_2 + C_3 W_3 + C_4 W_4 \quad (4.40)$$

where C_i are coefficients, and

$$\begin{aligned} W_1 &= \sin\left(\frac{\pi x}{l}\right); & W_2 &= \sin\left(\frac{2\pi x}{l}\right) \\ W_3 &= \sin\left(\frac{3\pi x}{l}\right); & W_4 &= \sin\left(\frac{4\pi x}{l}\right) \end{aligned} \quad (4.41)$$

The above four functions are the exact functions of the uncracked simply-supported beam for the first four modes. For a fixed-fixed beam, the trial functions are selected [83], from the exact first four mode functions of the uncracked fixed beam [see equation (3.18)], as

$$W = \sum_{i=1}^4 C_i W_i \quad (4.42)$$

where C_i are coefficients, and

$$W_1 = \sin\left(\frac{p_1 x}{l}\right) - \sinh\left(\frac{p_1 x}{l}\right) + B_1 \left[\cos\left(\frac{p_1 x}{l}\right) - \cosh\left(\frac{p_1 x}{l}\right) \right]$$

$$B_1 = \frac{\cos\left(\frac{p_1 x}{l}\right) - \cosh\left(\frac{p_1 x}{l}\right)}{\sin\left(\frac{p_1 x}{l}\right) + \sinh\left(\frac{p_1 x}{l}\right)} \quad (4.43)$$

$$p_1 = 4.73, \quad p_2 = 7.853, \quad p_3 = 10.996, \quad p_4 = 14.173 \quad (4.44)$$

To verify the convergence of Galerkin's method, more terms of trial functions are also used in the calculations. Table 4-1 and Table 4-2 show the frequencies obtained by the four terms Galerkin's method and eight terms Galerkin's method for a cracked beam (one crack) with a crack depth ratio of $a/h = 0.25$ and $a/h = 0.5$, respectively. The beam length is $3m$ and the crack is located at $c/l=0.8$. The results indicate that the four terms Galerkin's method has given acceptable frequencies, with minimal errors. It is also observed from the results shown in Table 4-1 and Table 4-2, that for the second mode of vibration the error obtained for a simply supported beam is greater than that for the fixed beam. This is due to the fact that the point of contra-flexure for the fixed beam (for the second mode) occurs near the crack location and consequently the crack presence does not influence the second frequency significantly; whereas for a simply supported beam, the presence of the crack affects the frequency significantly and as such a larger error is obtained for the second mode.

4.2.4 Experiments and Comparison with Theory

In order to verify the theory, vibration experiments for the cracked beam were carried out. The prismatic beam made of aluminum had a span length of 650 mm and a rectangular cross-section of $25.4 \times 25.4\text{ mm}$. Young's modulus of elasticity was $E = 62.1\text{ GPa}$, (supplied by the manufacturer) and material density was 2700 kg/m^3 ; also the variation in the cross section areas (across the whole beam length) was observed to be small and as such for the test it was assumed to be constant over the whole length. The crack was introduced by making fine saw cuts (0.4mm wide) at the middle of the beam ($c/l=0.5$) and perpendicular to the longitudinal axis; this allowed the crack to remain open always. The beam was simply supported at two ends as shown in Figure 4.4. From Figure 4.4 it can be seen that the ratio of bending stiffness between the thin connection and the remaining portion of the beam on the fixed end is $1/512$ [i.e. $(1/8)^3$] and ratio of axial stiffness between the two is $1/8$. Since only bending frequencies are considered in the study, the simply supported boundary conditions are almost properly simulated. The excitation was carried out by an electrodynamic shaker at the center of the beam. Seven accelerometers were evenly placed on the beam. Dual Channel Signal Analyzer (B&K type 2032) and the STAR analysis software [84] were used to extract the experimental results. The star analysis software carries out the modal averaging of response values (over 20 for sine sweep tests and even 100 for random responses) and as such the variance from the estimated values will be very small.

Figures 4.5 and 4.6 show experimental setup by side view. The beam model was clamped at each end, between two thick square steel plates, supported over a short and stiff steel H-section column. This was achieved by using two rectangular steel plates ($3/4$ " thick) with four holes each for bolting the beam model on the stiff supporting column. The exciter was suspended using a slotted square flat plate. The plate was fixed to the top beam (of the steel frame) by four threaded rods. This made possible the adjustment of the position of the exciter at any time a model was to be fixed.

By exciting the model at a point, and measuring the acceleration responses of the beam at different points on the beam model, it was possible to get all the frequency response functions between these positions which would lead to the extraction of the modal parameters. A fast sine sweep signal produced by the frequency generator, which was then amplified, was used to drive the exciter, which eventually transmitted the force to the beam model through the load cell. It is to be noted that the model was excited at a point which was a few millimeters away from the center of the model. This was done to avoid exciting the beam at a nodal point (of a mode), since the beam would not respond in that mode at that point.

The beam without crack was first tested; then the crack was made in the beam, varying from a crack depth ratio of $a/h = 0.1$ to $a/h = 0.5$. Therefore there were six sets of testing. For each set of testing, first three frequencies were measured, and the frequency ratios, i.e., the ratio of the frequency of the cracked beam to that of the uncracked beam, were calculated. The frequency ratio vs the crack ratio (first mode) is shown in Figure 4.7 and

compared with the theoretical results, obtained from this study, and experimental data from Christides and Barr [75]. It should be noted that the points are connected by a continuous curve, instead of a discretely jointed curve; the reason is that if the crack depth was increased in very small increments and the beam tested then the curve would be continuous curve. It can be seen that the theoretical and experimental results show a very good agreement; the test results seem to be slightly lower than the theoretical values. In addition, a parallel experimental study was carried out on 14 aluminum beams, seven with simply supported ends and the other seven with fixed ends. Careful experimental measurements and detailed analysis of the experimental results were carried out to verify the results of the numerical analysis reported [85]. Reference [85] can be consulted for more detailed results and analyses.

4.2.5 Results and Discussions

The natural frequencies and mode shapes for transverse vibration of the cracked beams are calculated using the MATLAB program. The crack is assumed to be always open. All beams considered here are of a solid rectangular cross section, with a depth of $0.2m$, a width of $0.1m$, and a length of $3m$. For the simply supported beam with a crack, the first four frequencies are obtained for different crack depths and locations. When the crack is located at the midpoint of the beam, the normalized frequencies are shown for different crack depths in Figure 4.8. The frequencies decrease by about 11.4% and 8.1% for the first and third modes as the crack grows up to half the beam height. However, the frequencies change marginally for the second and fourth modes; this is due to the fact

that the crack at the midpoint of the beam is located at the vibration nodes of the second and fourth modes. Since part of the beam around the crack region is also influenced by stress relief due to crack, small reductions of frequency values occur for second and fourth modes, even though the crack is located around the nodes of the second mode. For the sake of comparison, the normalized values of the parallel study reported earlier [85] is plotted in Figure 4.8. It is seen that there is a very good correlation between the theory developed in this study and measured crack growth development.

Figure 4.9 shows the normalized frequencies for various crack locations when the crack depth is kept constant at $a/h = 0.25$. As indicated in the figure, the crack occurring near the ends of the beam does not change the frequencies. For the first mode, the maximum change of frequency takes place as the crack occurs at the center. Generally, both the crack location and crack depth influence the natural frequencies of the cracked beam. The normalized frequencies vs. crack location and crack depth are shown in a three-dimensional plot in Figure 4.10. From these figures, it can be seen that the crack location and crack depth ratios are directly related to the frequency ratios.

For a simply supported beam containing two cracks, which are located at $c_1/l = 1/3$ and $c_2/l = 2/3$ from the left end, the normalized frequencies are shown in Figure 4.11 as both cracks grow to a depth of $a/h = 0.5$. The third mode has the smallest change of frequencies (about 5%), while the other modes have much larger changes, which are 15.5%, 16.9% and 12.8%, respectively; this is due to the fact that the nodes for the third mode are located near the crack locations.

For a fixed-fixed beam containing a crack, Figure 4.12 shows the normalized frequencies for different crack depths when the crack is located at the midpoint of the beam, and Figure 4.13 shows the normalized frequencies for different crack depths for the crack located at the end of the beam. The changes of frequencies are similar to that for a simply supported beam; however, the decrease of frequencies for the crack at the end of the beam is larger than that for the crack in the middle. For the crack in the middle, the frequency changes are 7.8% and 7.9% for the first and third modes (with crack depth ratio $a/h=0.5$); they are much smaller for the other two modes. For the crack at the end, the first frequency change is about 11.5% for a crack depth ratio of $a/h=0.5$. For the second mode, the change is much higher than that for the central crack; it is the same for fourth mode. For the third mode, the crack at the center produces larger changes than the crack at the end. This is due to the fact that the loss of stiffness at the center influences the frequencies much higher (due to fixed ends at both sides) than the crack at the end (which produces a partial fixed condition at one end when the crack becomes larger).

Figure 4.14 indicates the fluctuation of the normalized frequencies with crack depth $a/h = 0.25$ as the crack location moves along the beam. Unlike the simply supported beam, the maximum changes of frequencies for the first and second modes occur near the ends of the fixed-fixed beam. The reason is that the presence of a crack at these locations would reduce the stiffness much more near the supports (the boundary constraints) than near the center. The three-dimensional plot of normalized frequency vs. normalized crack location and depth are shown in Figure 4.15.

4.3 Crack Identification by Frequency Contours

As shown above, both crack location and depth have influences on the frequencies of the cracked beam. It turns out that one frequency could correspond to different crack depths and locations, as can be seen from Figure 4.10 and Figure 4.15. Based on this, the contour line which has the same normalized frequency change (the same frequency change resulting from different combinations of crack depths and locations) could be plotted in a figure having the crack location and depth as its axes. Figure 4.16 shows frequency contours for four modes of the simply supported beam with one crack, and Figure 4.17 shows contours for four modes of the fixed-fixed beam with one crack. To be clear and readable, the figures for each mode include only contours of three normalized frequency changes. The 0.98 contour means that the points on the curve have 2% decrease of frequency compared to the uncracked beam. The location and depth corresponding to any point on the curve would become the possible crack location and depth. A crack should and must belong to one contour line for each mode. The contour lines for different modes could be plotted together, and the intersection point(s) would indicate the crack location and crack depth. Since the frequencies could be measured accurately for lower modes and the contours for lower modes tend to be simple, two contours from lower modes (e.g. the first and second modes) are plotted together to obtain the intersection point(s). When more than one intersection point is obtained, the contour from another lower mode is also used to get the final point, which would indicate

the crack location and depth. When the crack location and vibration node coincide for a mode, the contour tends to disappear and no intersections are obtained; then the next mode is used. Basically, the first four frequencies are sufficient to identify the crack (depth and location) in the beam.

From the formulations given in equations (4.4) to (4.20), it can be seen that the frequency ratios are functions of a/h and c/l ratios. Hence the crack function G can be expressed as

$G = F\left(\frac{\omega}{\omega_0}, \frac{a}{h}, \frac{c}{l}\right)$ where F represents the composite function, and therefore the unique

location for the crack will be given by the intersection of any three frequency contours. For convenience and ease in calculations, the three lowest modes are used.

From the results in the above section, a crack, with $a/h = 0.25$, located at the middle of a simply supported beam, has the normalized frequencies of 0.9708 (i.e., a 2.92% decrease of frequency) for the first mode, 0.9744 for the third mode, and shows very small changes in frequencies for the other two modes (0.9972 and 0.994). The contour with the value of 0.9708 is retrieved from the first mode and is plotted in Figure 4.18. The contour with the value of the 0.9744 from the third mode is shown in the same figure. There are three intersection points for these two contours. Therefore, the contour from the second mode is also used to uniquely identify the crack location and depth. Three contours will give one intersection (location 2 in Figure 4.18), which indicates the crack depth and location very well. To consider the situation of a non-central crack, the case of a simply supported beam with a crack depth $a/h = 0.1$, located at $c/l = 0.4$, is illustrated in Figure 4.19. The changes in normalized frequencies for the above crack are given respectively by 0.9947,

0.9979 and 0.9978, for first three frequencies. The 0.9947 contour for the first mode, 0.9979 contour for the second mode and 0.9978 contour for the third mode are shown in Figure 4.19. The intersection points (locations 2 and 3 in Figure 4.19) indicate a crack depth $a/h=0.1$ and crack locations of $c/l=0.4$ or 0.6 . Due to structural symmetry in the simply supported beam, the three contours would give two probable crack locations. Actual location could be identified by adding an off-center mass to the beam, which would make the vibration modes asymmetric. When the modes are asymmetric, only one intersection point will be obtained. This is shown to be true in the following figures.

A lumped mass of one-tenth of beam mass per unit length is attached to the beam at the quarter point of the length. In case that no crack exists, the first four frequencies decrease about 4.7%, 8.1%, 3.5% and 0% (see Table 4-3), respectively, due to the off-center mass. When the beam contains a crack, normalized frequency changes against the crack depth ratios are shown in Figure 4.20. As crack location moves along the beam, the changes of normalized frequency are shown in Figure 4.21. It can be seen that the changes are not symmetric anymore due to the off-center mass. Figure 4.22 shows the normalized frequencies vs. crack depth ratios and crack location ratios. Three frequency contours for first four modes are plotted in Figure 4.23. Figure 4.24 shows the crack identification, which give the crack depth ratio of $a/h=0.1$ and crack location ratio of $c/l=0.4$. Due to the off-center mass, crack location ratio of $c/l=0.6$, which is identified as the possible crack location in the symmetric beam, is not a possible crack location.

4.4 Hollow Beam (Ship Backbone) Containing a Through Crack

4.4.1 Ship Model

A hydroelastic model, representing a 1/20th scale model of a version of the Canadian Patrol Frigate (CPF), was built several years ago for modal testing [86]. The model, 6.225m long, had six segments whose joints were located at .762m, 1.524m, 2.286m, 3.048m and 4.176m from the forward end. The six segments were rigidly connected to a backbone to construct a complete ship model. The backbone, which simulated the hull girder, primarily consisted of four continuous stiffeners of carbon fiber composite materials and a box made of lexan plates. The stiffeners were housed in the box by gluing and screwing them properly. The elastic backbone had a hollow rectangular section, which was continuous from the forward segment to the aft segment. While modal parameters and frequency responses for the model were obtained from experiments which were carried out at the Institute for Marine Dynamics (NRCC), St. John's, NF [87,88,89], a rigorous theoretical vibrational analysis of the model ship, with cracked and uncracked backbone, has not been carried out for the model. Such an analysis would help one to identify properly the modal frequencies and mode shapes of the model; in addition, it would also help to detect any crack present in the model and thus assist in preventing further damage to the model.

4.4.2 Simplified Formulation for the Hydroelastic Model

The hydroelastic model of the ship is shown in Figure 4.25. The backbone was centered transversely in the model and the vertical height of its centerline coincided with the model's vertical neutral axis at mid-ship. The rigid segments of the hydroelastic CPF model were mounted on the backbone by using aluminum plates, screwed onto hardwood supports which were glued and bolted on the backbone. The weight and length of the six segments are given in Table 4-4 [86]. There was a 10mm gap between two adjacent segments to allow for relative freedom of movement between each segment. The gap was closed by a flexible membrane so that water does not get in between the segments.

Since the backbone was the only continuous member in the ship model, and the segments only simulated the weight of the ship hull and transferred added mass due to its interaction with water, vibration analysis of the backbone should lead to the correct estimates of modal property for the whole model. The backbone was 4.85m long, 0.127m high, and had a varying width which was 0.132m at one end, 0.108m at the other end and 0.185m near the middle (see Figure 4.26). The vertical bending stiffnesses of the backbone at the joints of various segments are given in Table 4-5. The backbone is then modelled as a rectangular hollow section beam with average wall thickness of 3mm and composed of lexan material. This simplification was made to make use of the available stress intensity factors for computation of crack influence. If the composite material of the backbone was to be considered in analysis, as it exists, then new derivations had to be

obtained for SIF, including determination of complex modes of cracking. The material elastic modulus E is 145GPa and shear modulus G is 58GPa . Using the curve-fit method and values of bending stiffnesses given in Table 4-5[86], the continuous bending stiffness along the beam in vertical direction can be represented by [90]

$$EI = \sum_{i=0}^7 \alpha_i \prod_{j=0}^7 \frac{(x-x_j)}{(x_j-x_i)} \quad (4.45)$$

where

$$\begin{aligned} \alpha_0 &= 471,190, \alpha_1 = 515,733, \alpha_2 = 672,103 \\ \alpha_3 &= 787,894, \alpha_4 = 650,109, \alpha_5 = 562,134 \\ \alpha_6 &= 426,291, \alpha_7 = 328,404 \\ x_0 &= 0, x_1 = 0.4, x_2 = 0.968, x_3 = 2.138 \\ x_4 &= 2.919, x_5 = 3.697, x_6 = 4.474, x_7 = 4.85 \end{aligned} \quad (4.46)$$

Similarly the mass distribution along the beam, converted from the weights of the segments given in Table 4-4, can also be represented by

$$m_s = \sum_{i=0}^6 \beta_i \prod_{j=0}^6 \frac{(x-x_j)}{(x_j-x_i)} \quad (4.47)$$

where

$$\begin{aligned} \beta_0 &= 85, \beta_1 = 90, \beta_2 = 121, \beta_3 = 127 \\ \beta_4 &= 108, \beta_5 = 81, \beta_6 = 30 \end{aligned} \quad (4.48)$$

$$\begin{aligned} x_0 &= 0, x_1 = 0.4, x_2 = 1.553, x_3 = 2.528 \\ x_4 &= 3.308, x_5 = 4.086, x_6 = 4.85 \end{aligned} \quad (4.49)$$

Meanwhile, the mass of segments protruding out from the backbone beam are assumed to act as concentrated masses at the two ends of the backbone, which have the following values

$$\begin{aligned}
 M_{s0} &= 83.5 \text{ kg} \\
 M_{s'} &= 11.33 \text{ kg}
 \end{aligned}
 \tag{4.50}$$

It is also verified that the total mass obtained from the above continuous mass distribution and two concentrated masses at the ends added up to the values given in Table 4-4 along with the backbone mass.

Added fluid mass is added to the ship model during its vibration (heave and sway) in water. The added mass along the length is calculated using the equation given for a floating rectangular section [91] with a hull width of 0.95 m ($=2a$) and a waterline draft 0.31 m ($=b$). As is shown in Figure 4.27, the equation for calculation of added mass in vertical direction is given by

$$m_a = 2k_2 \rho a b \tag{4.51}$$

With $a=0.95/2$, $b=0.31$ and $k_2=1.19$ (see Figure 4.27), added mass is determined as

$$m_a = 2 * 1.19 * 1000 * 0.31 * 0.95 / 2 \text{ kg} / \text{m} = 350.46 \text{ kg} / \text{m} \tag{4.52}$$

Near the two ends of the model ship, the width contacting the water level became gradually narrowed to 0.50 m at one end and 0.0 m at the other end. Added masses at two ends (beyond the length of backbone) are calculated using the same equation (4.51). These two additional added water masses are considered as concentrated loads at the two ends of beam (backbone), which are given as

$$\begin{aligned}
 M_{s00} &= 293 \text{ kg} \\
 M_{s'0} &= 32 \text{ kg}
 \end{aligned}
 \tag{4.53}$$

4.4.3 Formulations for the Vertical Vibration of a Cracked Backbone Beam

4.4.3.1 Bending Stiffness of the Cracked Backbone Beam

For the backbone beam, without any crack, subjected to a bending moment M , the strain energy in the beam is given by

$$U = \frac{1}{2} \int_0^l \frac{M^2}{EI} dx \quad (4.54)$$

When the crack is formed on the upper flange of the beam, and grows from zero to $2a$ perpendicular to the centerline under a constant external bending moment, the energy consumed for crack growth, based on fracture mechanics, is

$$E_c = \int_0^{2a} G dA = \int_0^{2a} G t_c da \quad (4.55)$$

where t_c is the wall thickness of the beam, and G the strain energy release rate. For the vertical vibration of the beam, the crack is mainly subjected to an axial normal load and the shear stress can be neglected; therefore, only the first crack mode exists.

$$G = \frac{K_I^2}{E} \quad (4.56)$$

where K_I is the stress intensity factor for first crack mode, and E is the Young's modulus. For the hollow beam, K_I is given as [1]

$$\begin{aligned} K_I &= \sigma_0 \sqrt{\pi a} F \\ F &= 0.9 + 1.72 \left(\frac{a}{b+h} \right) - 11.42 \left(\frac{a}{b+h} \right)^3 + 140.17 \left(\frac{a}{b+h} \right)^5 \end{aligned} \quad (4.57)$$

where σ_0 is the nominal stress applied to the crack, b the beam width at the position of the crack, h the height of the beam, and

$$\sigma_o = \frac{Mh}{2I_w} \quad (4.58)$$

where I_w is moment inertia of the uncracked beam at the position of the crack. Finally equation (4.55) becomes

$$E_c = DM^2 \quad (4.59)$$

where

$$D = \frac{\pi h^2 F_A(a) I_c a^2}{2I_w^2 E}$$

$$F_A(a) = 0.81 + 4.13 \left(\frac{a}{b+h} \right) + 5.92 \left(\frac{a}{b+h} \right)^2 - 65.78 \left(\frac{a}{b+h} \right)^3 - 209.52 \left(\frac{a}{b+h} \right)^4 + 2306.8 \left(\frac{a}{b+h} \right)^5 + 9801.62 \left(\frac{a}{b+h} \right)^6 - 163915.92 \left(\frac{a}{b+h} \right)^8 + 3353195.33 \left(\frac{a}{b+h} \right)^{10} \quad (4.60)$$

If EI_c is bending stiffness of the cracked hollow beam, the final strain energy in the cracked beam could be alternatively expressed as

$$U_c = \frac{1}{2} \int_0^l \frac{M^2}{EI_c} dx \quad (4.61)$$

where I_c is moment inertia of the cracked beam.

From fracture mechanics, the stresses/strains are highly concentrated around the crack tip, and reach the nominal stress at a region far away from the tip. So it can be assumed that the increase of strain energy due to the crack growth under constant applied loads is mainly concentrated around the crack tip. Therefore, postulating that the distribution of E_c along the beam is similar to (as assumed earlier in sections 4.2.1 and 4.2.2)

$$\frac{Q}{1 + \left(\frac{x-c}{ka}\right)^2} \quad (4.62)$$

where Q and k are coefficients to be determined so that

$$E_c = \int_0^l \frac{Q}{1 + \left(\frac{x-c}{ka}\right)^2} dx \quad (4.63)$$

with c as the location of the crack on the beam. From equations (4.59) and (4.63), one obtains

$$Q = \frac{DM^2}{ka \left[\arctan\left(\frac{l-c}{ka}\right) + \arctan\left(\frac{c}{ka}\right) \right]} \quad (4.64)$$

Substituting equations (4.54), (4.61) and (4.63) into (3.110), one obtains

$$\frac{1}{2} \int_0^l \frac{M^2}{EI_c} dx = \frac{1}{2} \int_0^l \frac{M^2}{EI} dx + \int_0^l \frac{Q}{1 + \left(\frac{x-c}{ka}\right)^2} dx \quad (4.65)$$

From the above equation, one obtains the bending stiffness of the cracked hollow beam as

$$EI_c = \frac{EI}{1 + \frac{EIR}{1 + \left(\frac{x-c}{ka}\right)^2}} \quad (4.66)$$

where $R = \frac{2D}{ka \left[\arctan\left(\frac{l-c}{ka}\right) + \arctan\left(\frac{c}{ka}\right) \right]}$ (4.67)

At the location of the crack, i.e. at $x = c$, (neglecting lower order terms)

$$\frac{EI}{EI_c} = \frac{(bh^3 - (b-2t_c)(h-2t_c)^3)/12}{(bh^3 - (b-2t_c)(h-2t_c)^3)/12 - t_c 2ah^2/4} \quad (4.68)$$

Using equations (4.66) and (4.68),

$$k = 2F_A(a) \left[\frac{(bh^3 - (b-2t_c)(h-2t_c)^3)/12 - t_c 2ah^2/4}{(bh^3 - (b-2t_c)(h-2t_c)^3)/12} \right] \quad (4.69)$$

(notes: $\arctan\left(\frac{l-c}{ka}\right) + \arctan\left(\frac{c}{ka}\right) = \pi$ when the crack is not near the ends of the beam)

4.4.3.2 Characteristic Vibration Equation

For a cracked hollow beam vibrating in water, the equation of bending vibration is given by

$$\frac{\partial^2}{\partial x^2} \left[EI_c \frac{\partial^2 w}{\partial x^2} \right] + m \frac{\partial^2 w}{\partial t^2} + k_f w = 0 \quad (4.70)$$

where m is mass density along the beam length, which includes mass of segments and added mass m_a , and k_f is water stiffness.

$$\begin{aligned} m &= m_s + m_a + m_b \\ k_f &= 9310 \text{ N/m} \end{aligned} \quad (4.71)$$

where m_b is the mass density per unit length of the backbone, m_a is the added mass of water given by equation (4.52) and m_s is the distributed segmental mass give by equation (4.47). The fluid damping was not included in the formulation, since only frequency estimation was made at this stage. In order to consider the concentrated mass at the two ends of the beam, one can use delta functions and get the final vibration equation with the concentrated mass as

$$\frac{\partial^2}{\partial x^2} \left[EI_c \frac{\partial^2 w}{\partial x^2} \right] + m \frac{\partial^2 w}{\partial t^2} + k_f w + \delta(x-0) M_{e0} \frac{\partial^2 w}{\partial t^2} + \delta(x-l) M_{cl} \frac{\partial^2 w}{\partial t^2} = 0 \quad (4.72)$$

where

$$\begin{aligned} M_{e0} &= M_{s0} + M_{a0} \\ M_{cl} &= M_{sl} + M_{al} \end{aligned} \quad (4.73)$$

Let $w = W(x)H(t)$ and with $H(t) = e^{i\omega t}$, and substituting into the above equation, one obtains

$$\frac{d^2}{dx^2} \left[EI_c \frac{d^2 W}{dx^2} \right] - m\omega_c^2 W + k_f W - \delta(x-0) M_{e0} \omega_c^2 W - \delta(x-l) M_{cl} \omega_c^2 W = 0 \quad (4.74)$$

where ω_c is the natural frequency of the cracked hollow beam.

4.4.3.3 Solution

As the model ship floats on water, the boundary conditions for the hollow backbone beam are free/free at the ends. In order to get the first four frequencies and mode shapes, one can use a four-term Galerkin method. To satisfy the boundary conditions, the trial functions are selected from those used for the uncracked beam [83] as

$$W = \sum_{i=1}^4 C_i W_i \quad (4.75)$$

where C_i are coefficients, and W_i s are taken from equation (3.21) as

$$W_i = \sin\left(\frac{p_i x}{l}\right) + \sinh\left(\frac{p_i x}{l}\right) + B_i \left[\cos\left(\frac{p_i x}{l}\right) + \cosh\left(\frac{p_i x}{l}\right) \right]$$

$$B_i = \frac{\cos\left(\frac{p_i x}{l}\right) - \cosh\left(\frac{p_i x}{l}\right)}{\sin\left(\frac{p_i x}{l}\right) + \sinh\left(\frac{p_i x}{l}\right)} \quad (4.76)$$

$$p_1 = 4.73, \quad p_2 = 7.853, \quad p_3 = 10.996, \quad p_4 = 14.173 \quad (4.77)$$

4.4.4 Results and Discussions

The frequencies and mode shapes for vertical vibration are calculated using the MATLAB program. For the uncracked hollow backbone beam, the computed four natural frequencies as well as the ones from tests are shown in Table 4-6. Mode shapes are shown in Figure 4.28. Mode shapes obtained from the tests are shown in Figure 4.29[87]. It can be seen that the calculated frequencies agree well with the test results, but even-order frequencies in tests are missed in the calculation. It appears that the missed frequencies could be the frequencies for the (horizontal) flexural-torsional vibration of the backbone due to the eccentric nature of the added mass for transverse motion; the procedure to determine these frequencies are outlined in Chapter Five. The errors between the first three calculated and experimental frequencies are found to be -0.45%, +4.56% and +6.98% respectively. The stiff and long first segment of the experimental model seems to have affected the results of the measured and computed mode shapes, as can be seen from Figure 4.29; otherwise the first three computed mode shapes represent the measured mode shapes (obtained from six accelerometers only) very closely.

For a cracked backbone, the variation of frequencies against the length of crack at the middle of the backbone is plotted in Figure 4.30. All four frequencies decrease as the crack length increases. As long as the crack occurs in the upper flange only (a less than 0.088m, at the center of the backbone), the frequencies do not change much; this is due to the fact that the bending stiffness of the section is governed by the depth of the section than its width during vertical vibrations. Once the crack penetrates the side webs of the section, the frequencies begin to drop considerably. When the crack length ($2a$) has reached 0.2m (gone through the two side webs to a depth of about 12mm, respectively), the first frequency changes by nearly 11.3%. The second frequency is almost unchanged since the crack is located very close to the vibration node. As the location of the crack in the backbone changes, the four frequencies also get changed. Figure 4.31 shows how the frequencies decrease as the crack location changes along the backbone beam, for a crack length of 0.1m. For all the four modes, when the crack is near the ends, the frequencies remain almost unchanged. For the first mode, maximum frequency change occurs near the middle of the backbone where the bending moment during the vibration is very large. For other modes, there are some locations at which the frequencies do not decrease or decrease very little. This is due to the fact that these locations are vibration nodes corresponding to that mode. Using the modal changes that occur for any particular beam, the probable location of the crack could be easily located by examining different modes together.

Results from vertical vibration analysis agree well with the earlier test results for cracked beam [87], however, some frequencies, obtained from the tests, could not be calculated

from vertical vibration analysis. It is suggested that these frequencies could come from horizontal vibration, which would be coupled with torsional vibration due to asymmetric added fluid mass. Such coupled vibration as well as crack detection will be analyzed in the next chapter.

4.5 Closure

Variation of equivalent bending stiffness and depth (along the length) for the cracked beam are obtained using an energy-based model. Four modes are obtained for a simply supported beam and a fixed-fixed beam by selecting proper Galerkin's functions. Generally the crack would decrease the frequencies; however, the changes of frequencies are also dependent on the crack location. If the crack coincides with the vibration node of one mode, the frequency for that mode remains almost unchanged. The crack near the ends would influence the boundary constraints, and thus decrease the frequencies significantly as shown for the case of the fixed-fixed beam. The contour lines of frequency can be plotted for various modes for a beam containing one crack. The existing crack (in the beam) will belong to one particular contour in each mode. When these particular contours from different modes are plotted together, the intersection point(s) of the contours would provide the location and depth of the crack.

The ship model is modelled as a hollow beam with varying stiffness and mass. The interaction with water is taken into account by calculating the added fluid mass, and the beam is then assumed to vibrate in water with free-free boundary conditions. The results

of vertical vibration agree well with test results (for uncracked beam). When the backbone of the ship model contains a thickness-through crack, the frequencies decrease. When the crack size grows beyond the width of the backbone, the frequencies drop significantly because of massive loss of its stiffness at the crack location.

Table 4-1 Frequency comparison for four and eight terms Galerkin's method

 $(a/h=0.25, c/l=0.8)$

Particulars	Terms	First Freq.	Second Freq.	Third Freq.	Fourth Freq.
		$(C_1 \sqrt{\frac{EI}{\rho A}})$	$(C_2 \sqrt{\frac{EI}{\rho A}})$	$(C_3 \sqrt{\frac{EI}{\rho A}})$	$(C_4 \sqrt{\frac{EI}{\rho A}})$
		C_1	C_2	C_3	C_4
Simply Supported	4	1.09275	4.34286	9.74582	17.38584
	8	1.09265	4.34162	9.74220	17.38066
Cracked Beam	Difference (%)	0.009	0.028	0.037	0.03
Uncracked Beam		1.0966	4.3865	9.8696	17.5460
Fixed	4	2.4847	6.8241	13.32706	22.05678
Cracked Beam	8	2.48468	6.82344	13.32369	22.05164
	Difference (%)	0.008	0.01	0.025	0.023
Uncracked Beam		2.4859	6.8522	13.4347	22.2061

Table 4-2 Frequency comparison for four and eight terms Galerkin's method

 $(a/h=0.5, c/l=0.8)$

particulars	Terms	First Freq.	Second Freq.	Third Freq.	Fourth Freq.
		$(C_1 \sqrt{\frac{EI}{\rho A}})$	$(C_2 \sqrt{\frac{EI}{\rho A}})$	$(C_3 \sqrt{\frac{EI}{\rho A}})$	$(C_4 \sqrt{\frac{EI}{\rho A}})$
		C ₁	C ₂	C ₃	C ₄
Simply Supported	4	1.073681	4.163988	9.32906	16.89723
	8	1.071566	4.142127	9.27774	16.83074
Cracked Beam	Difference (%)	0.19	0.5	0.55	0.4
Ucracked Beam		1.0966	4.3865	9.8696	17.5460
Fixed	4	2.46262	6.64534	12.75247	21.34871
	8	2.46185	6.61838	12.65194	21.22287
Cracked Beam	Difference (%)	0.03	0.4	0.79	0.6
Ucracked Beam		2.4859	6.8522	13.4347	22.2061

Table 4-3 Frequency comparison between simply supported beam with and without off-center mass attached

Particulars	First Freq.	Second Freq.	Third Freq.	Fourth Freq.
	$(C_1 \sqrt{\frac{EI}{\rho A}})$	$(C_2 \sqrt{\frac{EI}{\rho A}})$	$(C_3 \sqrt{\frac{EI}{\rho A}})$	$(C_4 \sqrt{\frac{EI}{\rho A}})$
	C_1	C_2	C_3	C_4
Simply Supported Beam (no crack)	1.0966	4.3865	9.87	17.546
With Off-center Mass Attached (no crack)	1.045	4.0312	9.5246	17.546
Difference (%)	4.7	8.1	3.5	0
Simply Supported Beam (crack: $a/h=0.2, c/l=0.5$)	1.0767	4.3822	9.7065	17.5121
With Off-center Mass (crack: $a/h=0.2, c/l=0.5$)	1.0264	4.0271	9.365	17.5121
Difference (%)	4.7	8.1	3.5	0

Table 4-4 Properties of CPF hydroelastic model

Section at	Weight (N)	Length (m)
Segment 1	1643.5	1.965
Segment 2	1392.7	1.170
Segment 3	972.3	0.781
Segment 4	823.3	0.778
Segment 5	615.5	0.777
Segment 6	222.2	0.753
Total	5669.5	6.225

Table 4-5 Stiffness of the Backbone at the Connections of Segments

Between Segments	Bending Stiffness EI (Nm ²)
1-2	672,103
2-3	787,894
3-4	650,109
4-5	562,123
5-6	426,291

Table 4-6 Frequencies of Uncracked Backbone

Frequency (Hz)	1st	2nd	3rd	4th	5th	6th
Calculation	4.46	N/A	12.60	N/A	26.36	N/A
Test	4.48	6.35	12.05	19.63	24.64	38.65

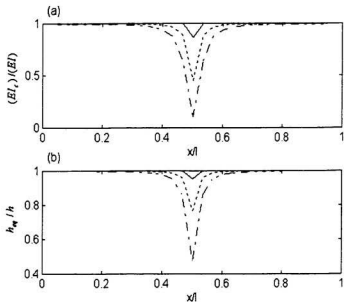


Figure 4.1 Variation of normalized bending stiffness and depth of a beam with a crack (crack location $c/l = 0.5$); — $a/h = 0.05$; $a/h = 0.25$; - - - $a/h = 0.5$

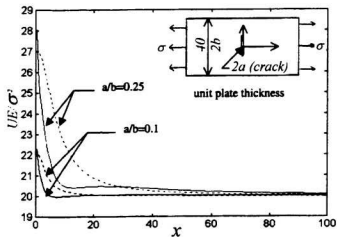


Figure 4.2 Energy distribution in x-direction for a finite cracked plate (U – the strain energy over plate width, E – the elastic modulus); — elastic fracture mechanics theory; theory used in this paper

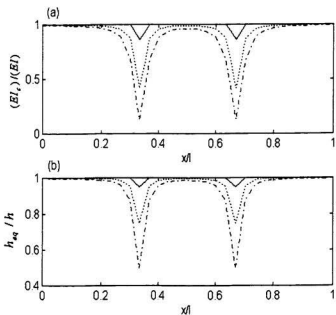


Figure 4.3 Variation of normalized bending stiffness and depth of a beam with two cracks (crack locations $c_1/l = 1/3$, $c_2/l = 2/3$); — $a/h = 0.05$; $a/h = 0.25$; - - - $a/h = 0.5$

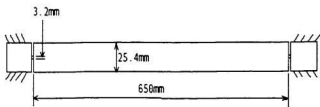


Figure 4.4 Simply supported experimental beam



Figure 4.5 Experimental set up showing the electronic equipment

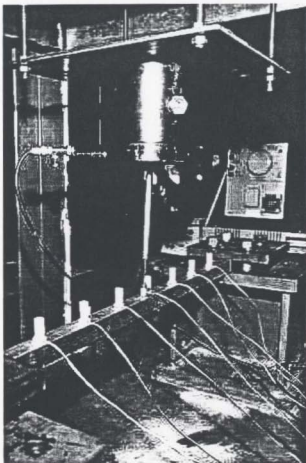


Figure 4.6 Experimental set up showing a connected beam

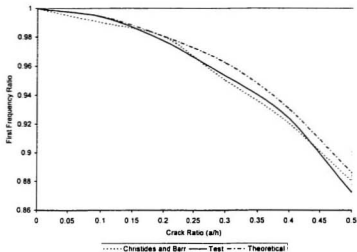


Figure 4.7 Comparison of experimental and theoretical values of frequency ratio

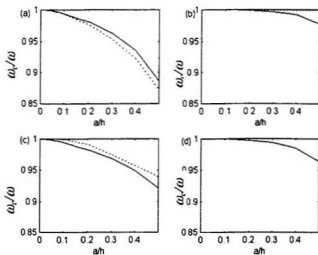


Figure 4.8 Variations of the first four frequencies as a function of crack depth for a simply supported beam (crack location $c/l = 0.5$, ω_n/ω – frequency ratio); (a) mode one; (b) mode two; (c) mode three; (d) mode four (--- experimental, — theory)

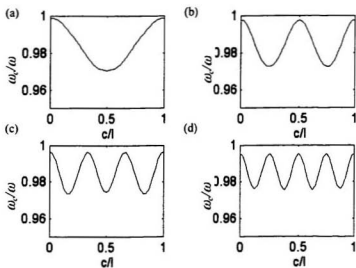


Figure 4.9 Variations of the first four frequencies as a function of crack location for a simply supported beam (crack depth ratio $a/h = 0.25$); (a) mode one; (b) mode two; (c) mode three; (d) mode four

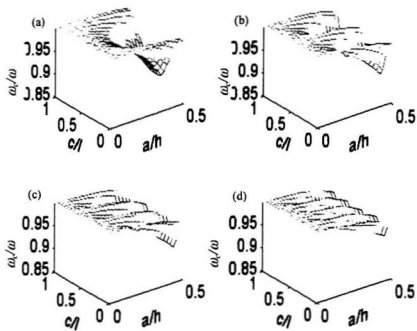


Figure 4.10 Frequencies vs. crack locations and depths for a simply supported beam; (a) mode one; (b) mode two; (c) mode three; (d) mode four

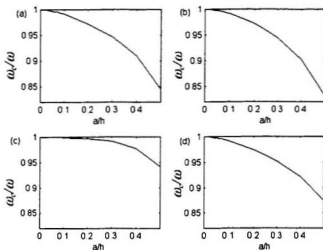


Figure 4.11 Variation of frequency as a function of crack depth for a simply supported beam with two cracks ($c_1/l = 1/3$, $c_2/l = 2/3$); (a) mode one; (b) mode two; (c) mode three; (d) mode four

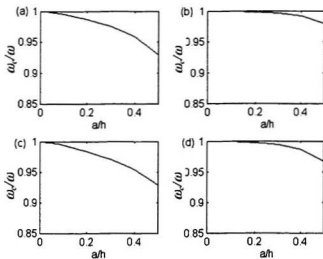


Figure 4.12 Variations of the first four frequencies as a function of crack depth for a fixed-fixed beam (crack location $c/l = 0.5$); (a) mode one; (b) mode two; (c) mode three; (d) mode four

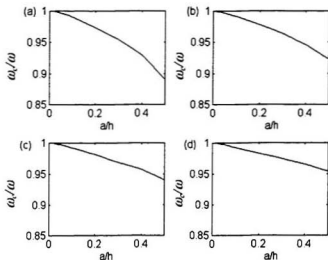


Figure 4.13 Variations of the first four frequencies as a function of crack depth for a fixed-fixed beam (crack location $c/l = 0$); (a) mode one; (b) mode two; (c) mode three; (d) mode four

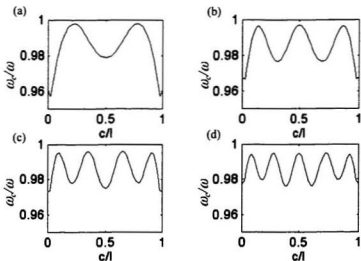


Figure 4.14 Variations of the first four frequencies as a function of crack location for a fixed-fixed cracked beam (crack depth ratio $a/h = 0.25$); (a) mode one; (b) mode two; (c) mode three; (d) mode four

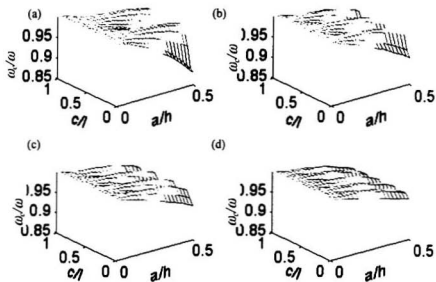


Figure 4.15 Frequencies vs. crack depths and locations for a fixed-fixed beam; (a) mode one; (b) mode two; (c) mode three; (d) mode four

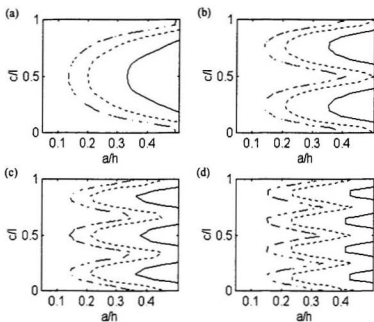


Figure 4.16 Frequency contours for a simply supported beam with a single crack; (a) mode one; (b) mode two; (c) mode three; (d) mode four; — $\omega_c/\omega = 0.95$; $\omega_c/\omega = 0.98$; - - - $\omega_c/\omega = 0.99$

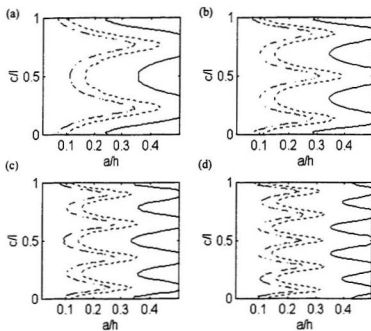


Figure 4.17 Frequency contours for a fixed-fixed beam with a single crack; (a) mode one; (b) mode two; (c) mode three; (d) mode four; — $\omega_c/\omega = 0.96$; $\omega_c/\omega = 0.98$; - - - $\omega_c/\omega = 0.99$

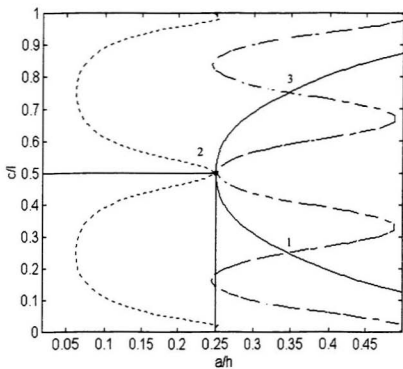


Figure 4.18 Crack identification by frequency contours from three different modes in a simply supported beam; — $\omega_c/\omega = 0.9708$; $\omega_c/\omega = 0.9972$; - - - $\omega_c/\omega = 0.9744$; (Deduction: $a/h = 0.25$, $c/l = 0.5$)

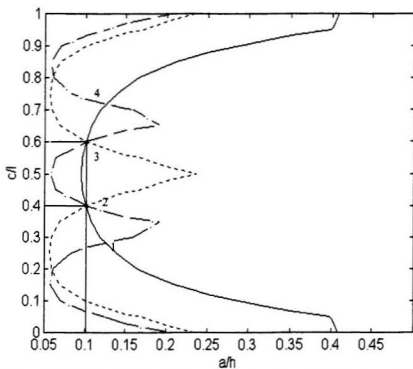


Figure 4.19 Crack identification by frequency contours from three different modes in a simply supported beam; — $\omega_c / \omega = 0.9947$; $\omega_c / \omega = 0.9979$; - - - $\omega_c / \omega = 0.9978$; (Deduction: $a/h = 0.1$, $c/l = 0.4$ or 0.6)

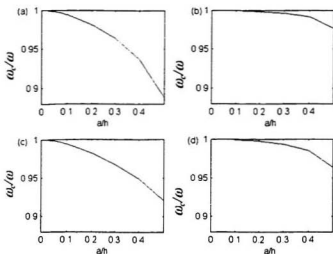


Figure 4.20 Variations of the first four frequencies as a function of crack depth for a simply supported beam with an off-center mass attached (crack location ratio $c/l = 0.5$); (a) mode one; (b) mode two; (c) mode three; (d) mode four

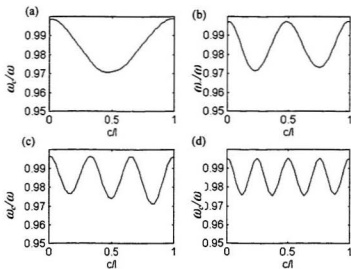


Figure 4.21 Variations of the first four frequencies as a function of crack location for a simply supported beam with an off-center mass attached (crack depth ratio $a/h = 0.25$); (a) mode one; (b) mode two; (c) mode three; (d) mode four

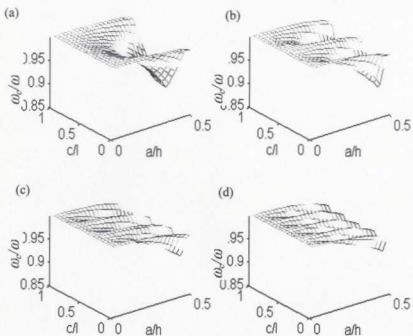


Figure 4.22 Frequencies vs. crack depths and crack locations for a simply supported beam with an off-center mass attached; (a) mode one; (b) mode two; (c) mode three; (d) mode four

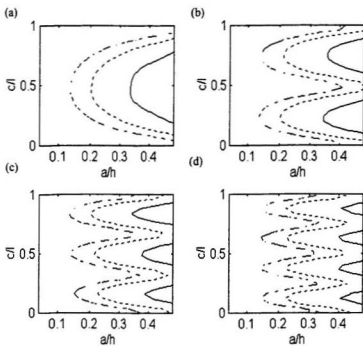


Figure 4.23 Frequency contours for a simply supported cracked beam with an off-center mass attached; (a) mode one; (b) mode two; (c) mode three; (d) mode four; — $\omega_c / \omega = 0.95$; $\omega_c / \omega = 0.98$; - - - $\omega_c / \omega = 0.99$

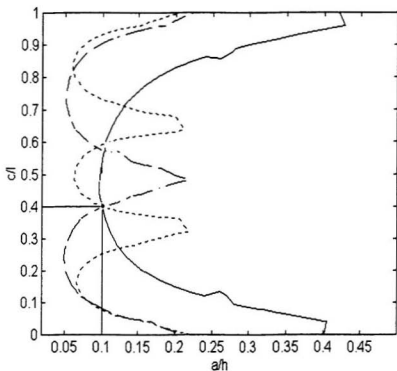


Figure 4.24 Crack identification by frequency contours from three different modes in a simply supported beam with off-center mass attached; — $\omega_c/\omega = 0.9946$; $\omega_c/\omega = 0.9976$; - - - $\omega_c/\omega = 0.9983$; (Deduction: $a/h = 0.1$, $c/l = 0.4$)

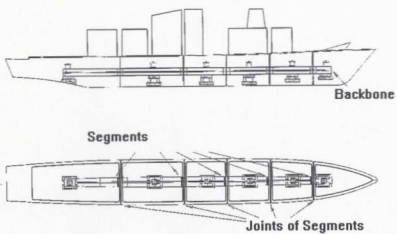


Figure 4.25 CPF ship model [87]

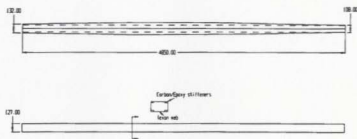


Figure 4.26 Backbone of ship model

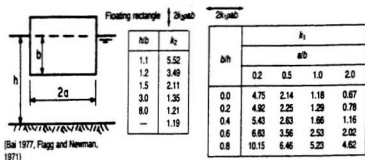


Figure 4.27 Added mass of two-dimensional body [91]

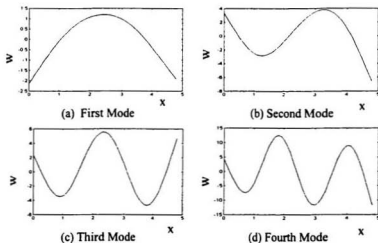


Figure 4.28 Mode shapes for the uncracked backbone, W —displacement, X —beam length

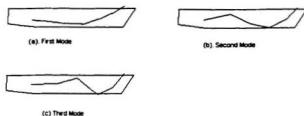


Figure 4.29 Mode shapes from tests for the uncracked backbone

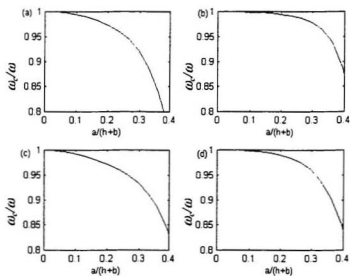


Figure 4.30 Variations of first four normalized frequencies as a function of crack length ratio for the ship beam (backbone) model (crack location ratio $c/l=0.5$); (a) mode one; (b) mode two; (c) mode three; (d) mode four.

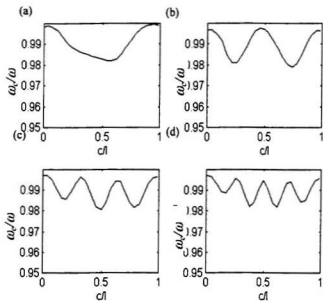


Figure 4.31 Variations of first four normalized frequencies as a function of crack location ratio for the ship beam (backbone) model (crack length ratio $a/(h+b)=0.17$); (a) mode one; (b) mode two; (c) mode three; (d) mode four.

Chapter 5

Coupled Bending-Torsional Vibration of a Cracked Hollow Beam Model in Water and Identification of Cracking

5.1 Introduction

In an earlier study, details of which are given in section 4.4, vertical vibration analysis of the model floating in water was carried out. For numerical analysis, the model was simplified as a hollow rectangular section beam of a single material with varying width, and the computed frequencies agreed with the results (odd-numbered frequencies) of tests (Table 4-6). However, even-numbered frequencies in tests were missed in the numerical analysis results. The missing frequencies must have come from some other vibrational modes which were not modelled in the numerical analysis. The floating model would vibrate vertically due to the heave exciting wave forces and horizontally due to the horizontal wave forces exerted on the model. It should also be remembered that the floating body would undergo horizontal flexural and torsional motions due to the eccentric nature of added mass and wave exciting force components. The combination of horizontal flexural and torsional vibrations would be the motions of missed frequencies obtained from modal tests. The study reported herein considers coupled horizontal flexural-torsional motions of the floating body through an approximate numerical procedure, based on Galerkin's weighted residual approach.

For the bending-torsional vibration of an Euler beam, Timshenko *et al* [92] derived the coupled bending-torsion equations for a channel whose cross section was asymmetric. They assumed a simple trigonometric-form solution in both transverse and torsional displacements, and obtained vibration frequencies. Rao [71] obtained the bending-torsion equations for an asymmetric beam without warping using Hamilton's principle. In 1987, Dokumaci [93] developed the exact solution for such coupled vibration equations without warping. After applying boundary conditions, the natural frequencies and mode shapes were determined by letting the determinant of six coefficients equal to zero. In 1999, Banerjee [94] presented essentially the same exact solution for coupled bending-torsional vibration. The frequencies and mode shapes were calculated using a computing package called REDUCE. Bishop *et al* [95] extended Dokumaci's solution to allow for warping. It was shown that warping could make a large difference to results for thin-walled beams of open cross section. Coupled bending-torsional vibrations of non-uniform Timshenko beams (including shear deflection and rotary inertia) with open cross-section were studied by Bishop and Price [96] and Bercin and Tanaka [97]. Warping was considered in Bercin and Tanaka's study, and numerical results were also provided.

Most of the studies in coupled bending-torsional vibration were carried out for asymmetric cross sections which had their shear centers misaligned with respect to their centroids, and thus generated bending vibration coupled with torsion. Also for a non-uniform beam, it would be difficult if not impossible to derive exact solutions. The present study will derive equations of coupled bending-torsional vibrations due to added

water mass applied on the lower portions of two flanks during vibration in water. For the varying-stiffness, varying mass, non-uniform hollow beam, Galerkin's method is applied to calculate frequencies and mode shapes. When the beam contains a crack, equivalent bending and torsion stiffnesses are determined by an energy procedure. Frequencies and mode shapes for cracked backbone are also calculated. Finally detailed analysis of the results is carried out to develop a method for identifying the crack size and location.

5.2 Parameters of Model

The weight and length of the ship model are given in Table 4-4. The vertical stiffnesses of the backbone at the joints of various segments are given in Table 4-5. Other properties (used for horizontal bending-torsional vibration) of the backbone at the joints of various segments are given in Table 5-1. The varying segmental stiffness of the backbone, given in Table 5-1 [86], was converted into a continuous stiffness distribution as shown in section 4.4.2. The segmental mass was also converted into a continuous varying mass as explained in section 4.4.2.

When the model of ship structure vibrates horizontally on water, fluid inertial effect is taken into account by considering added fluid mass as an extra distributed mass on the model. The added mass along the beam length is calculated using the equation given for a floating rectangular section [91] with a hull width of 0.95m and a waterline draft of 0.31m. For horizontal motion, the equation (see Figure 4.27) is given by

$$m_a = 2k_1 \rho a b \quad (5.1)$$

Interpolating the table in Figure 4.27, one obtains $k_1=0.89$, $a=0.95/2$ and $b=0.31$; then

$$m_a = 2 \times 0.89 \times 1000 \times 0.95 \times 0.31 / 2 = 262.105 \text{ (kg/m)} \quad (5.2)$$

The added mass is considered to act at 0.1m below neutral plane of the backbone, i.e.

$$z_0 = 0.1m \quad (5.3)$$

5.3 Equations of Coupled Vibrations in Water

Since the backbone is the only continuous and elastic member, and rigid segments are merely used to simulate the mass of ship hull, vibration analysis is applied to the backbone which is considered as a hollow rectangular Euler beam with varying width. In the horizontal direction, bending vibration will be accompanied by torsional motion due to added water mass. To develop the coupled bending-torsional vibration equations, Hamilton's principle was used.

Without considering warping (Figure 5.1), displacements of any point in the beam for horizontal bending and torsion are represented by (see Figure 5.2)

$$\begin{aligned} u_x &= -yv' \\ u_y &= v - z\theta \\ u_z &= y\theta \end{aligned} \quad (5.4)$$

where v is displacement of neutral axis in y direction, θ is torsional rotation of beam; x direction is parallel to the beam length. The prime in equation (5.4) denotes differentiation with respect to position x . Strains can be obtained as

$$\begin{aligned}
 \epsilon_{xx} &= -yv'' \\
 \gamma_{xy} &= -z\theta' \\
 \gamma_{xz} &= y\theta' \\
 \epsilon_{yy} = \epsilon_{zz} = \gamma_{yz} &= 0
 \end{aligned}
 \tag{5.5}$$

Strain energy is therefore determined by

$$\begin{aligned}
 U &= \frac{1}{2} \int_0^l \int (Ey^2v''^2 + Gz^2\theta'^2 + Gy^2\theta'^2) dx dA \\
 &= \frac{1}{2} \int_0^l (EI_z v''^2 + GI_p \theta'^2) dx
 \end{aligned}
 \tag{5.6}$$

where l is the length of the backbone beam.

$$\begin{aligned}
 I_p &= \int (z^2 + y^2) dA \\
 I_z &= \int y^2 dA
 \end{aligned}
 \tag{5.7}$$

Neglecting the axial inertia, velocities at any point in the beam are given by

$$\begin{aligned}
 \dot{u}_x &= 0 \\
 \dot{u}_y &= \dot{v} - z\dot{\theta} \\
 \dot{u}_z &= y\dot{\theta}
 \end{aligned}
 \tag{5.8}$$

where the dot denotes differentiation with respect to time t . The velocity of added mass is given by

$$\dot{u}_e = \dot{v} - z_0\dot{\theta}
 \tag{5.9}$$

where z_0 is the distance to neutral axis from the center of added mass. The total kinetic energy could be expressed as

$$\begin{aligned}
T &= \frac{1}{2} \int_0^l \int \rho \dot{v}^2 dx dA + \frac{1}{2} \int_0^l \int \rho (z^2 + y^2) \dot{\theta}^2 dx dA \\
&+ \int_0^l \int \rho (-z \dot{v} \dot{\theta}) dx dA + \frac{1}{2} \int_0^l m_a (\dot{v} - z_0 \dot{\theta})^2 dx \\
&= \frac{1}{2} \int_0^l (\rho A + m_a) \dot{v}^2 dx + \frac{1}{2} \int_0^l (\rho I_p + m_a z_0^2) \dot{\theta}^2 dx + \int_0^l m_a (-z_0 \dot{v} \dot{\theta}) dx
\end{aligned} \tag{5.10}$$

where ρA is mass of the model ship per unit length.

For free vibration, application of Hamilton's principle leads to

$$\begin{aligned}
\delta \int_{t_1}^{t_2} (T - U) dt &= \delta \int_0^l \int_0^{t_2} \left\{ \frac{1}{2} (\rho A + m_a) \dot{v}^2 + \frac{1}{2} (\rho I_p + m_a z_0^2) \dot{\theta}^2 \right. \\
&+ m_a (-z_0 \dot{v} \dot{\theta}) - \frac{1}{2} E I_z v''^2 - \frac{1}{2} G I_p \theta''^2 \left. \right\} dx dt = 0
\end{aligned} \tag{5.11}$$

Expansion of the above equation yields two coupled vibration equations, viz.,

$$\begin{aligned}
(E I_z v'')'' + (\rho A + m_a) \ddot{v} &= m_a z_0 \ddot{\theta} \\
-(G I_p \theta'')' + (\rho I_p + m_a z_0^2) \ddot{\theta} &= m_a z_0 \ddot{v}
\end{aligned} \tag{5.12}$$

The ship segments protruding outside the backbone are assumed to act as concentrated masses at the two ends of beam (backbone); so are the added water masses on these parts of ship model. According to the earlier discussions in section 4.4, the total concentrated masses at the two ends are as follows

$$\begin{aligned}
m_{e0} &= 319.9 \text{ kg} \\
m_{e1} &= 11.33 \text{ kg}
\end{aligned} \tag{5.13}$$

Effective radii of gyration for these concentrated masses are

$$\begin{aligned}
r_0 &= 0.075 \text{ m} \\
r_1 &= 0.068 \text{ m}
\end{aligned} \tag{5.14}$$

Concentrated masses could be considered using delta functions; so the final coupled vibration equations are given by

$$\begin{aligned} (EI_z v'')'' + (\rho A + m_a) \ddot{v} + \delta(x-0)m_{c0} \ddot{v} + \delta(x-l)m_{cl} \ddot{v} = m_a z_0 \ddot{\theta} \\ - (GI_p \theta'')' + (\rho I_p + m_a z_0^2) \ddot{\theta} + \delta(x-0)m_{c0} r_0^2 \ddot{\theta} + \delta(x-l)m_{cl} r_l^2 \ddot{\theta} = m_a z_0 \ddot{v} \end{aligned} \quad (5.15)$$

5.4 Natural Frequencies and Mode Shapes

Since the vertical motion is not coupled with the horizontal/torsional motion of the beam, the solutions are obtained separately; this was achieved in section 4.4 and the results are given in Table 4-6 and Figure 4.28. Here the frequencies and modal vectors are computed for the coupled horizontal bending-torsional vibration. In order to get approximate eigenvalues and eigenvectors for the problem, the hollow beam is first modelled as a uniform beam to determine the initial trial functions and frequency values required in Galerkin's procedure. For uniform beams, bending stiffness and torsion stiffness are constant; then the above equations (5.12) could be expressed as

$$\begin{aligned} EI_z v'''' + (\rho A + m_a) \ddot{v} = m_a z_0 \ddot{\theta} \\ - GI_p \theta'''' + (\rho I_p + m_a z_0^2) \ddot{\theta} = m_a z_0 \ddot{v} \end{aligned} \quad (5.16)$$

Equations (5.16) have exact solutions [93,94]. However, for equations (5.12) and (5.15), bending stiffness, torsion stiffness and line mass density are all varying along beam length due to varying width; hence it is difficult to find exact solutions for this beam. So Galerkin's method is used to calculate frequencies and mode shapes. First, average values of bending stiffness, torsion stiffness and line mass density for the whole ship length are calculated and used in equations (5.16), and the frequencies are computed using

MATLAB. Then, the obtained frequencies and mode shapes are selected as trial functions in Galerkin's method for coupled vibration.

Average values are obtained as (refer Table 5-1)

$$\begin{aligned}
 EI_z &= 958,986.8 \\
 GI_p &= 630,677.08 \\
 \rho A &= 94.5 \\
 \rho I_p &= 2.5174
 \end{aligned}
 \tag{5.17}$$

After introducing $v(x,t) = V(x)e^{i\omega t}$, $\theta(x) = \Theta(x)e^{i\omega t}$, equations (5.16) can be written as

$$\begin{aligned}
 EI_z V'''' - (\rho A + m_a)\omega^2 V + m_a z_0 \omega^2 \Theta &= 0 \\
 GI_p \Theta'' + (\rho I_p + m_a z_0^2)\omega^2 \Theta - m_a z_0 \omega^2 V &= 0
 \end{aligned}
 \tag{5.18}$$

The exact solution of the above equations are determined. The first four frequencies are obtained as

$$\omega_i = 29.2, 134.7, 261.4, 426.3 \text{ rad/sec } (i=1,2,3,4).
 \tag{5.19}$$

The first four modal vectors are obtained as

$$\begin{aligned}
 A_{ij} &= [1, -.98225, .99233, -.97085, -.006278, -.00173] \\
 &[1, -1.00084, .97864, -.96927, .00719, -.00793] \\
 &[1, -.99996, .95955, -.93923, -.00303, -.02119] \\
 &[1, -1.00000, .93923, -.90145, -.04656, -.04365]
 \end{aligned}
 \tag{5.20}$$

where $i=1,2,3,4$ for rows, $j=1,2,3,4,5,6$ for columns.

The corresponding modes could be written as

$$\begin{aligned}
V_i &= A_{11} \cosh(\alpha, x/l) + A_{12} \sinh(\alpha, x/l) + A_{13} \cos(\beta, x/l) \\
&\quad + A_{14} \sin(\beta, x/l) + A_{15} \cos(\gamma, x/l) + A_{16} \sin(\gamma, x/l) \\
\Theta_i &= k_m A_{11} \cosh(\alpha, x/l) + k_m A_{12} \sinh(\alpha, x/l) + k_m A_{13} \cos(\beta, x/l) \\
&\quad + k_m A_{14} \sin(\beta, x/l) + k_{c1} A_{15} \cos(\gamma, x/l) + k_{c1} A_{16} \sin(\gamma, x/l)
\end{aligned} \tag{5.21}$$

where

$$\begin{aligned}
\alpha_i &= [2(q_i/3)^{0.5} \cos(\phi_i/3) - a_i/3]^{0.5} \\
\beta_i &= [2(q_i/3)^{0.5} \cos((\pi - \phi_i)/3) + a_i/3]^{0.5} \\
\gamma_i &= [2(q_i/3)^{0.5} \cos((\pi + \phi_i)/3) + a_i/3]^{0.5} \\
q_i &= b_i + a_i^2/3 \\
\phi_i &= \arccos[(27a_i b_i c_i - 9a_i b_i - 2a_i^3) / \{2(a_i^2 + 3b_i)^{1.5}\}]
\end{aligned} \tag{5.22}$$

and

$$\begin{aligned}
a_i &= (\rho l_p + m_a z_0^2) \omega^2 l^2 / (G I_p) \\
b_i &= (\rho A + m_a) \omega^2 l^4 / (E I_z) \\
c_i &= 1 - m_a^2 z_0^2 / (\rho l_p + m_a z_0^2) / (\rho A + m_a) \\
k_m &= (b_i - \alpha_i^4) E I_z / (m_a z_0 \omega^2 l^4) \\
k_{m1} &= (b_i - \beta_i^4) E I_z / (m_a z_0 \omega^2 l^4) \\
k_{c1} &= (b_i - \gamma_i^4) E I_z / (m_a z_0 \omega^2 l^4)
\end{aligned} \tag{5.23}$$

For equations (5.15), assumption of a harmonic motion of frequency ω would lead to

$$\begin{aligned}
(E I_p V''')' - (\rho A + m_a) \omega^2 V - \delta(x-0) m_{c0} \omega^2 V - \delta(x-l) m_{c1} \omega^2 V + m_a z_0 \omega^2 \Theta = 0 \\
-(G I_p \Theta')' + (\rho l_p + m_a z_0^2) \omega^2 \Theta + \delta(x-0) m_{c0} r_0^2 \omega^2 \Theta + \delta(x-l) m_{c1} r_1^2 \omega^2 \Theta - m_a z_0 \omega^2 V = 0
\end{aligned} \tag{5.24}$$

Now solutions of equations (5.24) are selected as

$$\begin{aligned}
 V &= \sum_{i=1}^k C_i V_i \\
 \Theta &= \sum_{i=1}^k D_i \Theta_i
 \end{aligned}
 \tag{ 5.25}$$

where C_i and D_i are coefficients, V_i and Θ_i are trial functions which come from equations (5.21).

Upon making the residuals (Galerkin' s method) for each of the trial functions equal to zero, natural frequencies (bending-torsional) for the floating hydroelastic model vibrating on water could be calculated using MATLAB program. The first four frequencies are compared with the results of tests in Table 5-2. The mode shapes obtained for horizontal and torsional motions are shown in Figure 5.3. Figure 5.4 shows the mode shapes for bending motion only, and Figure 5.5 for torsion motion only.

5.5 Formulations for Cracked Backbone

When the hollow backbone contains a through crack, stiffnesses of backbone will decrease. Stiffnesses for cracked backbone will be determined using an energy procedure.

5.5.1 Horizontal Bending Stiffness of Cracked Beam

Under a constant external bending moment, strain energy of beam is increased after crack growth [72]. The increase of strain energy equals to the energy consumed by crack growth.

$$U_c = U + V_c \quad (5.26)$$

where U_c is the strain energy in beam after crack growth, U the strain energy prior to crack growth, V_c is energy for crack growth. For the uncracked backbone under constant external bending moment M in horizontal direction, the strain energy in the backbone could be written as

$$U = \frac{1}{2} \int_0^l \frac{M^2}{EI_z} dx \quad (5.27)$$

When a crack is formed in the flank (or even in the flange when the crack grows) of backbone under bending moment M in horizontal direction, and grows from zero to $2a$ (see Figure 5.6), the energy consumed for crack growth, based on fracture mechanics principle, would be

$$V_c = \int_0^{2a} \frac{K_I^2 t}{E} da \quad (5.28)$$

where K_I is the stress intensity factor for first crack mode, and t is the wall thickness of beam. For a rectangular hollow beam of close section, K_I is given as [1]

$$\begin{aligned}
 K_I &= \sigma_0 \sqrt{\pi a} F \\
 \sigma_0 &= \frac{Mb}{2I_z} \\
 F &= 0.9 + 1.72\left(\frac{a}{h+b}\right) - 11.42\left(\frac{a}{h+b}\right)^3 + 140.17\left(\frac{a}{h+b}\right)^5
 \end{aligned}
 \tag{5.29}$$

where h is the height of the beam, and $2b$ is the width at the position of the crack.

Substitution of eqn. (5.29) into eqn. (5.28) yields

$$V_c = DM^2 \tag{5.30}$$

where

$$D = \frac{\pi b^3 F_h(a) t a^2}{2 I_z^2 E} \tag{5.31}$$

and $F_h(a)$ is given in equation (4.60). If the horizontal bending stiffness of cracked hollow beam is denoted by EI_c , the strain energy in the cracked beam could be alternatively expressed as

$$U_c = \frac{1}{2} \int_0^l \frac{M^2}{EI_c} dx \tag{5.32}$$

As stated above, V_c equals the increase of strain energy in the beam after crack growth.

From fracture mechanics considerations, stresses/strains are very high around the crack tip, but remain unchanged in far field under constant load. Therefore, the increase of strain energy is mainly concentrated near the crack tip. Keeping this in mind, the distribution of V_c along the beam could be then assumed as

$$\frac{Q}{1 + \left(\frac{x-c}{ka}\right)^2} \tag{5.33}$$

where Q and k are coefficients to be determined so that

$$V_c = \int_0^l \frac{Q}{1 + \left(\frac{x-c}{ka}\right)^2} dx \quad (5.34)$$

where c is the crack location. It can be seen that equation (5.33) has the maximum value at crack location ($x = c$), and decreases quickly as x moves away from the crack. From equations (5.30) and (5.34), Q is determined as

$$Q = \frac{DM^2}{ka \left[\arctan\left(\frac{l-c}{ka}\right) + \arctan\left(\frac{c}{ka}\right) \right]} \quad (5.35)$$

Substitution of equations (5.27), (5.32) and (5.34) into (5.26) leads to

$$\frac{1}{2} \int_0^l \frac{M^2}{EI_c} dx = \frac{1}{2} \int_0^l \frac{M^2}{EI_z} dx + \int_0^l \frac{Q}{1 + \left(\frac{x-c}{ka}\right)^2} dx \quad (5.36)$$

From the above equation, the bending stiffness of cracked hollow beam is obtained as

$$EI_c = \frac{EI_z}{1 + \frac{EI_z R}{1 + \left(\frac{x-c}{ka}\right)^2}} \quad (5.37)$$

where

$$\begin{aligned} R &= \frac{2D}{ka \left[\arctan\left(\frac{l-c}{ka}\right) + \arctan\left(\frac{c}{ka}\right) \right]} \\ &= \frac{mb^3 F_n(a) t a}{EI_z k \left[\arctan\left(\frac{l-c}{ka}\right) + \arctan\left(\frac{c}{ka}\right) \right]} \end{aligned} \quad (5.38)$$

Moment of inertia I_z could be determined by the given dimensions of cross section of hollow beam. At the location of the crack, i.e. $x = c$, moment of inertia is decreased by

the area ($2ar$) of the crack multiplying square of the distance ($b/2$) from the crack to the neutral axis. So one has

$$\frac{EI_z}{EI_c} = \frac{[hb^3 - (h-2t)(b-2t)^3]/12}{[hb^3 - (h-2t)(b-2t)^3]/12 - 2atb^2/4} \quad (5.39)$$

Using equations (5.36) and (5.38), k is determined as

$$k = 2F_c(a) \frac{[hb^3 - (h-2t)(b-2t)^3] - 6atb^2}{[hb^3 - (h-2t)(b-2t)^3]} \quad (5.40)$$

5.5.2 Torsional Stiffness of Cracked Beam

Consider the hollow beam subjected to a constant external torque T . After a crack forms and grows, the strain energy in the beam will be equal to strain energy in the uncracked beam plus the energy consumed by crack growth. Following the same procedure given in section 5.5.1, the torsional stiffness of cracked hollow beam is obtained as

$$GI_c = \frac{GI_p}{1 + \frac{GI_p R_t}{1 + \left(\frac{x-c}{k,a}\right)}} \quad (5.41)$$

where

$$R_t = \frac{\pi F_c(a)a}{Eh^2b^2t} \frac{1}{k_t \left[\arctan\left(\frac{l-c}{k,a}\right) + \arctan\left(\frac{c}{k,a}\right) \right]} \quad (5.42)$$

and

$$\begin{aligned}
F_w(a) = & 2.25 + 2.28\left(\frac{a}{b+h}\right) - 37.04\left(\frac{a}{b+h}\right)^2 + 217.22\left(\frac{a}{b+h}\right)^3 - 248.25\left(\frac{a}{b+h}\right)^4 \\
& - 2693.65\left(\frac{a}{b+h}\right)^5 + 18061.02\left(\frac{a}{b+h}\right)^6 - 61797.91\left(\frac{a}{b+h}\right)^7 \\
& + 128352.09\left(\frac{a}{b+h}\right)^8 - 149257.97\left(\frac{a}{b+h}\right)^9 + 75335.7\left(\frac{a}{b+h}\right)^{10}
\end{aligned} \tag{5.43}$$

In equation (5.42), k_r is an undetermined parameter, and the crack geometry factor used for energy calculation is determined by following the procedure for determination of stress intensity factor for a box [1]. In reference [1], the crack geometry factor F_i is determined, based on stress intensity factor for a center cracked rectangular plate subjected to shear loading [98], as

$$F_i = 1.5 + 0.569\left(\frac{a}{b+h}\right) - 6.282\left(\frac{a}{b+h}\right)^2 + 25.0\left(\frac{a}{b+h}\right)^3 - 38.157\left(\frac{a}{b+h}\right)^4 + 21.0\left(\frac{a}{b+h}\right)^5 \tag{5.44}$$

k_r is determined using the dimensions of cross section in the location of the crack

$$k_r = \frac{I_{pc}(I_{pc} - tab^2/2 - 2ta^3/3)aF_w(a)}{2.5(tab^2/2 + 2ta^3/3)b^2h^2I} \tag{5.45}$$

where I_{pc} is polar moment inertia of uncracked hollow beam at $x=c$. Once the stiffnesses for cracked beam are determined, the natural frequencies and modal vectors can be calculated through equations (5.24) and (5.25), using the procedure outlined earlier.

5.6 Results and Discussions

Frequencies and mode shape vectors are calculated numerically using the MATLAB program. For bending-torsional and vertical vibration of uncracked backbone, the frequencies are compared with the test results in Table 5-2. It can be seen that the calculated frequencies agree well with test results. The missed frequencies in the earlier

vertical vibration analysis for this ship model are now given by the coupled (horizontal) bending-torsional vibration. Two analyses together, viz., vertical and coupled bending-torsional vibrations, have provided full verification of the test results. It is observed that sometimes the horizontal bending vibration (alone) gives better correlation with experimental results. This is due to the fact that the carbon/epoxy stiffener location was not exactly given and as such was assumed to be symmetrically located along a horizontal line with respect to the centroidal axis on the top and bottom flange of the hollow section. If the distances were not the same and the stiffeners were located at the corners of the box section, then the horizontal stiffnesses would be much higher in the horizontal direction at different sections along the beam length; this would have given much larger errors for the horizontal bending vibration. Frequencies and the trend of results would have been similar to the vertical vibration, where the test frequencies were less than the analytical values.

For a cracked backbone, the first four frequencies of horizontal bending-torsional vibration are obtained for different crack locations and crack depths. For a through crack occurring in one flank at the middle of beam length, the normalized frequencies (ratio of frequencies between the cracked one and uncracked one) are shown for different crack depths in Figure 5.7. All four frequencies decrease as the crack length increases. For second mode, the frequency has very little decrease even though the crack is large; this is due to the fact that the crack occurs near the vibration node of second mode. It can also be noticed that for other modes the decreases in frequency values are significant when the crack becomes larger. When crack length reaches $0.2m$ ($a/(b+h)=0.4$) which

considerably exceeds the width ($0.127m$) of flank at middle of the beam, the first frequency decreases by about 12.4%. It also means the stiffness of the beam is degraded severely. Figure 5.8 and Figure 5.9 show the normalized frequencies for different crack depths as the crack is located at other two positions $c/l=0.25$ and $c/l=0.75$, respectively. It is observed that (Figures 5.8 and 5.9) the crack influence is much higher for the second modes (of beam with crack at $c/l = 0.25$ and 0.75) due to the fact that the maximum bending moments tend to occur around these points.

For a constant crack length ($a/(b+h)=0.2$), normalized frequencies are shown for different crack locations in Figure 5.10. The changes in frequencies are very small when the crack is near the two ends. As crack location moves along the beam, frequencies decrease or increase showing a wave-type motion. There are some points where frequencies remain almost unchanged or change very little. These points are the vibration nodes of the structure. The crack close to vibration node appears to have very little influence on that vibration mode. This is due to fact that the crack is free of stresses/strains at vibration node for the free vibration of that mode. As is indicated, both crack depth and crack location affect the dynamic characteristics. Figure 5.11 and Figure 5.12 show normalized frequencies for different crack locations with the crack ratios of $a/(b+h)=0.08$ and $a/(b+h)=0.4$, respectively. Normalized frequencies versus crack depth and location are shown in Figure 5.13.

5.7 Crack Detection Procedure

The frequency values for a cracked beam are dependent on both crack location and depth. It turns out that one normalized frequency could correspond to different crack locations and crack depths, as can be seen from Figure 5.13. Based on this, the frequency contour line which has the same normalized frequency on the contour could be plotted in a figure having the crack location and depth as its axes. Figure 5.14 shows three contours (0.99, 0.98 and 0.96) for all the four modes of coupled horizontal bending-torsional vibration. The 0.99 contour means that the points on the contour have a 1% decrease of frequency compared to uncracked beam; the 0.96 contour has a 4% decrease. Similarly, any other contour can be plotted. If a crack is found to have the normalized frequency of a certain value, any point on the contour of that value could give the possible crack location and depth. A crack should and must belong to one contour for each mode. Each contour for different modes contains information about the crack. The contours for different modes could be plotted together, and the intersection point(s) would indicate the crack location and crack depth. Since the frequencies could be measured accurately for lower modes and contours for lower modes tend to be simple, the contours for lower modes (usually first and second one) are plotted together to obtain the intersection point(s). If more than one intersection points are obtained, the contour for another mode is used to get the correct location of the point, which would indicate the crack location and crack depth. If the crack location and vibration node coincide for a mode, the contour tends to disappear and no intersections are obtained; then the next mode is used. Basically, the first four frequencies are sufficient to identify the crack in the beam.

From the obtained results of coupled bending-torsional vibration, a crack with half-length $a/(b+h) = 0.2$ and location $c/l=0.5$ has normalized frequencies of 0.9816 for the first mode, 0.9786 for the third mode and 0.9922 for the fourth mode. These three contours for three different modes are plotted together in Figure 5.15. The three contours give one intersection which indicates crack location and depth very well. Figure 5.16 shows another example for a crack [$a/(b+h)=0.24$, $c/l=0.2$] which has the normalized frequency of 0.9848 for the first mode, 0.9756 for the second mode and 0.9820 for the third mode. The intersection of the three contours gives the crack depth and crack location.

5.8 Closure

The hydroelastic ship model has a pure vertical bending and a coupled (horizontal) bending-torsional vibrations due to added water mass in horizontal direction. Coupled and uncoupled vibration equations are developed using Hamilton's principle. Analysis of coupled vibration along with the vertical vibration provides a thorough theoretical dynamic analysis for the model, and gives a good verification for the test results of an uncracked hollow beam.

When the backbone of ship model contains a crack, reduced equivalent stiffnesses of the cracked backbone are determined using an energy procedure. Coupled vibration analysis is then carried out using Galerkin's method. Basically, the frequencies decrease as crack

length increases; however the decrease is also dependent on crack location. When a crack is located at (or close to) a vibration node of a mode, frequency for this mode remains almost unchanged. A crack identification procedure is developed by considering frequency contours that have the same normalized frequency on the contour line as that obtained for the cracked beam. The contours from different modes can be plotted together, and intersection point shows the crack location as well as crack depth.

Table 5-1 Properties of the Backbone [86]

Between Segments	Bending Stiffness EI_z (Nm^2) (horizontal)	Torsion Stiffness GI_p (Nm^2)	Mass Moment of Inertia ρI_p of Ship (kgm) (including masses of segments)
1-2	1,123,622	718,290	2.5198
2-3	1,401,778	875,868.2	2.5242
3-4	1,079,634	691,897.2	2.5191
4-5	723,853	514,394.8	2.5142
5-6	456,047	352,935.2	2.5097
Average	956,986.8	630,677.08	2.5174

Table S-2 Frequencies of Uncracked Backbone

Frequency(Hz)	1st	2nd	3rd	4th	5th	6th	7th	8th
Test results	4.48	6.35	12.05	19.63	24.64	38.65		
Torsional-bending vibration		6.469		17.9		36.94		61.8
% Errors from tests		1.84%		8.8%		4.4%		
Vertical vibration	4.46		12.6		26.36		44.20	
% Errors from Tests	0.45%		4.56%		6.98%			
Horizontal vibration		6.539		18.26		37.89		64.11
% Errors from tests		2.98%		6.98%		1.97%		

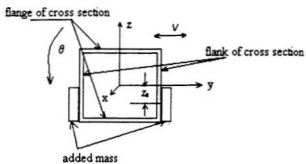


Figure 5.1 Cross section of backbone at a point considering added mass

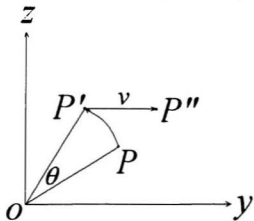


Figure 5.2 Displacement of a point P in coupled torsional-bending vibration of the beam.

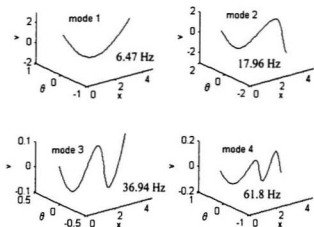


Figure 5.3 Mode shapes for coupled (horizontal) bending-torsional motion (v — horizontal displacement, θ — torsional angle)

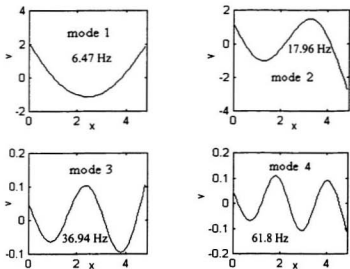


Figure 5.4 Mode shapes for horizontal motion only

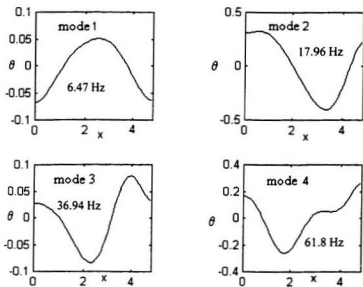


Figure 5.5 Mode shapes for torsional motion only

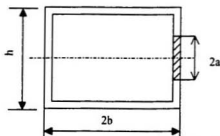


Figure 5.6 A crack ($2a$) is located at one flank of the hollow backbone.

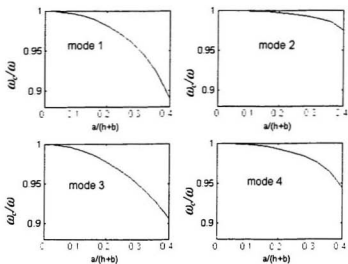


Figure 5.7 Normalized bending-torsional frequencies against crack length for a crack at $c/l=0.5$

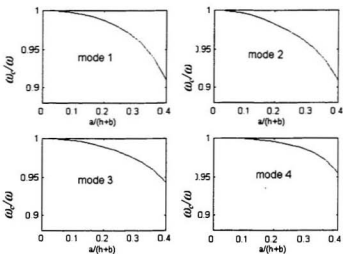


Figure 5.8 Normalized bending-torsional frequencies against crack length for a crack at $c/l=0.25$

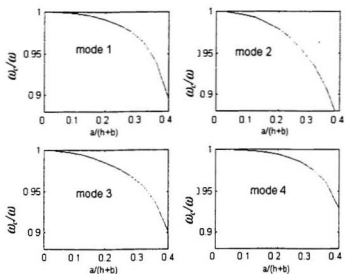


Figure 5.9 Normalized bending-torsional frequencies against crack length for a crack at $c/l=0.75$

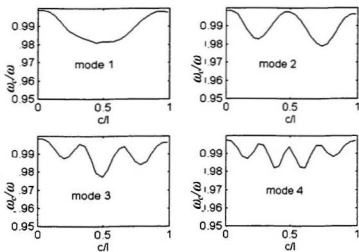


Figure 5.10 Normalized bending-torsional frequency against crack location ratio c/l ($a/(h+b)=0.2$)

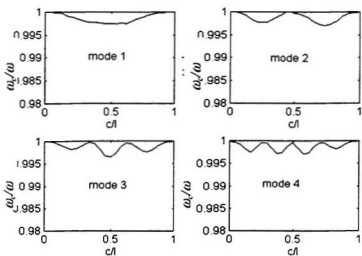


Figure 5.11 Normalized bending-torsional frequency against crack location ratio c/l ($a/(b+h)=0.08$)

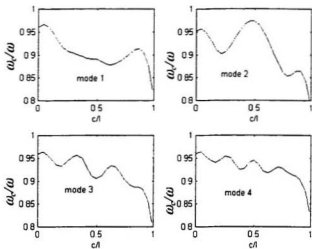


Figure 5.12 Normalized bending-torsional frequency against crack location ratio c/l ($a/(b+h)=0.4$)

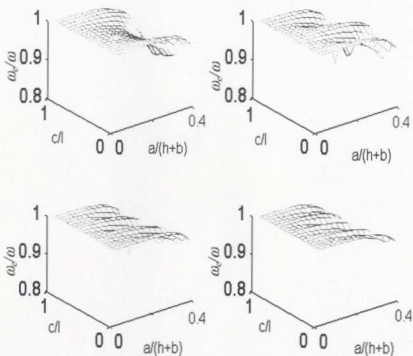


Figure 5.13 Normalized bending-torsional frequency against crack length and crack location

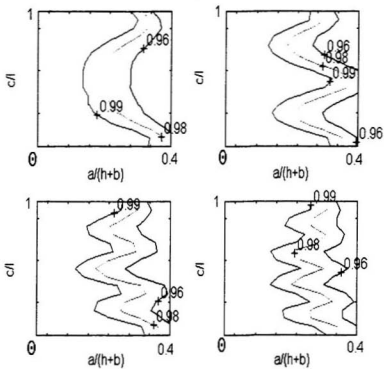


Figure 5.14 Three frequency contours for first four modes of bending-torsional motions

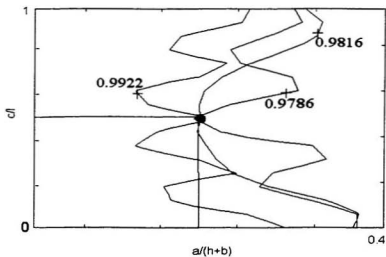


Figure 5.15 Crack identification by intersection of three contours for first, third and fourth modes (deduction: $a/(b+h)=0.2, c/l=0.5$)

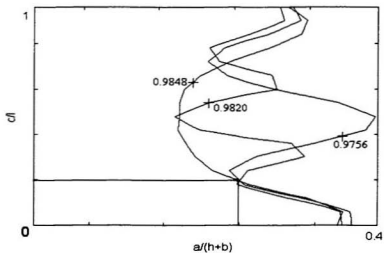


Figure 5.16 Crack identification by intersection of three contours for first, second and third modes (deduction: $a/(b+h)=0.24, c/l=0.2$)

Chapter 6

Vibration and Crack Detection in Timoshenko Beam with a Crack

6.1 Energy Conservation Law and Hamilton's Principle

If the kinetic energy of an elastic body is T , and the potential energy is V , then the total energy of the elastic body will be constant, if the non-conservative forces are zero. This leads to the conservation of energy principle [70], viz.,

$$T+V=\text{constant} \quad (6.1)$$

In case the non-conservative forces are not zero, the change of total energy will be equal to the work performed by non-conservative forces.

Hamilton's principle for a conservative system may be stated in the following form:

the real trajectory of the system is such that the integral [99]

$$\int_{t_1}^{t_2} (T - V) dt \quad (6.2)$$

remains stationary with respect to any compatible virtual displacement, arbitrarily chosen between both instants t_1 and t_2 but vanishing at the ends of the interval, i.e.,

$$\delta \int_{t_1}^{t_2} (T - V) dt = 0 \quad (6.3)$$

with $\delta q(t_1) = \delta q(t_2) = 0$ where q is the generalized coordinate.

6.2 Formulations of Vibration for a Timoshenko beam

For a short beam, shear deformation and rotary inertia should be considered in formulating the equation of motion. This is the case for a Timoshenko beam. The vibration equations of a Timoshenko beam are formulated using Hamilton's principle. For the transverse motion of the beam, the transverse displacement is given by [99]

$$w = w(x,t) \quad (6.4)$$

The shear deflection of the cross section is taken into account by introducing a new variable $\psi = \psi(x,t)$, the rotation of cross section. Both deformations are shown in figure 3.1. The axial displacement at any transverse location of the beam could be expressed as

$$u(x,z,t) = -z\psi \quad (6.5)$$

With small displacement approximation, one obtains the strain expressions as

$$\begin{aligned} \epsilon_{xx} &= \frac{\partial u}{\partial x} = -z \frac{\partial \psi}{\partial x} \\ \epsilon_{zz} &= \frac{\partial w}{\partial z} = 0 \\ \gamma_{xz} &= \left(\frac{\partial w}{\partial x} + \frac{\partial u}{\partial z} \right) = -\psi + \frac{\partial w}{\partial x} \end{aligned} \quad (6.6)$$

The bending moment is given by

$$M = EI \frac{\partial \psi}{\partial x} \quad (6.7)$$

where I is the moment of inertia of the cross section, $I = \int_A z^2 dA$. A is the area of the cross section and E the Young's modulus.

The shear force is given by

$$Q = k'GA\gamma_x = k'GA\left(-\psi + \frac{\partial w}{\partial x}\right) \quad (6.8)$$

where G is shear modulus and k' is a numerical factor depending on the shape of the cross section.

Strain energy of the beam could be written as

$$\begin{aligned} V &= \frac{1}{2} \int_A \int \left(\sigma_x \varepsilon_x + \tau_x \gamma_x \right) dx dA \\ &= \frac{1}{2} \int \left[EI \left(\frac{\partial \psi}{\partial x} \right)^2 + k'GA \left(-\psi + \frac{\partial w}{\partial x} \right)^2 \right] dx \end{aligned} \quad (6.9)$$

where EI is the bending stiffness of the cross section. The kinetic energy could be expressed as

$$T = \frac{1}{2} \int_0^l \int \rho (\dot{w}^2 + \dot{u}^2) dA dx = \frac{1}{2} \int_0^l (m\dot{w}^2 + mr^2\dot{\psi}^2) dx \quad (6.10)$$

where $m = \rho A$ is the mass per unit of beam length and $r^2 = \frac{I}{A}$.

Applying the Hamilton's principle to equation (6.3), one obtains (see [99,100])

$$\begin{aligned} \int_0^t (\delta T - \delta V) dt &= \int_0^t \left\{ \int \left[m\dot{w}\delta\dot{w} + mr^2\dot{\psi}\delta\dot{\psi} \right] dx \right\} dt \\ &+ \int_0^t \left\{ \int \left[-EI \frac{\partial \psi}{\partial x} \delta \left(\frac{\partial \psi}{\partial x} \right) - k'GA \left(\frac{\partial w}{\partial x} - \psi \right) \delta \left(\frac{\partial w}{\partial x} - \psi \right) \right] dx \right\} dt = 0 \end{aligned} \quad (6.11)$$

From the above equation, the equations of motion for the beam can be obtained as

$$\begin{aligned} \frac{\partial}{\partial x} \left[k'GA \left(\frac{\partial w}{\partial x} - \psi \right) \right] - m \frac{\partial^2 w}{\partial t^2} &= 0 \\ \frac{\partial}{\partial x} \left(EI \frac{\partial \psi}{\partial x} \right) + k'GA \left(\frac{\partial w}{\partial x} - \psi \right) - r^2 m \frac{\partial^2 \psi}{\partial t^2} &= 0 \end{aligned} \quad (6.12)$$

For an uniform beam ($k'GA$ and EI are constant), eliminating ψ , a fourth order differential equation in w is obtained as

$$EI \frac{\partial^4 w}{\partial x^4} - (r^2 m + \frac{mEI}{k'GA}) \frac{\partial^4 w}{\partial x^2 \partial t^2} + m \frac{\partial^2 w}{\partial t^2} + \frac{r^2 m^2}{k'GA} \frac{\partial^4 w}{\partial t^4} = 0 \quad (6.13)$$

The type of the motion could be assumed as

$$w = W(x)e^{i\omega t} \quad (6.14)$$

Substituting the equation (6.14) into (6.13), the following equation is obtained

$$EI \frac{d^4 W}{dx^4} + (r^2 m + \frac{mEI}{k'GA}) \omega^2 \frac{d^2 W}{dx^2} - m \omega^2 W + \frac{r^2 m^2}{k'GA} \omega^4 W = 0 \quad (6.15)$$

If we assume that

$$\psi = \Psi(x)e^{i\omega t} \quad (6.16)$$

the following equation could be obtained by using equation (6.12)

$$\Psi = \frac{1}{k'GA - \omega^2 m r^2} \left(EI \frac{d^3 \Psi}{dx^3} + \left(\frac{EI \omega^2 m}{k'GA} + k'GA \right) \frac{d\Psi}{dx} \right)$$

The solution to equation (6.15) would be of the form,

$$W = Ce^{sx} \quad (6.17)$$

Substitution into (6.15) yields the following algebraic equation,

$$EIs^4 + (r^2 m + \frac{mEI}{k'GA}) \omega^2 s^2 - m \omega^2 + \frac{r^2 m^2}{k'GA} \omega^4 = 0 \quad (6.18)$$

The roots of the above equation are

$$s^2 = \frac{-(r^2 m + \frac{mEI}{k'GA})\omega^2 \pm \sqrt{(r^2 m + \frac{mEI}{k'GA})^2 \omega^4 - 4EI(\frac{r^2 m^2}{k'GA} \omega^4 - m\omega^2)}}{2EI} \quad (6.19)$$

It can be seen that the roots are also dependent on the frequency; two of them are certainly complex values and other two are not complex values when

$$-4EI(\frac{r^2 m^2}{k'GA} \omega^4 - m\omega^2) > 0 \quad (6.20)$$

that is

$$\omega^2 < \frac{k'GA}{r^2 m} \quad (6.21)$$

To be valid for both cases, the solution of equation (6.15) is expressed in terms of the following functions, viz.,

$$W = C_1 e^{s_1 x} + C_2 e^{-s_1 x} + C_3 e^{s_2 x} + C_4 e^{-s_2 x} \quad (6.22)$$

For a simply supported beam, the boundary conditions are

$$\begin{aligned} W(0) = W(l) &= 0 \\ \left(\frac{d^2 W}{dx^2} \right)_{x=0} &= \left(\frac{d^2 W}{dx^2} \right)_{x=l} = 0 \end{aligned} \quad (6.23)$$

Applying the boundary conditions, the frequency equation is obtained as

$$(s_1^2 - s_2^2) \left(\frac{e^{s_1 l} - e^{-s_1 l}}{e^{s_2 l} - e^{-s_2 l}} \right) = 0 \quad (6.24)$$

Natural frequencies of a uncracked simply supported beam could be calculated using equation (6.24). Consider a rectangular cross section ($k' = 5/6$), beam length $l = 3m$, width $b = 0.1m$, modulus of elasticity $E = 62.1 \cdot 10^9 \text{ GPa}$, Density $\rho = 2700 \text{ kg/m}^3$, and shear modulus $G = 23.3 \cdot 10^9 \text{ GPa}$. For $l/h = 15$, the first four frequencies are compared

with the results of Euler beam in Table 6-1. Comparisons are also made for $l/h=10$ and $l/h=5$ in Table 6-2 and Table 6-3. It is seen from the results given in Table 6-1 to Table 6-3, that the differences between the Euler beam and Timoshenko beam become quite significant when the l/h ratio becomes smaller and smaller. Even for a beam with a l/h ratio of 15, the difference in the fourth frequency is more than 10%.

6.3 Timshenko Beam with a Crack

For a beam with a crack, the vibration equations are obtained using Hamilton' principle as

$$\begin{aligned} \frac{\partial}{\partial x} \left[k'GA_c \left(\frac{\partial w}{\partial x} - \psi \right) \right] - m \frac{\partial^2 w}{\partial t^2} &= 0 \\ \frac{\partial}{\partial x} \left(EI_c \frac{\partial \psi}{\partial x} \right) + k'GA_c \left(\frac{\partial w}{\partial x} - \psi \right) - r^2 m \frac{\partial^2 \psi}{\partial t^2} &= 0 \end{aligned} \quad (6.25)$$

where EI_c and $k'GA_c$ are bending stiffness and shear stiffness for the cracked beam, which are obtained using the same procedure described in Chapter 4. From equations (4.1) to (4.17), in Chapter 4,

$$EI_c = \frac{EI}{1 + \frac{EIR(a,c)}{1 + \left(\frac{x-c}{k(a)a} \right)^2}} \quad (6.26)$$

$$k'GA_c = \frac{k'GA}{\sqrt{1 + \frac{EIR(a,c)}{1 + \left(\frac{x-c}{k(a)a} \right)^2}}} \quad (6.27)$$

and

$$EIR(a, c) = \frac{3\pi F_c(a)a}{k(a)h \left[\arctan\left(\frac{l-c}{k(a)a}\right) + \arctan\left(\frac{c}{k(a)a}\right) \right]} \quad (6.28)$$

$$k(a) = \frac{3\pi F_c(a)(h-a)a}{[h^3 - (h-a)^3]h} \quad (6.29)$$

Similarly, assuming $w = W(x)e^{i\omega t}$ and $\psi = \Psi(x)e^{i\omega t}$, we obtain

$$\begin{aligned} \frac{d}{dx} \left[k'GAc \left(\frac{dW}{dx} - \Psi \right) \right] + m\omega^2 W &= 0 \\ \frac{d}{dx} \left(EI_c \frac{d\Psi}{dx} \right) + k'GAc \left(\frac{dW}{dx} - \Psi \right) + r^2 m\omega^2 \Psi &= 0 \end{aligned} \quad (6.30)$$

From the above equations, one could derive

$$W = \frac{\frac{d^2}{dx^2} (EI_c \frac{d\Psi}{dx}) + r^2 m\omega^2 \frac{d\Psi}{dx}}{m\omega^2} \quad (6.31)$$

Substitution of equation (6.31) into equation (6.30) yields

$$\begin{aligned} \frac{d}{dx} \left(k'GAc \frac{d^3}{dx^3} (EI_c \frac{d\Psi}{dx}) \right) + \frac{d^2}{dx^2} (EI_c \frac{d\Psi}{dx}) m\omega^2 + \frac{d}{dx} (k'GAc \frac{d^2\Psi}{dx^2}) r^2 m\omega^2 \\ - \frac{d}{dx} (k'GAc \Psi) m\omega^2 + r^2 m^2 \omega^4 \frac{d\Psi}{dx} = 0 \end{aligned} \quad (6.32)$$

Integrating the above equation, one has

$$\begin{aligned} k'GAc \frac{d^3}{dx^3} (EI_c \frac{d\Psi}{dx}) + \frac{d}{dx} (EI_c \frac{d\Psi}{dx}) m\omega^2 + k'GAc \frac{d^2\Psi}{dx^2} r^2 m\omega^2 \\ - k'GAc \Psi m\omega^2 + r^2 m^2 \omega^4 \Psi = 0 \end{aligned} \quad (6.33)$$

For a simply supported beam, the boundary conditions are

$$\frac{d^2}{dx^2} (EI_c \frac{d\Psi}{dx}) + r^2 m\omega^2 \frac{d\Psi}{dx} = 0 \quad \text{at } x = 0 \text{ and } x = l \quad (6.34)$$

$$EI \frac{d^2\Psi}{dx^2} = 0 \text{ at } x=0 \text{ and } x=l \quad (6.35)$$

Using the four term Galerkin's method, the solution is selected as

$$\Psi = C_1\Psi_1 + C_2\Psi_2 + C_3\Psi_3 + C_4\Psi_4 \quad (6.36)$$

where C_i are constants, and Ψ_i are trial functions chosen from the case of a simply supported uncracked Timoshenko beam, viz.,

$$\Psi_i = \cos\left(\frac{i\pi}{l}x\right), \quad i=1,2,3,4 \quad (6.37)$$

6.4 Frequency Changes Due to Crack

Natural frequencies of a simply supported beam could be calculated using equation (6.36) using a four term Galerkin method. Consider a cracked simply supported beam of rectangular cross section, $k' = 5/6$, beam length $l = 3m$, width $b = 0.1m$, modulus of elasticity $E = 62.1 \cdot 10^9 \text{ GPa}$, density $\rho = 2700 \text{ kg/m}^3$, shear modulus $G = 23.3 \cdot 10^9 \text{ GPa}$. For $l/h=15$ (which can be seen as a slender beam), normalized frequency against crack depth ratio is shown in Figure 6.1. For Euler beams, the frequencies are normalized by natural frequencies of the uncracked Euler beam. For Timoshenko beams, the frequencies are normalized by natural frequencies of the uncracked Timoshenko beam. It can be seen that normalized frequency decreases as crack depth increases, and Timoshenko beam shows almost no difference with the Euler beam for first two modes. For third and fourth modes, Euler beam shows a higher decrease in normalized frequency. For $l/h=10$, shown in Figure 6.2, Euler beam has a slightly larger decrease in normalized frequency compared to the Timoshenko beam. For $l/h=5$, shown in Figure 6.3, large decrease in

normalized frequency could be clearly observed in Euler beam compared to the Timoshenko beam. Difference between Euler and Timoshenko beams becomes significant as crack depth increases. Table 6-4 shows the normalized frequencies for Euler and Timoshenko beams with $a/h=0.5$. As the l/h ratio decreases (from slender to short), the Euler beam has larger and larger decrease in normalized frequency compared to the Timoshenko beam, even for the same crack. It is also observed that higher modes would show larger differences between Euler and Timoshenko beams. This is due to the fact that basic bending length (represented by the length of a sine wave between two adjacent nodes of vibration) by depth ratio becomes smaller and smaller and this has larger effect for higher modes; this makes the basic beam to be a very deep beam. Figures 6.4, 6.5 and 6.6 show the normalized frequencies for different crack locations. Variations of normalized frequencies for Euler and Timoshenko beams are similar. Frequency ratios obtained by Timoshenko and Euler formulations are also compared with test results of aluminum beam (with center cracks) in Figure 6.7. It is seen that the differences between Euler beam results and Timoshenko beam results are marginal for the first two modes; the differences become apparent for the third and fourth modes. The frequency contour procedure, outlined in Chapter 4, can also be used for crack detection in Timoshenko beams.

6.5 Closure

Vibration equations and solutions for a cracked Timoshenko beam are developed. Analysis results show that when length-to-height ratio of the beam is less than 10, the

error for first frequency (between Euler and Timoshenko beams) will be greater than 1.7%. The error will be larger for higher frequencies; thus Timoshenko beam analysis is necessary for lower length-to-height ratios to take account of the effect of shear deformation and rotary inertia effect. For cracked beams, decreases of frequencies due to the presence of the crack are almost the same for Euler and Timoshenko beams, having large length-to-height ratios (>15). For low length-to-height ratios (<10), differences become significant, especially for higher modes, and the cracked Euler beam has larger normalized frequency decrease than the cracked Timoshenko beam. This would indicate a larger crack to be present in the beam than it is actually existing in the structure.

Table 6-1 First four frequencies for Euler and Timoshenko beams with $l/h = 15$

	First Freq. (rad/s)	Second Freq. (rad/s)	Third Freq. (rad/s)	Fourth Freq. (rad/s)
Euler Beam	303.64	1214.56	2732.77	4858.26
Timoshenko Beam	301.34	1179.28	2565.03	4366.67
Relative Error	0.76%	2.9%	6.1%	10.1%

Table 6-2 First four frequencies for Euler and Timoshenko beams with $l/h = 10$

	First Freq. (rad/s)	Second Freq. (rad/s)	Third Freq. (rad/s)	Fourth Freq. (rad/s)
Euler Beam	455.46	1821.85	4099.15	7287.39
Timoshenko Beam	447.84	1710.02	3599.00	5918.77
Relative Error	1.7%	6.1%	12.2%	18.8%

Table 6-3 First four frequencies for Euler and Timoshenko beams with $l/h = 5$

	First Freq. (rad/s)	Second Freq. (rad/s)	Third Freq. (rad/s)	Fourth Freq. (rad/s)
Euler Beam	910.92	3643.72	8198.31	14574.77
Timoshenko Beam	855.01	2959.38	5643.7	8551.5
Relative Error	6.1%	18.8%	31.2%	41.3%

Table 6-4 Normalized frequencies for Euler and Timoshenko beams with $a/h=0.5$, $c/l=0.5$

		ω_{k1}/ω_1	ω_{k2}/ω_2	ω_{k3}/ω_3	ω_{k4}/ω_4
$l/h=15$	Euler Beam	0.8860	0.9808	0.9197	0.9683
	Tim. Beam	0.8868	0.9813	0.9246	0.9716
$l/h=10$	Euler Beam	0.8301	0.9603	0.8922	0.9414
	Tim. Beam	0.8326	0.9627	0.9043	0.9523
$l/h=5$	Euler Beam	0.6903	0.8759	0.8269	0.8578
	Tim. Beam	0.7031	0.8969	0.8707	0.9093

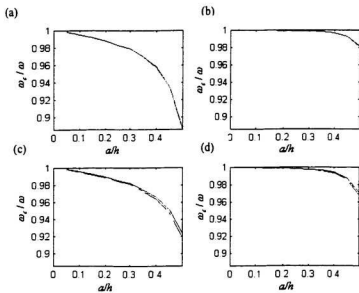


Figure 6.1 Normalized frequency vs crack depth ratio for $l/h=15$, $c/l=0.5$. --- Euler beam, — Timoshenko beam; (a) mode one, (b) mode two, (c) mode three, (d) mode four.

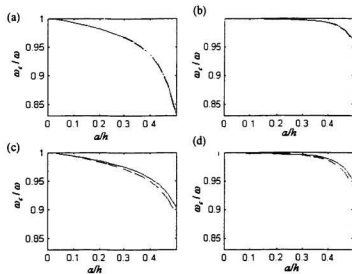


Figure 6.2 Normalized frequency vs crack depth ratio for $l/h=10$, $c/l=0.5$. --- Euler beam, — Timoshenko beam; (a) mode one, (b) mode two, (c) mode three, (d) mode four.

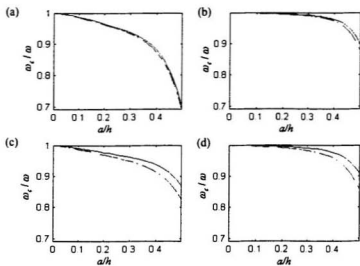


Figure 6.3 Normalized frequency vs crack depth ratio for $l/h=5$, $c/l=0.5$. — Euler beam, — Timoshenko beam; (a) mode one, (b) mode two, (c) mode three, (d) mode four.

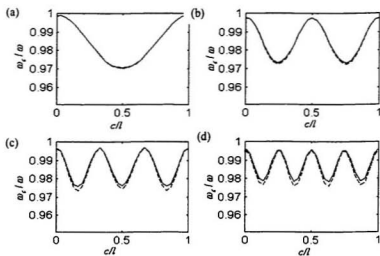


Figure 6.4 Normalized frequency vs crack location ratio for $l/h=15$, $a/h=0.2$. — Euler beam, — Timoshenko beam; (a) mode one, (b) mode two, (c) mode three, (d) mode four.

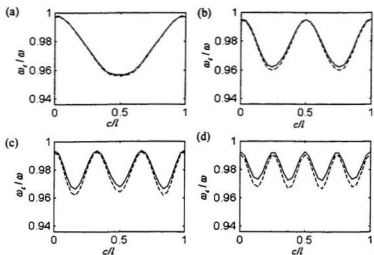


Figure 6.5 Normalized frequency vs crack location ratio for $l/h=10$, $a/h=0.2$. --- Euler beam, — Timoshenko beam; (a) mode one, (b) mode two, (c) mode three, (d) mode four.

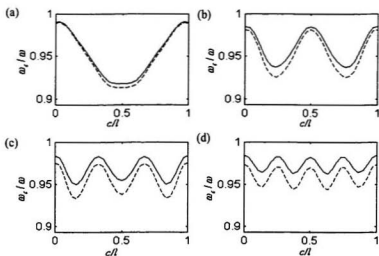


Figure 6.6 Normalized frequency vs crack location ratio for $l/h=5$, $a/h=0.2$. --- Euler beam, — Timoshenko beam; (a) mode one, (b) mode two, (c) mode three, (d) mode four.

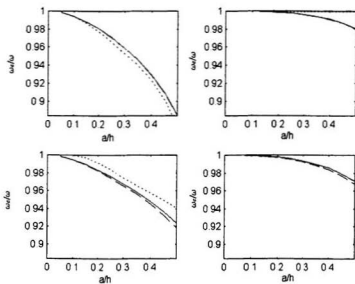


Figure 6.7 Frequency ratio comparisons among Timoshenko beam, Euler beam and test results, $c/l=0.5$. --- Euler beam, — Timoshenko beam, test results of aluminum beam.

Chapter 7

Forced Vibration of a Cracked Beam and Crack

Identification

7.1 Formulations for Forced Beam Vibration with a Crack

For a cracked solid Euler beam, subject to a concentrated harmonic force excitation, the flexural vibration motion is given by

$$(EI_c w'')'' + c\dot{w} + m\ddot{w} = f_0 e^{j\omega t} \delta(x - x_c) \quad (7.1)$$

where EI_c is bending stiffness for the cracked beam which is determined earlier in equation (4.16), c is damping, m is line mass density and f_0 is the amplitude of excitation force which is applied at $x=x_c$. The damping is assumed to be the equivalent structural damping which could be uncoupled for modal analysis; therefore, to make the normal modes orthogonal, the damping is selected as [101]

$$c\dot{w} = \alpha m \dot{w} + \beta (EI_c w'')'' \quad (7.2)$$

where α and β are arbitrary constants.

If q_i are modal coordinates, the response w could be represented by

$$w(x, t) = \sum_{i=1}^{\infty} \bar{W}_i(x) q_i(t) \quad (7.3)$$

where \overline{W}_i s are normalized mode functions which are obtained from mode shapes (W_i s) for free vibration of the cracked beam given in Chapter 4. The normalizing is done such that

$$\int_0^l m \overline{W}_i^2 dx = 1 \quad (7.4)$$

where

$$\overline{W}_i = \frac{W_i}{\sqrt{\int_0^l m W_i^2 dx}} \quad (7.5)$$

Substituting equation (7.3) into equation (7.1), multiplying by \overline{W}_i , and integrating over the beam length, one obtains

$$\ddot{q}_i + 2\xi_i \omega_i \dot{q}_i + \omega_i^2 q_i = \int_0^l f_0 e^{j\omega t} \delta(x-x_r) \overline{W}_i dx \quad (7.6)$$

where ξ_i s are damping ratios or modal damping factors which are dependent on the damping c . Due to the presence of delta function, equation (7.6) is simplified as

$$\ddot{q}_i + 2\xi_i \omega_i \dot{q}_i + \omega_i^2 q_i = f_0 e^{j\omega t} \overline{W}_i(x_r) \quad (7.7)$$

Let

$$q_i = Q_i e^{j\omega t} \quad (7.8)$$

where Q_i is the complex response amplitude. Then following the procedure for one-degree-of-freedom system, the modal frequency response function of equation (7.7) could be obtained as

$$Q_i = \frac{f_0 \overline{W}_i(x_r)}{\omega_i^2 - \omega^2 + 2j\xi_i \omega_i \omega} \quad (7.9)$$

From equations (7.3), (7.8) and (7.9), the frequency response at $x=x_1$ could be derived as

$$w(x_1, x_1, t) = \sum_{i=1}^{\infty} \frac{f_0 \bar{W}_i(x_1) \bar{W}_i(x_1) e^{i\omega t}}{\omega_i^2 - \omega^2 + 2\xi_i \omega_i(j\omega)} \quad (7.10)$$

with the force excitation acting at $x=x_1$. Therefore, based on equation (7.10), the frequency transfer function for displacement is obtained as

$$H(x_1, x_1, j\omega) = \sum_{i=1}^{\infty} \frac{\bar{W}_i(x_1) \bar{W}_i(x_1)}{\omega_i^2 - \omega^2 + 2\xi_i \omega_i(j\omega)} \quad (7.11)$$

Acceleration response at x_1 for excitation at x_1 , would be

$$A_1(x_1, x_1, j\omega) = \sum_{i=1}^{\infty} \frac{-f_0 \bar{W}_i(x_1) \bar{W}_i(x_1) \omega^2}{\omega_i^2 - \omega^2 + 2\xi_i \omega_i(j\omega)} \quad (7.12)$$

For a specified location of the excitation, the displacement response varies along the beam length. Therefore, differentiation with respect to x_2 , will give the frequency response function for the slope, viz.,

$$S(x_1, x_1, j\omega) = \sum_{i=1}^{\infty} \frac{\bar{W}'_i(x_1) \bar{W}_i(x_1)}{\omega_i^2 - \omega^2 + 2\xi_i \omega_i(j\omega)} \quad (7.13)$$

Similarly, the frequency response function for curvature would be given by

$$C(x_1, x_1, j\omega) = \sum_{i=1}^{\infty} \frac{\bar{W}''_i(x_1) \bar{W}_i(x_1)}{\omega_i^2 - \omega^2 + 2\xi_i \omega_i(j\omega)} \quad (7.14)$$

7.2 Crack Identification by Acceleration Curvature Response

The presence of a crack in a beam would result in some changes in mode shapes of the beam; these changes would inevitably introduce changes in displacement and acceleration frequency transfer function compared to the uncracked beam. However, these changes are global, not local. The crack could not be located by directly looking at the acceleration responses of the cracked beam. Figure 7.1 and Figure 7.2 show the frequency transfer functions for the uncracked and cracked beams. Figure 7.3 and Figure 7.4 show the acceleration response for the uncracked and cracked beams (beams discussed in section 4.2.5). From these four figures, we can see that considerable global changes occur due to the presence of the crack, but it would be difficult to indicate the crack location or size from these figures.

In order to identify the crack, one can define the acceleration curvature response (ACR) over the beam length as

$$ACR(x_1, x_2, j\omega) = \sum_{i=1}^n \frac{-f_0 \overline{W}_i(x_1) \overline{W}_i(x_2) \omega^2}{\omega_i^2 - \omega^2 + 2\xi_i \omega_i(j\omega)} \quad (7.15)$$

Due to differentiation twice over the beam, the local information of the crack is incorporated into the acceleration curvature response (ACR) which could be used to identify the crack. For a single frequency excitation (natural frequency would be better), and at the fixed excitation location, the acceleration curvature response could be calculated directly from measured acceleration response along the beam, using a numerical method called central-difference formula.

$$ACR_m = \frac{A_m(x+d) - 2A_m + A_m(x-d)}{d^2} \quad (7.16)$$

where ACR_m is acceleration curvature response, A_m is measured acceleration response, d is the distance between adjacent acceleration sensors. To get accurate acceleration curvature response from measurement, there should be enough acceleration sensors placed over the beam.

To examine the acceleration curvature response (ACR), a simply supported aluminum beam is taken as an example for computation. The beam length is $3m$, its depth is $0.2m$ and its width is $0.1m$. The material Young's modulus $E=62.1GPa$ and the damping is set to be 0.01 . The natural frequencies and mode shapes for free vibration of a cracked beam obtained in Chapter Four by Galerkin's method are used in equation (7.15).

The excitation point could be located at the middle point of the beam which would generate larger response (large amplitude) for first mode as well as third modes. However, the response for second mode would be very small, because the point is close to its vibration node. If the second mode alone is of interest, the excitation point should move to the location of one fourth of the beam length. For all modes (of interest), the excitation force could be located at the point which is not close to any node of vibration modes so that all these modes, which one expects to examine, can be excited. Consider that the cracked beam is subjected to unit harmonic excitation. For a crack with depth ratio $a/h=0.5$ and crack location ratio $c/l=5/6$, Figure 7.5 shows the acceleration response along the beam for excitation at the middle of the beam. It is observed that the second mode is almost not excited. Figure 7.6 shows the acceleration response along the beam

for excitation location at one quarter of the beam. All the three modes are excited when the excitation location is not at a nodal point. To identify the crack, Figure 7.7 shows the resonant acceleration curvature response for a cracked beam. It can be seen that at the crack location the curve has an abrupt peak which would be a better crack indicator. Figure 7.8 shows resonant acceleration curvature response at the first resonant frequency. The crack is identified at $c/l=5/6$. A larger crack has a larger abrupt peak. It is also seen that even for the small crack depth ratio of $a/h=0.1$, there is a clearly observed discontinuity in the acceleration response curvature at the crack location. Figure 7.9 shows resonant acceleration response curvatures for different crack depth ratios at the crack location. The peak amplitude increases as the crack size grows and the increase is quite significant; this is much higher than the increase observed for frequencies during cracking. This resonant acceleration curvature response amplitude could be used to detect the crack size and location.

From equation (7.15), it is known that the acceleration curvature response (ACR) is also dependent on the excitation frequency and amplitude of excitation force. When the excitation frequency is close to the natural frequencies, the acceleration curvature response will have larger values including values near the crack location. Figure 7.10 shows ACRs for different excitation frequencies. When the excitation frequency is close to the first natural frequency, the indication for the crack is quite noticeable. So the excitation frequency should be always selected to be the resonant frequency of a cracked structure. This is facilitated when a fast sine sweep, sweeping over the requisite natural frequency ranges, is used for excitation. As for the excitation force, the ACRs will

increase as the force increases. Hence in order to get sharp and well-defined responses, an optimal magnitude of excitation force should be used.

7.3 Crack Indication Using Resonant Acceleration Amplitude Contour

Resonant amplitude for acceleration response could be expressed as

$$A_k(x_s, x_r) = \sum_{i=1}^{\infty} \frac{-f_0 \bar{W}_i(x_s) \bar{W}_i(x_r) \omega_i^2}{\omega_i^2 - \omega_k^2 + 2\zeta_i \omega_i (j\omega_k)}, \quad k = 1, 2, 3, 4, \dots \quad (7.17)$$

where s and r are locations of response measurement and excitation. It is found that resonant amplitude would change depending on crack depth and crack location. When excitation and measurement points are located at the middle of the beam, Figure 7.11 shows resonant acceleration amplitudes (normalized by that of an uncracked beam) against the crack depth (crack location: $c/l=1/6$). It can be seen that amplitudes for the first and third modes decrease while the crack size increases. Against this decrease, the amplitudes for the second and fourth modes would increase as the crack size increases. For the second and fourth modes, acceleration response would be near zero for the uncracked beam because the middle point is the vibration node. However, the presence of the excitation point at the center will slightly change mode shapes and vibration nodes; therefore vibration node for the second and fourth modes will move slightly away up and down along with the excitation point, and yield the increasing acceleration response as crack size increases. The crack will reduce the local stiffness, and consequently increase the local acceleration response and generally decrease response at a point away from the crack. If the response point is taken to be away from the vibration nodes, the influence related to vibration nodes could be neglected. For the crack located at $c/l=1/3$, the

resonant acceleration amplitude against crack depth plot is shown in Figure 7.12. It can be seen that the curves follow similar patterns shown in Figure 7.11. For the third mode, the crack is located at its vibration node; therefore crack has very little influence on resonant acceleration amplitude. When the crack is located at the middle point of the beam, normalized resonant acceleration amplitude against the crack depth ratio is shown in Figure 7.13. For the first and third modes, the resonant acceleration amplitudes increase as the crack size increases, while, for the second and fourth modes, the resonant acceleration amplitudes decrease as the crack size increases. For the first and third modes the crack is not close to the vibration node; the reduced local stiffness results in the increase of response. However, for the second and fourth modes, the crack is located at its vibration node, and crack acts like a reducer of restraints which causes the responses of other points to increase. The acceleration resonant amplitude also changes depending on the crack location. Figure 7.14 shows normalized resonant acceleration amplitude against crack location for crack depth ratio $a/h=0.25$. Figure 7.15 shows normalized resonant acceleration amplitude against crack location for crack depth ratio $a/h=0.5$. To give an overall view of resonant acceleration amplitude, Figure 7.16 shows normalized resonant acceleration amplitude against both crack location and crack size.

In order to identify the crack using normalized resonant acceleration amplitude, the resonant acceleration amplitude contours are plotted. Figure 7.17 shows three contours (0.95, 0.97, and 0.99) for first four modes. Figure 7.18 shows another three contours (0.96, 1.2, and 1.6) for first four modes. On one contour curve, amplitude value is same for different crack sizes and crack locations. Same amplitude value for different modes

will have different curves. A crack will show different amplitude values for different modes. Contours for these values from different modes could be plotted together, and intersection point would indicate the crack location and crack size. Figure 7.19 shows the crack location is $c/l=0.5$ and the crack depth is $a/h=0.2$. The intersection point comes from three contours, the first one is 1.0191 from the first mode, the second one is 1.0646 from third mode and the third one is 0.9729 from the fourth mode. Figure 7.20 shows the crack location is $c/l=1/3$ or $2/3$ and the crack depth is $a/h=0.4$. The intersection point comes from three contours, the first one is 0.9878 from the first mode, the second one is 0.9997 from third mode and the third one is 1.2256 from the fourth mode. Further refinements could be made by using an off-center mass (as shown in Figure 4.20 to Figure 4.24) and the correct crack location is identified.

7.4 Closure

The forced vibration response for a cracked beam under a single harmonic excitation is developed. The acceleration response and frequency transfer functions for displacement, slope and curvature are obtained over the beam length. Due to the fact that acceleration response is easy to measure (using accelerometers), acceleration curvature response is utilized to identify the crack. The abrupt peak on the acceleration curvature response would be the indication of the location of the crack.

Resonant acceleration amplitude is also dependent on crack location and crack size. Unlike natural frequencies for cracked beams, it could decrease, but could also increase

as the crack size increases. It is determined by the fact whether the crack location is close to the measurement point and vibration node or far away from them. The crack would increase local acceleration response if vibration node has no significant influence. Normalized resonant acceleration amplitude contours are plotted. A crack will generate different contour values for different modes. These contours from different modes are plotted together, and the intersection point of the three curves is used to identify the crack.

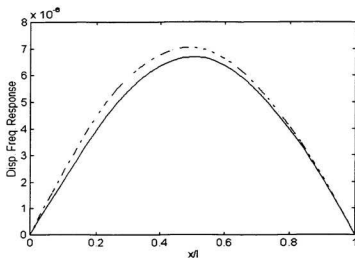


Figure 7.1 Displacement frequency responses for cracked and uncracked beam excited at first natural frequency ($a/h=0.5$, $c/l=1/6$, excitation at the middle point), --- cracked beam, — uncracked beam.

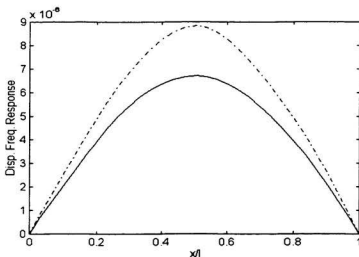


Figure 7.2 Displacement frequency responses for cracked and uncracked beam excited at first natural frequency ($a/h=0.5$, $c/l=1/2$, excitation at the middle point), --- cracked beam, — uncracked beam.

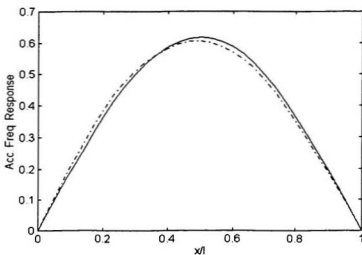


Figure 7.3 Acceleration frequency responses for cracked and uncracked beam excited at first natural frequency ($a/h=0.5$, $c/l=1/6$, excitation at the middle point), --- cracked beam, — uncracked beam.

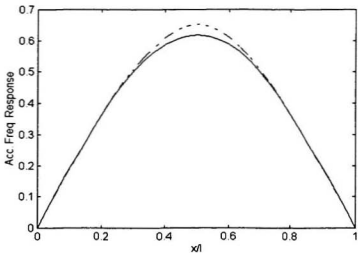


Figure 7.4 Acceleration frequency responses for cracked and uncracked beam excited at first natural frequency ($a/h=0.5$, $c/l=1/2$, excitation at the middle point), --- cracked beam, — uncracked beam.

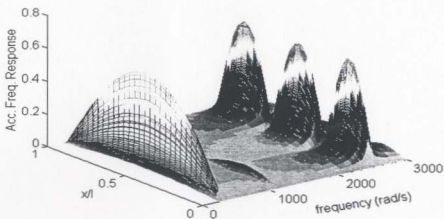


Figure 7.5 Acceleration response along beam length for different excitation frequencies (excitation at the middle point of the beam, $a/h=0.5$, $c/l=5/6$)

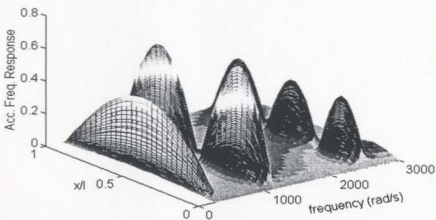


Figure 7.6 Acceleration response along beam length for different excitation frequencies (excitation at the quarter point of the beam, $a/h=0.5$, $c/l=5/6$)

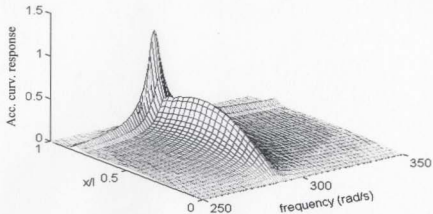


Figure 7.7 Acceleration curvature response along with beam length at different excitation frequencies (with crack location $c/l=5/6$, crack depth $a/h=0.5$, excitation at the middle point)

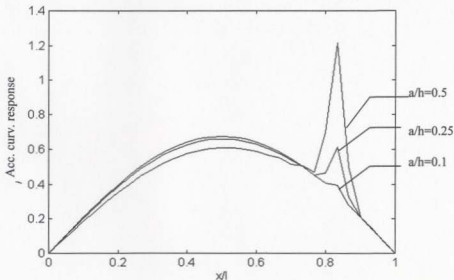


Figure 7.8 Acceleration curvature response along with beam length at the first resonant frequency (crack location $c/l=5/6$, excitation at the middle point of the beam)

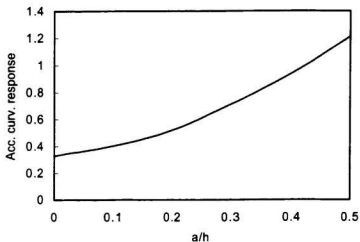


Figure 7.9 Acceleration curvature response (at the crack location) against crack depth at the first resonant frequency (crack location $c/l=5/6$, excitation at the middle point of the beam)

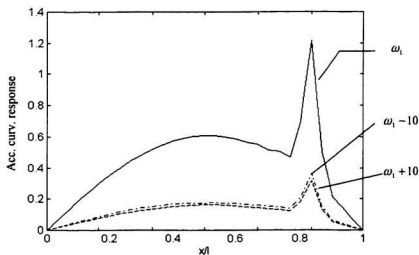


Figure 7.10 Acceleration curvature responses for the first resonant and non resonant frequency excitations (excitation at the middle point)

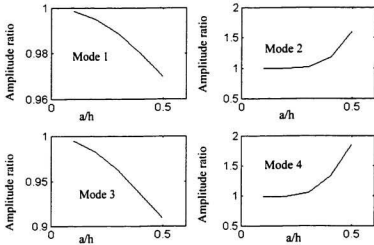


Figure 7.11 Resonant acceleration amplitude against crack depth (crack location $c/l=1/6$; excitation at the middle point, response at the middle point)

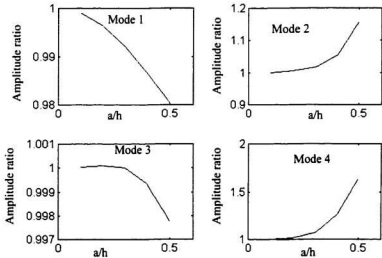


Figure 7.12 Resonant acceleration amplitude against crack depth (crack location $c/l=1/3$; excitation at the middle point, response at the middle point)

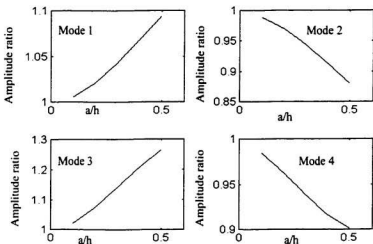


Figure 7.13 Resonant acceleration amplitude against crack depth (crack location $c/l=0.5$; excitation at the middle point, response at the middle point)

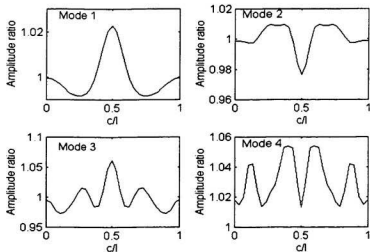


Figure 7.14 Resonant acceleration amplitude against crack location (crack depth $a/h=0.25$; excitation at the middle point, response at the middle point)

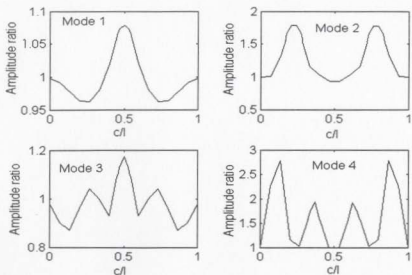


Figure 7.15 Resonant acceleration amplitude against crack location (crack depth $a/h=0.5$; excitation at the middle point, response at the middle point)

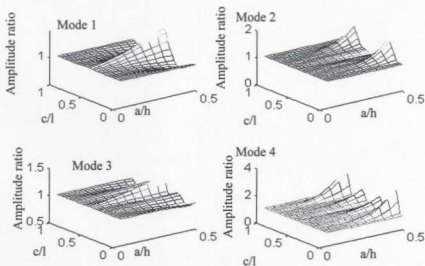


Figure 7.16 Resonant acceleration amplitude vs. crack depth and location (excitation at the middle point, response at the middle point)

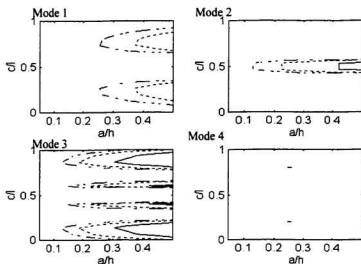


Figure 7.17 Resonant acceleration amplitude contours for first four modes
(— 0.95, --- 0.97, - - - 0.99)

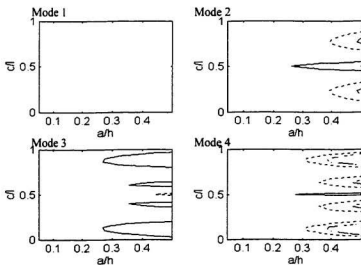


Figure 7.18 Resonant acceleration amplitude contours for first four modes (— 0.96, --- 1.2, - - - 1.6)

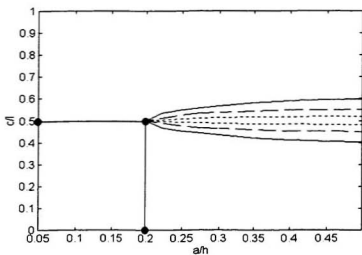


Figure 7.19 Crack identification by the intersection of three contours from three different modes (deduction: $a/h=0.2$, $c/l=0.5$) (— 1.0191: first mode, ----1.0646: third mode, -.-.- 0.9729: fourth mode)

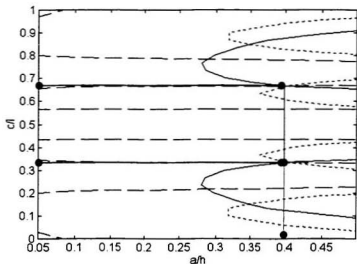


Figure 7.20 Crack identification by the intersection of three contours from three different modes (deduction: $a/h=0.4$, $c/l=1/3$ or $2/3$) (— 0.9878: first mode, ----0.9997: third mode, -.-.-1.2256: fourth mode)

Chapter 8

Summary and Conclusions

A vibration model has been developed for cracked beam structures by energy considerations. The stiffness of the beam changes not only at the crack location, but also along the beam length (mostly around the crack region), due to stress relief around the crack. This stiffness change around the crack region has been modelled by considering strain energy in the beam that would change due to the presence of a crack. Total strain energy change is calculated under dead-load loading using fracture mechanics principles. Actual energy change around the crack region is determined from classical solution for stresses around crack regions and compared with the approximate formulations used in this study, for different crack length ratios; final stiffness for cracked beam is obtained using this approximate formulation. Due to this approach, the stiffness becomes a continuously varying parameter over the beam length. It has a minimum value at the crack location, and tends quickly to the stiffness of uncracked beam away from the crack location; using this formulation, the continuous beam vibration equation is derived. Due to lack of close-form solutions, Galerkin's method is used to solve the equation, in which the trial functions are chosen from that of uncracked beams.

Free vibration analyses are carried out for simply supported rectangular beams and fixed-fixed rectangular beams. One and two edge cracks are considered. Application of

Galerkin's method to vibration equations yields the natural frequencies and mode shapes of cracked beams.

Natural frequencies vary depending on crack size and crack location. Consequently normalized frequency contours have been drawn for various modes with crack depth ratios along x-axis and crack location ratios along y-axis. From these contours, it is observed that a crack depth ratio could correspond to different frequency ratios and crack locations for different modes. In order to identify a crack that gives predefined normalized frequency ratios (obtained from experimental measurements on cracked structures) for a number of modes, frequency contours for these modal frequency changes could be drawn from previously computed values (for different modes) and plotted in a single diagram; the intersection point would indicate the crack location and crack depth.

In addition to the above, a number of other studies have been carried out. A hollow beam model representing a ship hull (which was tested earlier in the nearby Institute for Marine Dynamics [NRCC], for dynamic response) has been investigated. The hollow beam, with varying stiffness and varying thickness, vibrates in water with free-free boundary conditions. Added water masses are considered. Vertical bending vibration responses, and coupled torsional-bending (horizontal) vibration responses, are determined without and with a through-thickness crack. The natural frequencies and mode shapes are obtained. Frequency contours are used to identify the crack, using the methodology developed earlier.

To consider the influence of shear deformation and rotary inertia in vibration of cracked beams, the Timoshenko beam vibrations are examined with/without a crack for different length-to-height ratios. Comparisons of natural frequencies are made between the Timoshenko beam and Euler beam, with/without a crack.

Forced vibration response of a cracked beam has also been determined, using the above procedure. Excitation is considered as a concentrated harmonic force. The natural frequencies and mode shapes used for calculation are taken from results obtained previously in Chapter 4. Frequency transfer function, acceleration response, acceleration curvature response and resonant acceleration amplitude are obtained.

The acceleration curvature response along the beam length shows that the acceleration response curvature has a large increase at the crack location, which could be used to identify the crack location; the crack depth could be determined by curvature value at the location. Another crack detection procedure uses resonant acceleration amplitude contours. The resonant acceleration amplitude also varies according to the crack size and crack location. Similar to frequency contours, the resonant acceleration amplitude contours are also plotted. The contours for different modes are plotted together, and the intersection point is used to identify the crack size and location.

The following observations, contributions and conclusions have been made from the above study:

1. The vibration model developed in this study is able to easily solve for dynamic characteristics of cracked beam structures. It has included stress concentration at the crack tip and stress relief around the crack region which leads to stiffness reduction around the crack region. The crack is thus better modeled. The obtained results using the model agree very well with experimental results and other research results, giving better agreement than others.
2. Results for simply supported and fixed-fixed beams show that the natural frequencies would decrease as the crack size increases. The natural frequencies also vary depending on the crack location. For a simply supported beam, the maximum decrease of the first natural frequency is at the middle point, and the half-height crack has 11.6% decrease of frequency. For a fixed-fixed beam, the maximum decrease of the first natural frequency occurs at the ends, and the half-height crack has 11.5% decrease of frequency.
3. Normalized frequency contour plots present a clear view of how natural frequencies change as the crack size and its location change. Frequency contours contain explicit information to analyze influence of crack on dynamic behavior. For crack detection, frequency contour procedure provides an easy way to identify the crack, giving its size and location even for small cracks ($a/h=0.05$ to 0.10). The similar frequency reductions (crack at ends and at center) obtained for both fixed and simply-supported beams (first mode) indicate that failure is generated by identical conditions, in spite of their different boundary conditions.

4. Frequency contour procedure requires at least two natural frequencies, and usually three natural frequencies, to generate the unique intersection point that would identify the crack. The three frequencies are selected from lower modes (first four) since frequencies for the lower modes could be accurately measured and contours for lower modes tend to be simple.
5. For symmetric beam structures, frequency contour procedure would indicate two possible crack locations. Adding an off-center mass to the beam would make vibration modes asymmetric, and thus give the unique crack location.
6. The studies carried out in this thesis have clearly identified the additional frequencies obtained during an earlier dynamic testing of a hydroelastic ship model as that due to coupled torsional-bending (horizontal) motion of the ship. Coupled horizontal torsional-bending vibration is not due to structural asymmetry, but due to mass asymmetry caused by added water mass. The agreement between earlier experimental results and present analysis has been found to be very good.
7. For the backbone with a crack, the natural frequencies would decrease. For vertical bending vibration, when the crack size grows beyond the flange of the backbone and goes into two flanks, the stiffness drops significantly and natural frequencies have a large decrease.

8. Bending vibration analyses of Timoshenko beams show that frequency differences between Timoshenko beam and Euler beam are very small for slender beams ($l/h=15$), with a difference of 0.76% for the first mode; but the differences become considerable for higher modes, being more than 10.1% for the fourth mode. For a short beam with $l/h=5$, the difference is 6.1% for the first, and becomes 41.3% for fourth mode.
9. For cracked beams, when $l/h \geq 15$, the results between Timoshenko beam and Euler beam are very close. For short cracked beams with $l/h < 15$, the Timoshenko beam analysis becomes essential. Analyses show that Euler beam gives larger frequency decrease than that of Timoshenko beam; this would indicate that the crack present in the structure is much larger than its actual value.
10. Forced vibration analyses show that frequency transfer function and acceleration frequency response for a cracked beam change globally over the beam length compared to an uncracked beam. It is difficult to use them to identify the crack directly when the crack depth is small.
11. Acceleration curvature response has very large local change near the crack. The local abrupt increase would indicate the crack location. The value of curvature could be used to infer the crack size. Acceleration curvature response should be obtained from resonant frequency excitation.

12. Resonant acceleration amplitudes vary according to crack sizes and crack locations.

Unlike natural frequencies, resonant acceleration amplitudes will not always decrease. At some crack locations, the resonant acceleration amplitudes will increase as crack size increases; while at other crack locations they will decrease. Resonant acceleration amplitude contours also could be used to identify the crack.

For future research, the following recommendations are made:

1. The crack considered in this study remains always open. This is a limitation of this study; since cracks open and close during their dynamic response, fully or partially, this would influence the results obtained in this study. Hence it would be worthwhile to consider the influence of crack opening and closing on the dynamic behavior along with the stress relief considered in this study.
2. The acceleration response function, and acceleration curvature response function, have been considered only for lower modes. From the results given in this study, it appears that better indication of crack size and location could be obtained by considering a few more higher order modes.
3. Further studies could be carried out (using the methodology developed in this thesis) to relate the crack size, crack location and the remaining life of a cracked structure.

-
-
-
4. In addition to the above, studies could also be carried out on frames, plates, shells and other complex structures, utilizing the methodology developed in this investigation.

REFERENCES

1. A. Rytter, "Vibration Based Inspection of Civil Engineering Structures", Ph.D thesis, Submitted to the Department of Building Technology and Structural Engineering, University of Aalborg, Denmark, April 1993, pp. 20-22, 40-45, 58-60, 185-193.
2. S.W. Doebling, C.R. Farrar, M.B. Prime and D.W. Shevitz, *Damage Identification and Health Monitoring of Structural and Mechanical System from Changes in Their Vibration Characteristics: A Literature Review*, Los Alamos National Laboratory, New Mexico, 1996.
3. W. Elber, "Fatigue Crack Closure Under Cyclic Tension", *Engineering Fracture Mechanics*, Vol. 2, No. 1, July 1970, pp. 37-45.
4. W. Elber, "The Significance of Fatigue Crack Closure," *Damage Tolerance in Aircraft Structures*, ASTM STP 486, American Society for Testing and Materials, 1971, pp. 230-240.
5. G. Marci and P.F. Packman, "The Effects of the Plastic Wake Zone on the Conditions for Fatigue Crack Propagation", *International Journal of Fracture*, Vol. 16, No. 2, 1980, pp.133-153.
6. J. Tirosh and A. Ladelski, "Note on Residual Stresses Induced by Fatigue Cracking", *Engineering Fracture Mechanics*, Vol. 13, 1980, pp. 453-461.
7. P.G. Kirsmer, "The Effect of Discontinuities on the Natural Frequency of Beams", *Proceedings of the American Society for Testing and Materials*, Vol. 44, 1944, pp. 897-904.

8. W.T. Thomson, "Vibration of Slender Bars with Discontinuities in Stiffness", *Journal of Applied Mechanics*, Vol. 16, 1949, pp. 203-207.
9. H.J. Petroski, "Simple Static and Dynamic Models for the Cracked Elastic Beams", *International Journal of Fracture*, Vol. 17, 1981, pp. R71-R76.
10. M.M.F. Yuen, "A Numerical Study of the Eigenparameters of a Damaged Cantilever", *Journal of Sound and Vibration*, Vol. 103, No. 3, 1985, pp. 301-310.
11. A.K. Pandey, M. Biswas and M.M. Samman, "Damage Detection from Changes in Curvature Mode Shapes", *Journal of Sound and Vibration*, Vol. 145, No. 2, 1992, pp. 321-332.
12. O.S. Salawu and C. Williams, "Damage Location using Vibration Mode Shapes", *Proc. of 12th International Modal Analysis Conference*, 1994, pp. 933-939.
13. T. Mura and T. Koya, *Variational Methods in Mechanics*, Oxford University Press, New York, 1992, p.244.
14. W.M. Ostachowicz and M. Krawczuk, "Analysis of the Effect of Cracks on the Natural Frequencies of a Cantilever Beam", *Journal of Sound and Vibration*, Vol. 150, No. 2, 1991, pp. 191-201.
15. G.R. Irwin "Fracture Mechanics", *Structural Mechanics*, Proc. of 1st Symposium on Naval Structural Mechanics, 1960, p. 564.
16. H. Okamura, K. Watanabe and T. Takan, "Applications of the Compliance Concept in Fracture Mechanics", *Progress in Flaw Growth and Fracture Toughness Testing*, ASTM, STP 536, 1972.

17. F.D. Ju, M. Akgun, E.T. Wong and T.L. Lopez, "Modal Method in Diagnosis of Fracture Damage in Simple Structures", Productive Application of Mechanical Vibrations, ASME AMD, Vol. 52, 1982, pp. 113-126.
18. A.D. Dimarogonas and S.A. Paipetis, Analytical Methods in Rotor Dynamics, Elsevier Applied Science, London, 1983, pp. 160-164.
19. C.A. Papadopoulos and A.D. Dimarogonas, "Coupling of Bending and Torsional Vibration of a Cracked Timoshenko Shaft", Ingenieur-Archiv, Vol. 57, 1987, pp. 257-266.
20. M.-H.H. Shen and Y.C. Chu, "Vibration of Beams with a Fatigue Crack", Computers and Structures, Vol. 45, No. 1 1992, pp. 79-93.
21. Y.C. Chu and M.-H.H. Shen, "Analysis of Forced Bilinear Oscillators and the Application to Cracked Beam Dynamics", AIAA Journal, Vol. 30, No. 10, 1992, pp. 2512-2519.
22. M. Krawczuk and W.M. Ostachowicz, "Parametric Vibration of Beam with Crack", Archives of Applied Mechanics, Vol. 62, 1992, pp. 463-473.
23. W.M. Ostachowicz and M. Krawczuk, "Vibration Analysis of a Cracked Beam", Computers and Structures, V. 36, No. 2, 1990, pp. 245-250.
24. M. Krawczuk and W.M. Ostachowicz, "Forced Vibrations of a Cantilever Timoshenko Beam with a Closing Crack", ISMA 19-Tools for Noise and Vibration Analysis, 1994, pp. 1067-1078.
25. R.L. Actis and A.D. Dimarogonas, "Non-linear Effects Due to Closing Cracks in Vibrating Beams", ASME Design Engineering Division Publication DE-Structural Vibration and Acoustics, V. 18, No. 3, 1989, pp. 99-104.

26. G.-L. Qian, S.-N. Gu and J.-S. Jiang, "The Dynamic Behavior and Crack Detection of a Beam with a Crack", *Journal of Sound and Vibration*, Vol.138, No. 2, 1990, pp.233-243.
27. M. Imregun and K.Y. Sanliturk, "Natural Frequency and Damping Changes Produced by Fatigue Cracks", *Proc. of 15th International Seminar on Modal Analysis*, 1990, pp. 791-805.
28. M.B. Prime and D.W. Shevitz, "Linear Method for Detecting Cracks in Beams", *Proc. of 14th International Modal Analysis Conference*, 1996, pp. 363-368.
29. B.G.Lamonaca, C. Valente and F. Brancaleon, "Crack Identification in Non-Linear Vibration", *Proc. of 15th International Modal Analysis Conference*, 1997, pp. 1808-1814.
30. J.R. Maguire, "Assessing the Dynamic Properties of Existing Bridge Structures by Hammer Testing", *Proc. of 1st International Conference on Bridge Management, Inspection, Maintenance Assessment and Repair*, Elsevier, March 1990, pp. 596-605.
31. J.K. Vandiver, "Detection of Structural Failure on Fixed Platforms by Measurement of Dynamic Response", *Proc. of 7th Annual Offshore Technology Conference*, 1975, pp. 243-252.
32. J.K. Vandiver, "Detection of Structural Failure on Fixed Platforms by Measurement of Dynamic Response", *Journal of Petroleum Technology*, March 1977, pp. 305-310.
33. R.M Kenley and C.J. Dodds, "West Sole WE Platform: Detection of Damage by Structural Response Measurements", *Proc. of 12th Annual Offshore Technology Conference*, 1980, pp. 111-118.

34. J.J Tracy and G.C. Pardoen, "Effect of Delamination on the Natural Frequencies of Composite Laminates", *Journal of Composite materials*, Vol. 23, 1989, pp. 1200-1215.
35. X.T. Man, L.M. McClure, Z. Wang, R.D. Finch, P.Y. Robin and B.H. Jansen, "Slot Depth Resolution in Vibration Signature Monitoring of Beams Using Frequency Shift", *Journal of the Acoustic Society of America*, Vol. 95, No. 4, 1994, pp. 2029-2037.
36. F.K. Choy, R. Liang and P. Xu, "Fault Identification of Beams on Elastic Foundation", *Computers and Geotechnics*, Vol. 17, 1995, pp. 157-176.
37. R.D. Adams, P. Cawley, C.J. Pye and B.J. Stone, "A Vibration Technique for Non-destructively Assessing the Integrity of Structures", *J. of Mechanical Engineering Science*, Vol. 20, 1978, pp. 93-100.
38. N. Stubbs and R. Osegueda, "Global Non-destructive Damage Evaluation in Solids", *Modal Analysis: The International J. of Analytical and Experimental Modal Analysis*, Vol. 5, No. 2, 1990a, pp. 67-79.
39. N. Stubbs and R. Osegueda, "Global Damage Detection in Solids - Experimental Verification", *Modal Analysis: The International J. of Analytical and Experimental Modal Analysis*, Vol. 5, No. 2, 1990b, pp. 81-97.
40. G. Hearn and R.B. Testa, "Modal Analysis for Damage Detection in Structures", *J. of Structural Engineering*, V. 117, No. 10, 1991, pp. 3042-3063.
41. D. Sanders, D.I. Kim and R.N. Stubbs, "Non-destructive Evaluation of Damage in Composite Structures using Modal Parameters", *Experimental Mechanics*, V. 32, 1992, pp. 240-251.

42. P.S. Skjaerbaek, S.R.K. Neilsen and A.S. Cakmak, "Assessment of Damage in Seismically Excited RC-Structures from a Single Measured Response", Proc. of 14th International Modal Analysis Conference, 1996, pp. 133-139.
43. W.M. West, "Illustration of the Use of Modal Assurance Criterion to Detect Structural Changes in an Orbiter Test Specimen", Proc. of Air Force Conference on Aircraft Structural Integrity, 1984, pp. 1-6
44. P.F. Rizos, N. Aspragathos and A.D. Dimarogonas, "Identification of Crack Location and Magnitude in a Cantilever Beam From the Vibration Modes", J. of Sound and Vibration, V. 138, No. 3, 1990, pp. 381-388.
45. C.H.J. Fox, "The Location of Defects in Structures: A Comparison of the Use of Natural Frequency and Mode Shape Data", Proc. of 10th International Modal Analysis Conference, 1992, pp. 522-528.
46. N.A.J. Liewen and D.J. Ewins, "Spatial Correlation of Mode Shapes, the Coordinate Modal Assurance Criterion (COMAC)", Proc. of 6th International Modal Analysis Conference, 1988, pp. 690-695.
47. J.M. Ko, C.W. Wong and H.F. Lam, "Damage Detection in Steel Framed Structures by Vibration Measurement Approach", Proc. of 12th International Modal Analysis Conference, 1994, pp. 280-286.
48. T.Y. Kam and T. Y. Lee, "Detection of Cracks in Structures using Modal Test Data", Engineering Fracture Mechanics, V. 42, No. 2, 1992, pp. 381-387.
49. O.S. Salawu and C. Williams, "Bridge Assessment using Forced-Vibration Testing", J. of Structural Engineering, V. 121, No. 2, 1995, pp. 161-173.

50. P. Cornwell, S.W. Doebling and C.R. Farrar, "Application of the Strain Energy Damage Detection Method to Plate-Like Structures", Proc. of 15th International Modal Analysis Conference, 1997, pp.1312-1318.
51. N. Stubbs, J.-T. Kim and C.R. Farrar, "An Efficient and Robust Algorithm for Damage Localization in Offshore Platforms", Proc. of ASCE 10th Structures Conference, 1992, pp. 543-546.
52. A.S.J. Swamidas and Y. Chen, "Damage Detection in a Tripod Tower Platform (TTP) Using Modal Analysis", ASME Offshore Technology, 1-B, 1992, pp. 577-583.
53. J. Chance, G.R. Tomlinson and K. Worden, "A Simplified Approach to the Numerical and Experimental Modeling of the Dynamics of a Cracked Beam", Proc. of 12th International Modal Analysis Conference, 1994, pp. 778-785.
54. D.I. Nwosu, A.S.J. Swamidas, J.Y. Guigne and D.O. Olowokere, "Studies on Influence of Cracks on the Dynamic Response of Tubular T-Joints for Non-destructive Evaluation", Proc. of 13th International Modal Analysis Conference, 1995, pp. 1122-1128.
55. A.K. Pandey and M. Biswas, "Damage Detection in Structures Using Changes in Flexibility", J. of Sound and Vibration, V. 169, No. 1, 1994, pp. 3-17.
56. T. Toksoy and A.E. Aktan, "Bridge-condition Assessment by Modal Flexibility", Experimental Mechanics, V. 34, 1994, pp. 271-278.
57. R.L. Mayes, "An Experimental Algorithm for Detecting Damage Applied to the I-40 Bridge over the Rio grande", Proc. of 13th International Modal Analysis Conference, 1995, pp. 219-225.

58. Z. Zhang and A.E. Atkan, "The Damage Indices for Constructed Facilities", Proc. of 13th International Modal Analysis Conference, 1995, pp. 1520-1529.
59. P.-L. Liu , "Identification and Damage Detection of Trusses using Modal Data", J. of Structural Engineering , V. 121, No. 4, 1995, pp. 599-608.
60. H.M. Kim and T.J. Bartkowicz, "Damage Detection and Health Monitoring of Large Space Structures", Sound and Vibration, V. 27, No. 6, 1993, pp. 12-17.
61. S.W. Doebling, F.M. Hemez, L.D. Peterson and C. Farhat, "Improved Damage Location Accuracy Using Strain Energy-Based Mode Selection Criteria", AIAA Journal, Vol. 35, No. 4, April 1997, pp.693-699.
62. K.R. Colins, R.H. Plaut and J. Wauer, "Detection of Cracks in a Rotating Timoshenko Shaft Using Axial Impulses", J. of Vibration and Acoustics, V. 113, 1991, pp. 74-78.
63. M.I. Friswell and J.E. Penny, "A Simple Non-Linear Model of a Cracked Beam", Proc. of 10th International Modal Analysis Conference, 1992, pp. 516-521.
64. O.N.L. Abraham and J.A. Brandon, "The Modelling of the Opening and Closure of a Crack", Journal of Vibration and Acoustics, Vol. 117, July 1995, pp. 370-377.
65. J. Kudva, N. Munir and P.Tan, "Damage Detection in Smart Structures Using Neural Networks and Finite Element Analysis", Proc. of ADPA/AIAA/ASME/SPIE Conference on Active Materials and Adaptive Structures, 1991, pp. 559-562.
66. W.J. Leath and D.C Zimmerman, "Analysis of Neural Network Supervised Training with Application to Structural Damage Detection", Damage and Control of Large Structures, Proc. of 9th VPI/SU Symposium, 1993, pp. 583-594.

67. P.Z. Szewczyk and P. Hajela, "Damage Detection in Structures Based on Feature-Sensitive Neural Networks", *ASCE J. of Computing in Civil Engineering*, V. 8, No. 2, 1994, pp. 163-178.
68. J. C. Newman and W. Weber, *Mechanics of Fatigue Crack Closure*, ASTM, PA, USA, 1988, pp.172.
69. J. Backlund, A. F. Blom and C. J. Beeves, *Fatigue Thresholds*, EMAS, UK, 1981, pp.1123.
70. L. Meirovitch, *Principles and Techniques of Vibrations*, Published by Prentice Hall, New Jersey, 1997.
71. J.S. Rao, *Advanced Theory of Vibrations*, New York/Toronto, John Wiley & Sons, Inc., 1992, pp. 339-348.
72. E.E. Gdoutos, *Fracture Mechanics*, Kluwer Academic Publishers. 1993, pp. 79-94.
73. C. Hu, *Fracture Mechanics and Its Applications in Engineering*, Beijing, 1989, pp. 10-14.
74. H.M Westergaard, "Bearing Pressure and Crack", *Journal of Applied Mechanics*, Vol. 61, 1939, pp. 49-53.
75. S. Christides and A. D. S. Barr, "One-Dimensional Theory of Cracked Bernoulli-Euler Beams", *International Journal Mechanics Sciences*, Vol. 26, 1984, pp. 639-648.
76. Hai-Chang Hu, "On Some Variational Principles in the Theory of Elasticity and Plasticity", *Scientia Sinica*, Vol. 4, 1955, pp. 33-55.
77. K. Washizu, *Variational Methods in Elasticity and Plasticity*, 3rd Edition, Pergamon Press, Oxford, 1982.

78. M.–H. H. Shen and C. Pierre, "Free Vibration of Beams with a Single-Edge Crack", *Journal of Sound and Vibration*, Vol. 170, 1994, pp.237-259.
79. M. –H. H. Shen and Y. C. Chu, "Vibrations of Beams with a Fatigue Crack", *Computers and Structures*, Vol. 45, 1992, pp.79-93.
80. T. G. Chondros and A. D. Dimarogonas, "Vibration of a Cracked Cantilever Beam", *Journal of Vibration and Acoustics*, Vol. 120, 1998, pp.742-746.
81. T. G. Chondros, A. D. Dimarogonas and J. Yao, "A Continuous Cracked Beam Vibration Theory", *Journal of Sound and Vibration*, Vol. 215, 1998, pp.17-34.
82. A. Almar-Ness, *Fatigue Handbook*, Tetric, Trondheim, Norway, 1985.
83. D. J. Gorman, *Free Vibration Analysis of Beams and Shafts*, John Wiley and Sons, Inc., 1975, p.1-14.
84. STAR System, *Reference Manual*, 1994, Santa Clara, California: GenRad, Inc.
85. G.M. Owolabi, *Crack Identification Procedures in Beams Using Experimental Modal Analysis*, Master Thesis, Memorial University of Newfoundland, 2001.
86. Hardiman, K. and Daley, C., "Final Reports – Construction of a Hydroelastic Canadian Patrol Frigate Model for Testing in Sever Seas," Reports 3838C, Fleet Technology Limited, 1993.
87. Chen, Y. and Swamidas, A. S. J., "Modal Property Measurements of Canadian Patrolling Frigate (CPF) Hydroelastic (Segmented) Model," Project Report Submitted to Fleet Technology Ltd., Ontario, June 1993.
88. Rowsell, C., "Modal Property Tests of a Hydroelastic Ship Model," IMD Report LM-1993-13, IMD, 1993.

89. Cumming, D. and Mackay, M. and Datta, I., "Experimental Investigation of Hull Lateral Force Distribution Using a Partly Captive Hydroelastic Model," IMD Report IR-1998-06, IMD, 1998.
90. E. R. Champion (Jr.), Numerical methods for engineering applications, Published by Marcel Dekker, New York, 1993, p.442.
91. Reddy, D. V. and Arockiasamy, M., Offshore Structures, Krieger Publishing Company, 1991, pp. 252-259.
92. S. Timoshenko, D.H. Young and W. Weaver, Vibration Problems in Engineering, New York, John Wiley & Sons, Inc., 1974, pp. 471-475.
93. E. Dokumaci, "An Exact Solution for Coupled Bending and Torsion Vibrations of Uniform Beams Having Single Cross-Sectional Symmetry", Journal of Sound and Vibration, Vol. 119, No. 3, 1987, pp. 443-449.
94. J.R. Banerjee, "Explicit Frequency Equation and Mode Shapes of a Cantilever Beam Coupled in Bending and Torsion", Journal of Sound and Vibration, Vol. 224, No. 2, 1999, pp. 267-281.
95. R.E.D. Bishop, S.M. Cannon and S. Miao, "On Coupled Bending and Torsional Vibration of Uniform Beams", Journal of Sound and Vibration, Vol. 131, No. 3, 1989, pp. 457-464.
96. R.E.D. Bishop and W.G. Price, "Coupled Bending and Twisting of a Timoshenko Beam", Journal of Sound and Vibration, Vol. 50, No.4, 1977, pp. 469-477.
97. A.N. Bercin and M. Tanaka, "Coupled Flexural-Torsional Vibrations of Timoshenko Beams", Journal of Sound and Vibration, Vol. 207, No. 1, 1997, pp. 47-59.

98. Y. Murakami [Editor-in-chief], *Stress Intensity Factors Handbook*, Pergamon Press, 1987, pp. 931-932.
99. M. Geradin and D.Rixen, *Mechanical Vibrations, Theory and Application to Structural Dynamics*, John Wiley and Sons, New York, 1994.
100. I.N. Sneddon, *Application of Integral Transforms in the Theory of Elasticity*, Springer-Verlag, 1975.
101. D. E. Newland, *Mechanical Vibration Analysis and Computation*, Longman Scientific and Technical, 1989.

